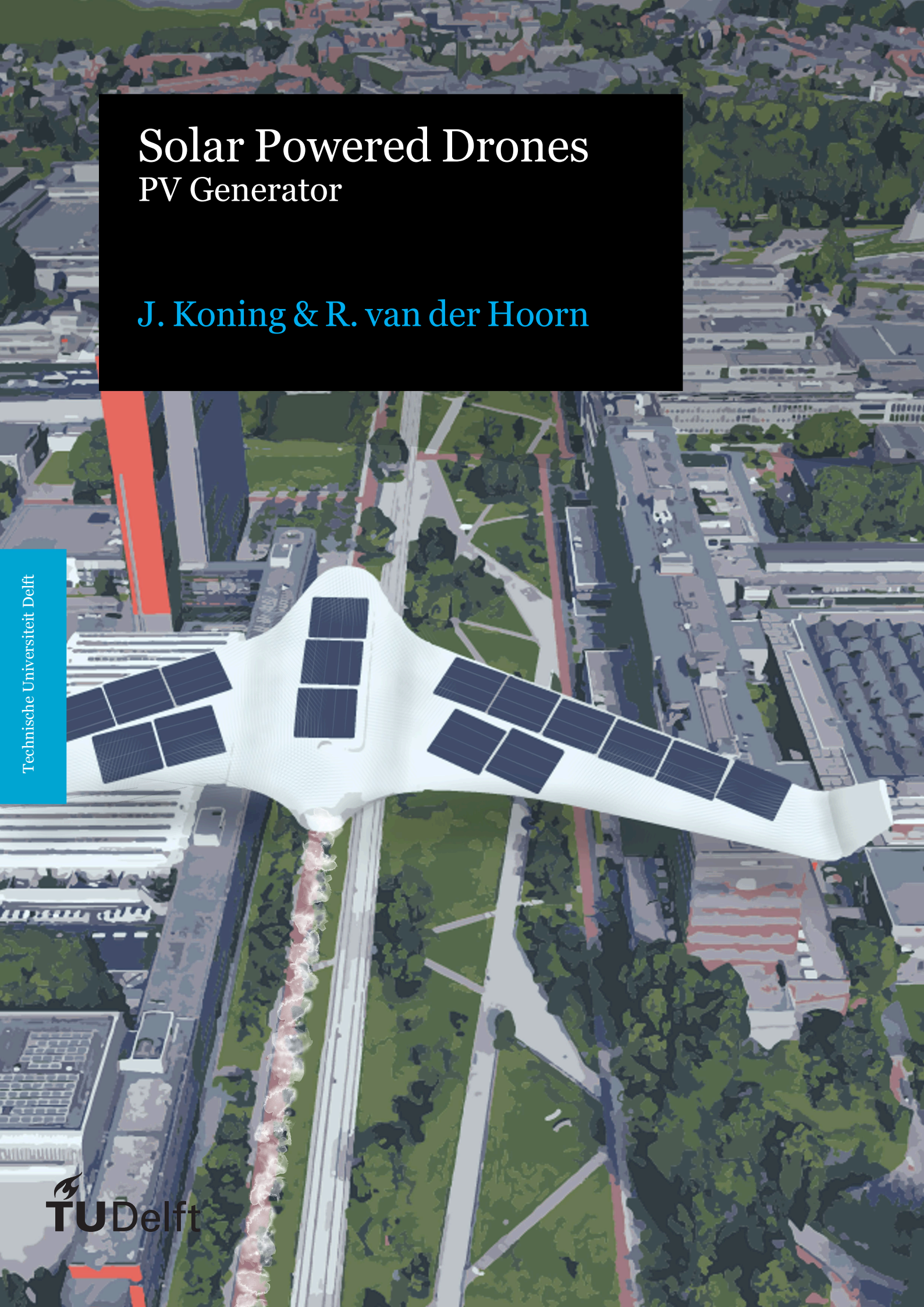

Solar Powered Drones
PV Generator

J. Koning & R. van der Hoorn

Technische Universiteit Delft

TU Delft

Solar Powered Drones

PV Generator

by

J. Koning & R. van der Hoorn

to obtain the degree of Bachelor of Science
at the Delft University of Technology,
to be defended on Tuesday June 30, 2020 at 15:00 PM.

Student numbers:	4329759 (Koning), 4571150 (Hoorn)	
Project duration:	April 20, 2020 – July 3, 2020	
Thesis committee:	Prof. dr. P.J. French,	TU Delft, Jury Chair
	Dr. P. Manganiello,	TU Delft, Supervisor
	Dr. Ir. G.R. Chandra Mouli,	TU Delft, External Assessor
	Dr. M. Muttillo,	TU Delft

TU Delft

Abstract & Preface

Drones are unmanned flying vehicles, which can be used for a broad spectrum of different applications. One of these applications is the generation of albedo maps. However, it could take some time to map an area. Therefore problems can occur the with respect to its flight range, which typically lies between 20 to 45 km for mini UAVs. The goal of this project is to design a PV powered drone that can create an albedo map of an area that is equal or bigger than the area of the Technical University of Delft. This is done by choosing and modelling an UAV system, where after choosing and modelling a PV generator system. Based on these models, power dynamics and flight ranges are calculated. The usability is tested for different weather conditions of Delft. The UAV system with PV generator without protection layers has a flying range between 129 and 250 km, depending in the irradiance. For the same system with protective layers, the flight range varies from 117 to 208 km. the total flight range that is needed to map the area of the TU Delft is 48.75 km. Therefore, there can be concluded that in both cases our goal has been achieved. When these results are compared to the weather conditions of the TU Delft, it can be concluded that on average a UAV system with PV generator will increase the flight range. However, when comparing this system to a system with additional batteries, the latter will achieve better results. In order to make sure that the PV generator system will guarantee a longer flight range, limitations regarding times, periods and places are made. Keep in mind that since these results are solely based on models of systems, it's best to create and test the physical system to validate the found results.

This thesis is written in context of the Bachelor Graduation Project. We would like to express our gratitude to our daily supervisor Patrizio Manganiello and our supervisors Andres Calcabrini and Mirco Muttillo for their guidance during the project. Finally we would like to thank our colleagues: Laura Muntenaar and Sjoerd de Groot of the control algorithm project and Jetse Spijkstra and Martin Geertjes of the power electronics project for an enjoyable and productive collaboration.

J. Koning & R. van der Hoorn
Delft, June 2020

Contents

1 Introduction 1
- 1.1 Problem definition . . . 1
- 1.2 Goal of the project . . . 1
- 1.3 Thesis synopsis . . . 1

2 Requirements 2
- 2.1 Requirements of total system . . . 2
  - 2.1.1 Assumptions . . . 2
  - 2.1.2 Mandatory functional requirements . . . 2
  - 2.1.3 Mandatory non-functional requirements . . . 2
  - 2.1.4 Trade off requirements . . . 3
- 2.2 PV generator Requirements . . . 3
  - 2.2.1 Mandatory functional requirements . . . 3
  - 2.2.2 Mandatory non-functional requirements . . . 3
  - 2.2.3 Trade off requirements . . . 3

3 State of the art 4
- 3.1 PV cell technology . . . 4
  - 3.1.1 PV cell specifications . . . 4
  - 3.1.2 PV cell types . . . 5
- 3.2 PV cell model . . . 6
  - 3.2.1 Ideal model . . . 6
  - 3.2.2 Single-diode model . . . 7
  - 3.2.3 Two-diode model . . . 7
  - 3.2.4 Characteristic curves . . . 7
  - 3.2.5 Parameter value estimation . . . 8
- 3.3 PV configurations . . . 8
  - 3.3.1 Configuration types . . . 8
  - 3.3.2 Configuration specifications . . . 9
- 3.4 PV generator protection . . . 10
- 3.5 Weather impact . . . 11

4 Design choices 12
- 4.1 PV cell type . . . 12
- 4.2 PV cell protection . . . 13
- 4.3 Cell placement . . . 13
- 4.4 PV configuration . . . 14
- 4.5 PV cell wiring . . . 15
- 4.6 Partial shading . . . 16

5 Modeling choices 17
- 5.1 Weather case creation . . . 17
- 5.2 Parameter value estimation . . . 18
- 5.3 Sandia thermal model . . . 18
- 5.4 Single diode model . . . 18

6 Implementation 19
- 6.1 Total PV configuration . . . 19
- 6.2 Weather model . . . 20
- 6.3 Parameter value estimation . . . 20
- 6.4 Sandia thermal model . . . 20

6.5 Single diode model 20

7 Results **22**
7.1 Weather analysis and cases 22
7.2 PV cell values and characteristics 23
7.3 PV system characteristics and power output 24
7.4 UAV flight range and comparison 26

8 Discussion and conclusion **28**
8.1 Discussion and conclusion 28
8.2 Recommendations 29
8.3 Future work 30

A Appendix **31**
A.1 Symbols 31
A.2 Derivation of parameter value estimation 32

B Figures **34**
B.1 Cell placement 35
B.2 Characteristic curves 37

C MATLAB code **38**
C.1 Weather 38
C.2 Parameter value estimation 43
C.3 PV cell analysis 44
C.4 PV power output 47
C.5 UAV flight range 48

D Drone Documentation **52**

E Datasheets **87**
E.1 SunPower Maxeon datasheet 87

Bibliography **90**

1

Introduction

Drones are flying vehicles.They are by definition unmanned and are therefore also called unmanned aerial vehicles (UAVs). The broad spectrum of possible applications of UAVs led to the invention of various types with different sizes and weights. One of these applications is the generation of albedo maps. Generation of albedo maps could take some time as a large area needs to be captured, therefore problems can occur the with respect to the flight range of UAVs. In this chapter the problem definition and goal of the project are explained, where after a synopsis of the thesis is stated.

1.1. Problem definition

As was already said, problems regarding flight range can occur when an area is being (albedo) mapped. Typical UAVs that do not require licensing, which are categorised as micro and mini UAVs, handle on average a flight range between 25 to 40 kilometers [11]. Taking in mind that an UAV should create multiple flight lines with a certain amount of overlap to be able to generate useful images for (albedo) mapping, there can be concluded that with this flight range only a small area can be covered. Therefore, to be able to cover more area without intermediate battery changes, it is very much needed to improve this flight range.

1.2. Goal of the project

The overall goal of this project is to design a PV powered drone that can create an albedo map of an area that is equal or bigger than the area of the Technical University of Delft. To test this, first an UAV needs to be selected and modelled, where after a PV generator configuration is chosen, its model is added and results between the two systems are compared. The first part, where the UAV and its components are selected and modelled can be seen as preparatory work, and is therefore added as an appendix in this report. In appendix D is stated which frame is used and which components are chosen. Based on these components an aerodynamic and electrical model are made, which are used to simulate power dynamics and flight ranges of the drone. The second part of this project, which is the selection, design, modeling and implementation of a PV generator system is elaborated in this report.

1.3. Thesis synopsis

This thesis is build up as followed. Chapter 2 starts out with explaining the boundaries of the project and the requirements of the subsystems. Chapter 3 is called the State of the Art, and describes the necessary background information that is needed in order to make correct design choices. Chapter 4 describes the design of the PV generator based on the requirements and the state of the art. Chapter 5 then elaborates on the design of the models that are used to simulate the PV system. Next the sub systems need to be implemented, which is described in chapter 6. In chapter 7 the results are stated and explained. And finally, a conclusion, discussion, further recommendations and some future work are given in chapter 8.

2

Requirements

2.1. Requirements of total system

The goal of this project is to implement solar panels on a UAV to increase its range, where the minimum flight range should cover the area of the TU Delft. This is in order to enable an on board camera to capture an an albedo map of the area.

2.1.1. Assumptions

We assume the following conditions are met to operate our UAV.

- There is a large enough grass field nearby the location of operation to take off and land a fixed wing UAV.
- The operator flying the UAV is at least certified for ROC and the necessary permits for flying in the area are obtained.

2.1.2. Mandatory functional requirements

These are the requirements of the functions the system needs to adhere to.

1. The UAV should be able to capture an area the size of the TU Delft campus in a single flight in a maximum time of 60 minutes.
2. The UAV should be able to fly 5 times during one day, 2 times before noon, 1 time at noon and 2 times after noon, between flights the battery should be replaced or recharged.
3. The UAVs minimum flight altitude is 100m to improve area coverage for mapping and maximum flight altitude is 120m due to Dutch regulations.
4. The UAV should be able to fly with and without solar panels.
5. The components of the UAV should be able to be attached into the UAV.
6. The weight and size of the components should not prevent the UAVs ability to fly.
7. The camera should be able to create images suited for albedo mapping with a GSD (Ground Spatial Distance) of at least 20 cm at a flight height of 120 meters.
8. The UAV should be controllable using an autopilot for efficient albedo mapping.
9. The UAV should be able to take off and land in a controllable manner.

2.1.3. Mandatory non-functional requirements

These are the requirements which specify how the system should work.

1. The UAV should be less than 4kg to fall within the legal classification of a small UAV.
2. The UAV should be able to operate at temperatures ranging from -10 to + 40$^{\circ}C$.
3. Components should be commercial available.
4. The safety aspects of the UAV should be able to meet the dutch safety regulations for privately owned drones and UAVs
5. Maintainability:The average lifespan of the UAV should be at least 2 years when used for the

predestined purpose.

2.1.4. Trade off requirements

1. The weight of the UAV should be as low as possible to increase flight time.
2. The flight path should be optimized to increase area efficiency.
3. The effective wing area should be as high as possible to increase power generated by the PV generator.
4. The drone should be fast enough to cover the required surface but it shouldn't affect image quality.

2.2. PV generator Requirements

The goal of this project is to implement PV system on a UAV to increase its range, whereas the minimum flight range should cover the area of the TU Delft. This is in order to enable an albedo map to be captured of the area.

2.2.1. Mandatory functional requirements

These are the requirements of the functions the system needs to adhere to.

1. The minimal energy generation of the PV generator should be higher than the energy the added PV generator costs.
2. The addition of PV generator to the drone should not affect the controllability of the UAV due to aerodynamics changes.
3. The weight of the PV generator should not affect the drone's ability to fly.
4. The PV generator need to be able to be mounted onto the drone.

2.2.2. Mandatory non-functional requirements

These are the requirements which specify how the system should work.

1. The PV generator should be protected to optimize lifespan.
2. The price of the PV cells should be in line with market conformity.
3. The addition of PV generator should not reduce the usage safety.
4. The PV system should not be able to be damaged due to wet weather conditions.

2.2.3. Trade off requirements

1. The aerodynamics of the drone should be affected as little as possible.
2. The power to weight ratio of the PV generator should be as high as possible.
3. The power to area ratio of the PV cells should be as high as possible.
4. The area of the drone surface should be covered with PV cells as efficiently as possible.
5. Partial shading of the PV array should affect the power generation as little as possible by using the best configuration.
6. The angle of the irradiance should affect the efficiency of a PV cell as little as possible.

3

State of the art

3.1. PV cell technology

In this section, information is stated regarding PV cell technology. This includes cell specifications and cell types.

3.1.1. PV cell specifications

When it comes to analysing PV cells there are multiple specifications to take into account. Relevant specifications for designing a PV generator for UAV flights are stated and explained in this section. Important to keep in mind is that the specifications of solar cells can be tested via different standards. The most common standard is the STC, which are test conditions which specify a solar cell temperature of 25 $^{\circ}C$ and irradience of 1,000 W/m^2 [15].

Maximum power point (MPP)

The maximum power point (MPP) is the point on the current-voltage curve (I-V curve) for which the PV generator reaches the highest power output, as is shown in picture 3.1. Since power is a product of current and voltage, the largest maximum power is found by obtaining the largest possible rectangle on the curve. The MPP is dependant not only on connection losses and tracking losses of the Maximum power point tracking (MPPT) unit, but it's mostly influenced by temperature and illumination profiles [16]. This is shown in figures 3.1a and 3.1b.

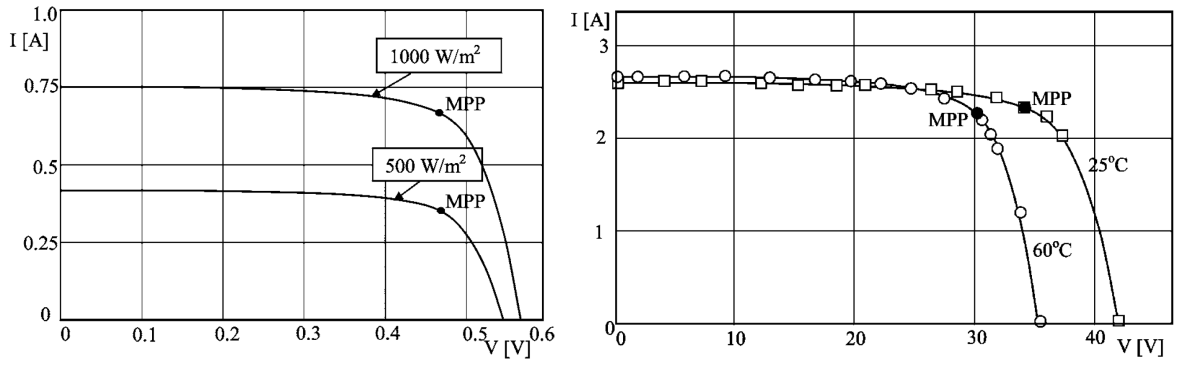

(a) Current-Voltage output curves of a typical single crystal silicon PV cell of 100 cm2 at different irradiances

(b) Current-Voltage characteristics of the ASE-100-DGL-SM module measured at 25°C, 60°C and irradiance level of 840 W/m2

Figure 3.1: Maximum power point influenced by (a) irradiance and (b) temperature [16]

Efficiency

The efficiency of a solar cell tells something about how much solar energy is actually turned into electrical energy. In other words, the efficiency is defined by the ratio of the maximum power point MPP

and the total power input from the sun P_{in}. It is dependant on the temperature of the solar cell and the irradiance of the sunlight.

$$\eta = \frac{MPP}{P_{in}} \tag{3.1}$$

Power temperature coefficient

A solar cell's power generation is dependant on the temperature of the solar cell. A higher temperature will result in a less efficient solar cell. The power temperature coefficient states at what the percentile decrease in power is per degree Celsius (mW/C) [4]. It's coefficient should ideally be as close to zero as possible, in that way the solar cell is least dependant on varying temperatures.

Power to area

The power to area ratio specification demonstrates how much power is generated per cm^2. When choosing solar cells for a solar powered UAV, this specification plays an important role since there will only be a limited amount of area available. A high power to area ratio will therefore be beneficial.

Power to weight

The power to weight ratio expresses the power that is generated per kilogram. This is an important specification when designing a solar powered UAV because a UAV has a limited payload. A payload is the amount of weight that can be carried without including the fixed components. The power to weight ratio varies a lot between different types of solar cells. Therefore it's urgent to keep this specification in mind when choosing the right solar cell type for a solar powered UAV.

Adjustability

Another non-functional specification to have a closer look at is the solar cells' adjustability. This aspects covers questions such as; to what angular degree is it possible to bend the solar cells without affecting it's photovoltaic properties or significantly impact it's lifespan? And is it possible to slice the PV cells into smaller parts while maintaining its usability? The adjustability could have a great advantage when designing a solar powered UAV, since surfaces are likely to have curves and the ability to slice cells could assure a large effective area.

Robustness

Robustness of a cell is important to assure a certain lifespan. Factors such as being shockproof, waterproof and heatproof could be useful when developing an UAV that is used for outdoor purposes. When landing, drones could experience a relatively high shock.

3.1.2. PV cell types

Over the past decade solar cells have been evolving rapidly, where now efficiencies higher than 20% are fairly common. Whereas silicon cells have been the norm for a long time, now different types of solar cells are emerging too. The different categories and types are further explained in this chapter. Here, the analyzed types are restricted to single junction solar cells, as multi junction solar cells are at this point under development, which means that they are not currently commercially available or feasible. A single-junction solar cell consists of only one p-n junction and is therefore limited to be sensitive to only a certain range of wavelength (corresponding to the characteristics of the used elements). Different types can be seen in figure 3.2, where they can be categorized by wafer based- and thin film technologies. A wafer based solar cell is a cell that consists of a thin slice of semiconductor material [19]. Wafer based solar cell technologies have been the norm for a long time, in particular crystalline silicon wafers. Thin film solar cells on the other hand, are made by placing one or more thin layers of photovoltaic material on a substrate. Thin film solar cells tend to be more flexible, lower in weight and have less drag because their thickness is significantly lower than that of silicon wafer [2].

Monocrystalline and polycrystalline silicon solar cells

Monocrystalline and polycrystalline solar cells are a type of wafer based technologies. Monocrystalline solar cells has a different structure design, therefore it outperforms polycrystalline cells when it comes to efficiency. Monocrystalline wafers are made out of a single crystal while polycrystalline wafers use

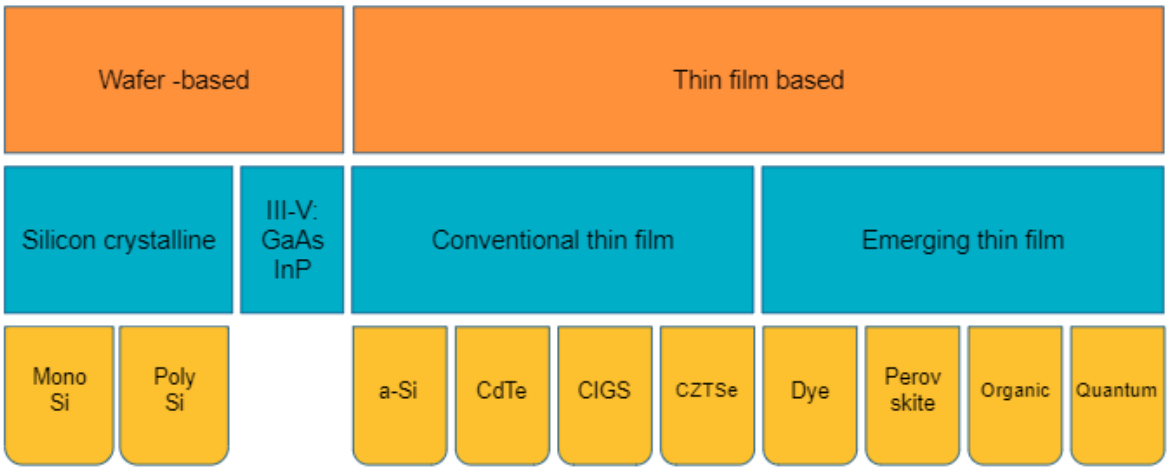

Figure 3.2: Overview of PV cell types

an amalgam of silicon fragments when produced [17]. However, this difference does result in higher pricing as well.

CdTe solar cells

Cadmium telluride is a thin film solar cell. The technology accounted for more than half of the thin film market in 2013 [2]. This could be due to the fact that it's the only thin film technology that is less expensive than the current silicon cell market leader. While CdTe technologies were being outperformed by silicon solar cells when it comes to efficiency, they significantly improved over the years, and lab cell efficiency for CdTe is now beyond 21% [2].

CIGS solar cells

A copper indium gallium selenide solar cell or CIGS cell is a technology that is produced by creating a thin layer on glass or plastic backing. Compared to other semiconductors a much thinner film is needed because of its high absorption coefficient [2]. Improvements in efficiency has made CIGS a relevant competitor in the solar cell industry as its lab efficiency is now beyond 23%.

3.2. PV cell model

The performance of a PV cell under different operating conditions can be obtained using an experimental setup or by simulating a model. In case of a experimental setup, the characteristic curves, the I-V and P-V curves of a PV cell, can be created by using empirical data and a curve fitting tool. However to create the characteristic curves for the entire range of irradiances and operating temperatures, a lot of measurements under controlled conditions have to be done. Therefore a better method to create the characteristic curves is by modeling a PV cell and simulating the different operating conditions. Modeling a PV cell should be done with great care since the results should deviate as little as possible from the actual performance. In this section various equivalent circuits of a PV cell are discussed.

3.2.1. Ideal model

An ideal PV cell can can be described with only two components, a current source and a diode, as seen in figure 3.3. The current source models the photocurrent I_{PV} generated due the photovoltaic effect caused by illumination. The diode current represents effects caused by the P-N junction in the PV cell. The output current as a function of the voltage is given by equation 3.2. The current through the diode is described with Shockley's diode current equation with saturation current I_s. All the symbols with the corresponding units used are listed in appendix A.1.

$$I = I_{pv} - I_s \left[exp\left(\frac{V}{aV_T}\right) - 1 \right], \quad with \;\; V_T = \frac{kT_c}{q} \tag{3.2}$$

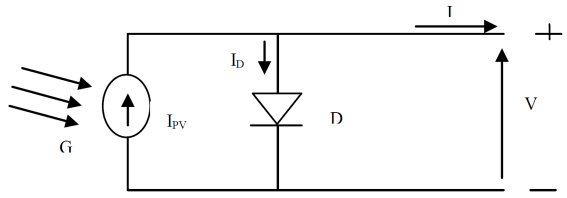

Figure 3.3: Ideal model of a PV cell [3]

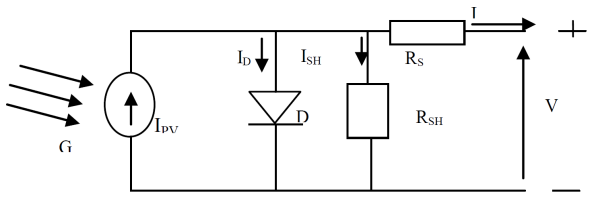

Figure 3.4: Single-diode model of a PV cell [3]

3.2.2. Single-diode model

A more realistic model is the single-diode model where a series resistance R_s and the shunt resistance R_{sh} are added, which can be seen in figure 3.4. The shunt resistance is in parallel to the output and should therefore be as large as possible to maximize the power output. The shunt resistance represents the leakage due to non-idealities in the P-N junction. The series resistance is in series with the output and represents the bulk resistance of the semiconductor and the metal electrodes, and the contact resistance between the semiconductor and the metal electrodes. The series resistance should be as low as possible to maximize the output power. The output current is reduced due to the current through the shunt resistance which is expressed by equation 3.3.

$$I = I_{pv} - I_s \left[exp\left(\frac{V + IR_s}{aV_T} \right) - 1 \right] - \frac{V + IR_s}{R_{sh}} \tag{3.3}$$

3.2.3. Two-diode model

The single-diode model can be expanded into the two-diode model, where a second diode added in parallel to the first diode, as shown in figure 3.5. This diode is included to provide a more accurate I-V characteristic curve where the two diodes model the currents due to diffusion and recombination effects [3]. The two diodes have different ideality factors a_1 and a_2 and saturation currents I_{s1} and I_{s2}. The output current of the two-diode model can be calculated according to equation 3.4.

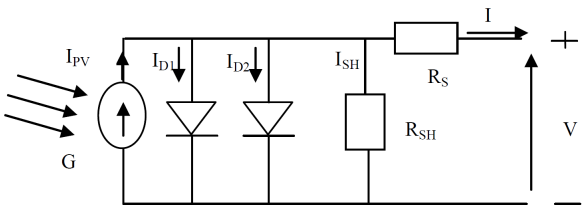

Figure 3.5: Two-diode model of a PV cell [3]

$$I = I_{pv} - I_{s1} \left[exp\left(\frac{V + IR_s}{a_1 V_T} \right) - 1 \right] - I_{s2} \left[exp\left(\frac{V + IR_s}{a_2 V_T} \right) - 1 \right] - \frac{V + IR_s}{R_{sh}} \tag{3.4}$$

3.2.4. Characteristic curves

For creating the characteristic I-V and P-V curves of the PV cell, the irradiance G and cell temperature T_c should be known to calculate the corresponding current I for every voltage V. The parameters I_{pv}, I_s and R_{sh} are dependent on the irradiance and temperature [6] and can be calculated according to equations 3.5, 3.6 and 3.7. The values for $I_{pv,ref}$, $I_{s,ref}$ and $R_{sh,ref}$ should be estimated using data from the modeled PV cell. From equations 3.3 and 3.5 until 3.7 becomes clear that the I-V and P-V relationships of a PV cell are implicit and nonlinear and depend on both irradiance and operating temperature. The output power and the short circuit current are strongly related to the amount of irradiance, since the photocurrent is linearly related to the irradiance, equation 3.5. The temperature has also a significant effect on the maximum output power and the open circuit voltage as can be seen in figure 3.6.

$$I_{pv} = [I_{pv,ref} + K_i(T_c - T_{ref})] \cdot \frac{G}{G_{ref}} \tag{3.5}$$

$$I_s = I_{s,ref} \cdot \left(\frac{T_c}{T_{ref}}\right)^3 \cdot exp\left(\frac{E_{g,ref}}{ak_{ev}T_{ref}} - \frac{E_g}{ak_{ev}T_c}\right), \quad with \;\; E_g = 1.17 - 4.73 \cdot 10^{-4} \cdot \frac{T_c^2}{T_c + 636} \tag{3.6}$$

$$R_{sh} = R_{sh,ref} \cdot \frac{G_{ref}}{G} \tag{3.7}$$

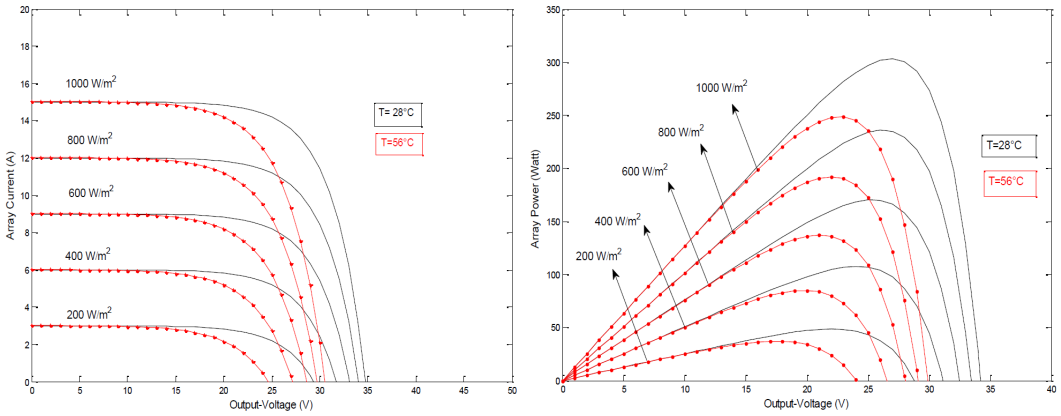

(a) I-V characteristics (b) P-V characteristics

Figure 3.6: Characteristics curves at various irradiances and temperatures [3]

3.2.5. Parameter value estimation

To create the characteristic curves of a PV cell for a specific operating condition, the irradiance G and cell temperature T_c have to be provided. However besides these input parameters, the other parameter values have to be known when using one of the three PV models mentioned in section 3.2. For the ideal model the photocurrent $I_{pv,ref}$, the saturation current $I_{s,ref}$ and the ideality factor a have to be known. For the single-diode model the series resistance R_s and the shunt resistance $R_{sh,ref}$ are required as well. For the two-diode model additional information is needed since for both diodes the saturation current $I_{s,ref}$ and the ideality factor a are needed. The parameter values depend on the PV cell and are almost never listed on the datasheet of the manufacture. Hence, the values of these parameters have to be estimated using known data of the PV cell. The parameter value estimation can be done using the datasheet from the manufacture or based on experimental data with many different approaches [8]. In general, the more data is available the better the values of the parameters can be approximated. In section 5.2 an approach will be chosen and elaborated.

3.3. PV configurations

In this section, relevant configuration types are stated and relevant specifications are explained.

3.3.1. Configuration types

There are many different configurations when it comes to PV arrays. The basic elements consist of series and parallel formations. Based on these formations, there are different configuration types, each causing a different output regarding voltages and currents. Even though more complex configurations are sometimes less affected by partial shading, they are not feasible to implement on the Skywalker X8 because of their complex connectivity and are therefore not further researched. Three feasible configurations are further explained in the following sections.

Series

In a series configuration, PV cells are placed in line one after another, as can be seen in image a) in figure 3.7. PV cells that are put in series maintain the same current as is provided by one solar cell.

Their voltage output however can be multiplied by the number of cells put in series. This configuration is particularly sensitive to partial shading, since shade on one solar cell can obstruct current flow throughout the whole configuration. To fix this, bypass diodes can be used. However, multiple peaks may arise in the I-V curve due to the use of bypass diodes.

Parallel

In parallel formation, PV cells are placed next to each other, as can be seen in image b) in figure 3.7. In this configuration, the voltage remains the same value as the voltage of one solar cell, while the currents of all solar cells can be added. A parallel configuration is less affected by partial shading, as shade on one cell will only disconnect this cell. However, sometimes high currents are generated in this configuration, which can be problematic for power converters.

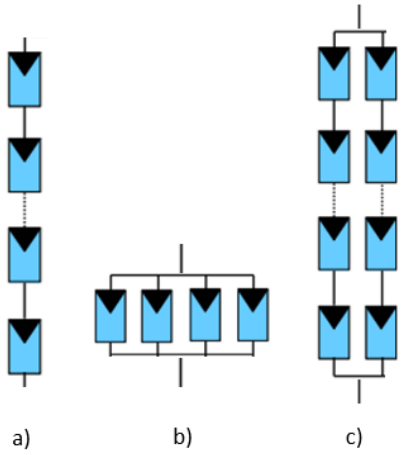

Figure 3.7: Configurations: a) series, b) parallel, c) series-parallel

Series-parallel

In SP configuration, as shown in image (c) figure 3.7 , modules are connected in series forming strings, where after these strings are connected in parallel. This configuration type is the most commonly used configuration in PV systems as it is easily constructed and fairly cheaply produced due to no redundant connections. However, when involved in partial shading, an SP configuration can generate multiple Maximum Power Point (MPP) peaks, which impacts the overall power performance.

3.3.2. Configuration specifications

In this section, relevant configuration specifications are stated and elaborated on.

Maximum power point

The maximum power output, which is more thoroughly explained in paragraph 3.1.1, is the point on the current-voltage curve (I-V curve) for which the PV generator defines the highest power output. Mismatch losses could result in differences in maximum power values of different configurations. Also, partial shading conditions could lead to multiple-power peaks in the power-voltage curves, which could be a problem for most Maximum Power Point Tracking (MPPT) algorithms.

System losses

Due to the fact that PV systems generally have a low energy yield, it is important that the efficiency of power transfer within the PV generator is as high as possible. Power loss can vary between 10% to 70% depending on different reasons which affect the PV system performance [13]. Therefore, it is essential to keep energy losses as low as possible by eliminating factors that cause these losses. Different types of losses are explained:

Cable losses Cable losses also affect the system performance and are dependant on the cross sectional area of the cable and its length. Since a PV configuration on a UAV can be considered as a small PV system, cable losses can therefore be considered negligible.

Thermal losses PV panels can't convert the entire solar energy into electrical energy, the conversion rate of PV panels mostly lie within a range of 5-25%. Therefore, other energy that is not converted to electrical energy is mainly converted to heat. This heat will affect PV cells, correspondingly to their power temperature coefficient, causing thermal losses.

Mismatch losses Mismatch losses are almost always present in photovoltaic arrays, simply because electrical characteristics in photovoltaic devices are not identical for each element of the array. The difference between the output power of the array and the sum of the output powers of its elements represent the amount of mismatch losses [14].

Complexity of installation

The complexity of the installation can be seen as how hard it is to implement the configuration onto the predestinated surface. In this particular case, the surface of a UAV is meant. Different types of configurations will involve a different complexity of installation. In order to investigate the feasibility, the configuration will have to be modelled onto the UAVs surface.

3.4. PV generator protection

PV cells need protection against many types of electrical and weather related issues. For example, there is electrical protection needed in case there is a load in balance or cell defect and weather protection is needed against rain, humidity, dust and UV irradiation. There are different types of protective layers that can help against these problems. The function of each particular layer, as can be seen in figure 3.8, is explained the following paragraph. Next to these protective layers, diodes are also explained, as they too play a role in protection of PV generators.

Frames and glass

Frames and glass are used to give solar cells stability and to protect the cells front surface from damages caused by shocks and flexion.Frames are often made of metal materials. For glass the most common types are tempered glass, which is highly resistant against breakage, and low iron content glass which has a high light transmittance. Even though frames and glass can offer important advantages, it could also potentially add quite some weight.This can have a negative impact on the power output for PV generators on UAVs.

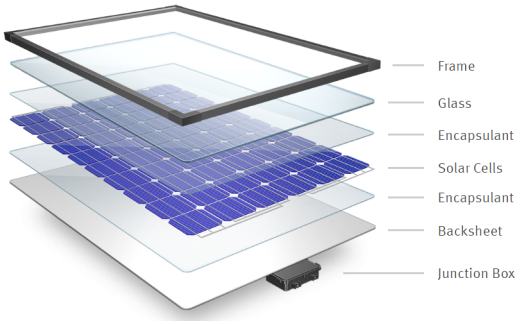

Figure 3.8: General protective layer setup [7]

Front- and back sheets

Front- and back sheets protect solar cells from ultraviolet radiation, weather conditions (such as humidity, dryness, dust, etc) and scratches. They also provide electrical insulation for enhanced performance and safety. In the case of using a front sheet, it is necessary to assure transparency for optimal light transmittance. Most solar panel manufacturers use TPT for a solar backsheet which is a Tedlar-PET-Tedlar film.

Encapsulants

Encapsulants are a polymer envelop that neatly surround PV cells. They are used to deliver protection for the most sensitive portions of solar panels against UV damage and weathering. Also, encapsulants protect the fragile solar cells from impact and enable the transmission of sunlight to the solar cells. A commonly used material is a copolymer of ethylene and vinylacetate (EVA). This is a polymer with a high resistivity and high transparency.

Diodes

For electrical protection diodes can be added, namely bypass diodes and blocking diodes. Bypass diodes are placed in parallel to the PV cell to create an alternative path for the current, as seen in figure 3.9. When a PV cell is defect or shaded, it will generate less current and without a bypass diode, the PV cell is force to transmit the current of the PV cells in series. This will create a negative voltage across the defect/shaded PV cell and thus consume power which can further damage the PV cell since it will heat up and also reduces the PV array performance.

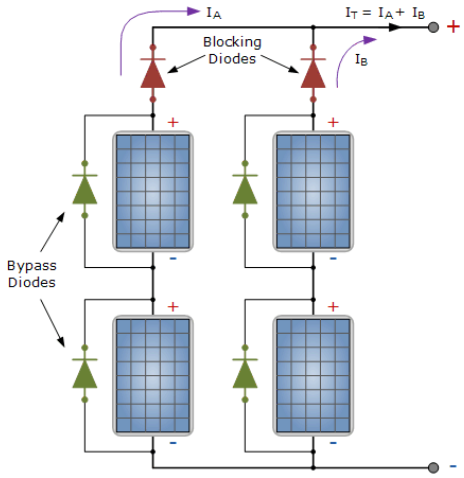

Figure 3.9: Blocking- and bypass diodes [1]

Blocking diodes are added in series to each string of PV cells, this can be seen in 3.9. Blocking diodes

prevent a reverse current through a string of PV cells coming from another string of PV cells connected in parallel. Without blocking diodes a reverse current can arise when there is a potential difference between strings of PV cells, this can be caused by for example partial shading of a PV array. When a PV array is connected to a battery blocking diodes can prevent discharge of the battery through the PV cells at low irradiances.

3.5. Weather impact

The output power of a PV cell strongly depends on the irradiance and the cell temperature as mentioned in section 3.2.4. The total irradiance on a PV cell is the sum of the direct normal irradiance G_{DNI}, the diffuse irradiance G_{DIFF} and the reflected irradiance G_{REFL} [6], as shown in equation 3.8.

$$G_{TOT} = G_{DNI} \cdot cos(\theta) + G_{DIFF} \cdot \left(\frac{1 + cos(\beta)}{2}\right) + G_{REFL} \cdot \left(\frac{1 - cos(\beta)}{2}\right) \tag{3.8}$$

The solar incidence angle Θ on the PV cell is calculated by:

$$cos(\theta) = cos(z) \cdot cos(\beta) + sin(z) \cdot sin(\beta) \cdot sin(\alpha - \gamma) \tag{3.9}$$

Where z the sun zenith angle, β the PV cell tilt, α the sun azimuth angle and γ the angle between the cell and the south direction as shown in figure 3.10.

The irradiance on the cell surface G is lower than the total irradiance, since a protective layer will be added to protect the PV cell. This protective layer will result in reflective losses at the interface and absorption within the layer. This will be discussed in section 4.2.

Besides the irradiance, the cell temperature has a significant effect on the power output of the PV cell. The higher the cell temperature gets, the less power it will generate. The cell temperature mainly depends on the ambient temperature, the irradiance and the wind speed. To estimate the temperature of the cell many different empirical equations have been proposed [6] [18].
The wind has a cooling effect on the cell and plays a significant role. Since the equations are determined empirically, they contain coefficients that have to be determined with measurement data. However this will not be possible for this research project, therefore the availability of data has to be taken into account when selecting a equation for the cell temperature. The choice of equation of the cell temperature will be done in section 5.3.

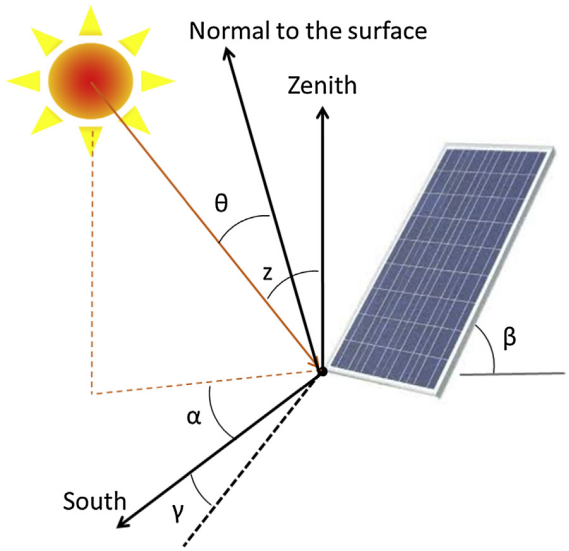

Figure 3.10: Solar characteristics angles [6]

Another possible major impact on PV generators is partial shading. Partial shading is the effect where part of the modules of the PV array receive solar irradiation, while other modules receive less radiation due to shades. Partial shading can play a huge role when it comes to losses and is mainly characterized by the shading factor and the number of shaded modules [9]. It is one of the main causes of overheating of shaded cells and reduced energy yield of the module [12]. Use of bypass diodes and modifying interconnections can significantly reduce the amount of power lost in a module due to partial shading. The impact of partial shading will be discussed in section 4.6.

4

Design choices

In this chapter, decisions are made regarding the design of the PV generator. First, the chosen components are stated, which are the cell types, the cell protection and the cell wiring. After this, the chosen PV configuration and cell placement is explained. As partial shading could play a role in configuration decisions, this subject will also be touched upon.

4.1. PV cell type

As is stated in section 3.1.2, there are many types of PV cells, each differing in the way they are manufactured and the materials they are made out of. To decide on which type of PV cell is best suited for our purpose, first a decision should be made about which specifications are important. The relevant specifications to access the PV cells on are chosen based on the Program of Requirements. As was stated as a non-functional requirement, the PV cells should be attachable to the UAV. This means that the PV cell should be bendable with a curvature that can be represented by a circle with a radius of 12 cm. When in comes to affordability, the chosen cell should be commercially available and have market conform prices. Another very important aspect is that it should generate as much power as possible. This means that it should weigh as least as possible while having a high efficiency factor and power to area ratio.

When analyzing these specifications for all different PV cells, some types are easily dismissed. For example, the 3rd generation emerging thin film category is at this point not yet commercially available and is not yet able to create high enough efficiencies. While III-V type PV cells can reach extremely high efficiencies, these cells do not meet our specifications when it comes to affordability, as these cells are extremely expensive and are mainly used for airspace applications. Lastly, polycrystalline silicon-, amorphous silicon- and CZTSe PV cells are not explored any further as their efficiency factors are significantly lower than some of the other options.

This leaves us to analyze the monocrystalline silicon-, CIGS- and CdTe solar cells more thoroughly. This analysis can be found in table 4.1, where their specifications are stated. The monocrystalline silicon solar cell type is chosen, based on the fact that CIGS and CdTe technologies are sold as modules. These available modules are too large to efficiently attach to the UAV. Since adjusting these modules into smaller pieces is not possible, these PV cell technologies are not considerable for our configuration.

Table 4.1: Specifications of analyzed solar cells

	Monocrystalline Si Maxeon Gen III - Sunpower	CIGS FLEX-03N-130W Misole	CdTe 144W Flexible thin film solar module Xi'an Runda Recourse Technology Co.
Efficiency [%]	24.3	17	15.5
Power to Area $[mW/cm^2]$	24.84	14.45	7.07
Power to Weight $[Wp/kg]$	155.8 (protection incl)	65.0	27.2
Power temperature coefficient $[\%/^\circ C]$	-0.29	-0.40	-0.279
Attachable	Yes	No	No
Bendable	Yes	Yes	Yes

Within the monocrystalline silicon PV cell technology, the Maxeon Gen III Le3 – SunPower cell is chosen. This cell is chosen for its high efficiency, which will outweigh the negative effects of the relatively low power to weight ratio (compared to CIGS and CdTe cells). This PV cell also has a high power to area ratio and a low power temperature coefficient. Even though a concrete numerical value for the bendability for the Maxeon Gen III cell is not available, the image stated in Appendix B.2 shows that this cell can easily bend with a radius of 12 cm. This makes the Maxeon Gen III cell suited for our purpose. More specifications for this PV cell are found in table 4.2 and an image of the cell can be found in figure B.1 in the appendix.

Table 4.2: Specifications of SunPower Maxeon Gen III - Le3 cell

Specification	**Unit**
PV cell model	SunPower Maxeon Gen III - Le3
Maximum power point	3.84 W
Vmpp	0.634 V
Impp	6.06 A
Voc	0.724 V
Isc	6.43 A
Efficiency	24.8 %
Power temp. coeff.	-0.29 $\%/°C$
Voltage temp. coeff.	-1.74 $mV/°C$
Current temp. coeff.	2.9 $mA/°C$
Cell size	125mm x 125mm
Cell area	155.09 cm^2
Cell weight	6.6 g
Cell price	8.8 $ (excl. tax)

4.2. PV cell protection

There are multiple different layers that can be used to protect a solar cell, as is explained in paragraph 3.4. For our design, a frontsheet, encapsulant and backsheet are used. No frame or glass top layers were used for our setup as their benefits do not outweigh the negative impact they cause for adding extra weight.

For the encapsulant, the Z1261C encapsulant for flexible solar panels was chosen. This layer would be placed directly above and below the solar cells and will protect the most sensitive parts from impact by sealing it. Also it will stimulate the transmission of sunlight into the solar cells. Due to it's low weight, and bendability it is suitable for our application. As a front- and back-sheet the Transparent 1500V Jingmao was chosen. These sheets will be used as outer layers of the configuration. These will protect the solar cells from external factors such as ultraviolet radiation, ambient temperature and physical damage (such as rain, hail, shocks, etc). Next to this, it will also help with internal factors such as improving its performance and safety by providing electrical insulation. The low weight and bend ability make these sheets suitable for our application. Specifications of both protective layers can be found in table 4.3.For the protective layers an irradiance absorption of 3% is estimated. However, this is a rough estimation and should be further researched in furture work.

Table 4.3: Specifications of protective layers

Type	Front/backsheet	Encapsulant
Product	Transparent 1500V Jingmao	Z1261C encapsulant for flexible solar panel
Material	PVDF/PET/PVDF	EVA(28-33% VA content)
Thickness	300 μm	200-300 μm
Weight/area	340 g/m^2	237.5 g/m^2

4.3. Cell placement

After choosing a PV cell, the cells have to be mounted on the UAV. The dimensions of a PV cells are 125mm x 125mm and have a thickness of 150 $\mu m \pm 20\mu m$. The curvature of the frame is important to consider since the cells can only be bend along a single axis. A cell can be cut in half to fit the cells more effectively on the UAV. Since the cells will be connected at least partially in series, all the cells should make the same angle with the sun. Therefore the cells can only be placed on the wings and on the middle section of the body and not on the sides of the body because this has a different slope as can be seen in figure B.4. In this section only the top view of the half cell placement and full cell placement are shown, figure 4.1 and 4.2 respectively. In appendix B.1 more detailed figures are shown of the cell placement and curvature of the entire UAV, figure B.3.

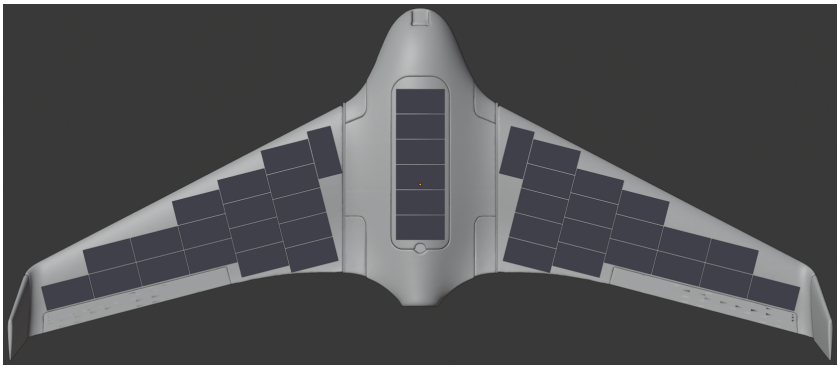

Figure 4.1: Top view placement of half cells

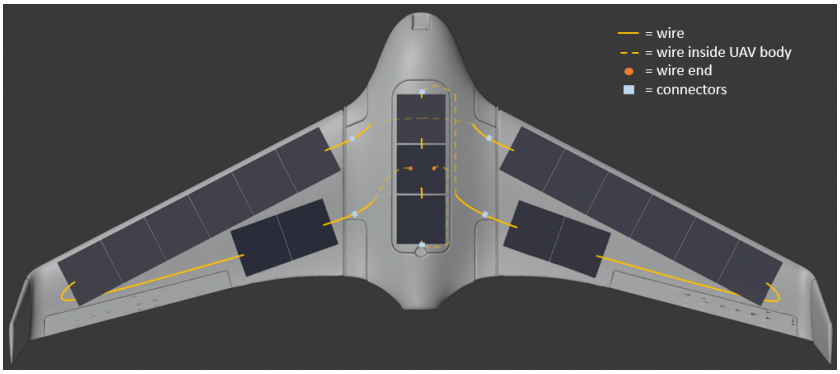

Figure 4.2: Configuration with wires

The cells are quiet flexible and should be able to handle the maximum curvature with a radius of 12cm. With the placement careful attention has been paid that the cell only have to bend along a single axis. For the placement of full cells, 8 cells are placed on both wings and 3 cells on the body, which results in a total of 19 cells. For the half cell placement, 18 cells can be placed on the wings and 6 cells on the body, resulting in 42 half cells in total, equal to 21 full cells. All the cells are place with almost the same slope, which will help with the performance and configuration.

4.4. PV configuration

In last section was concluded that for a half cell setup 42 cells can be placed, equal to 21 full cells. For the full cell setup 19 cell can be placed, however the number of PV cell is not the only aspect that determines the range increase due to PV power generation. As stated in section 2.2, trade-off requirement 2 ”The power to weight ratio of the PV generator should be as high as possible”, so the weight of the configuration should be taken into account as well. From UAV simulations becomes clear that power consumption of the motor due to weight increase, increases with 39.8 W/kg, as shown in appendix D. Therefore the weight of the half and full cell setup has to be calculated. Beside the weight of the cells, the weight of the protection layers have to be considered since with more cells a larger area has to be cover with protection. The weight of the protection layers is $1155 g/m^2$, two times a front/back sheet and encapsulant weighing $340 g/m^2$ and $237.5 g/m^2$ respectively. The area covered with protection is calculated using the cell area with an extra $3mm$ all round extension as margin for proper protection. This results in an area of $131mm$ x $131mm$ for full cells and an area of $131mm$ x $68.5mm$ for half cells. Combining the total area covered with protection, with the weight of the protection per square meter and the cell weight, the combined weight can be calculated for both setups. The power generation by PV generator is calculated using the maximum power point power at STC of a cell multiplied by the number of cells, and divided in half to estimate a power generation that is realistic in the Netherlands. Finally the net power generation is calculated by combining the power generation with the power consumption increase to indicate the performance increase for both the full and half cell setup. In table

4.4, the calculated values are listed and it becomes clear that the net generated power differs only by $1W$.

Table 4.4: Full and half cell setup comparison

	Full cell	Half cell
Weight protection $[g/m^2]$	1155	1155
Area protection incl. margin $[m^2]$	0.32606	0.37689
Weight cells + protection $[g]$	502.0	573.9
Power increase motor due to weight $[W]$	20.00	22.84
Power generation PV ($500W/m^2$, $298K$) $[W]$	36.48	40.32
Net power generation PV $[W]$	16.48	17.48

After analysing the possible setups, the possible configurations of both setups have to be discussed. To reduce restive losses and allow for thinner lighter wiring the current to voltage ratio should be as low as possible. Hence cell should be placed in series for the lowest I/V ratio. Using the maximum power point specifications of a single cell listed in table 4.2, the maximum power point specification for different configurations can be estimated and are shown in table 4.4.

Table 4.5: Maximum power point for various configurations

Maximum power point at STC	Full cell series	Half cell series	Half cell series-parallel
Voltage $[V]$	12.05	26.63	13.31
Current $[A]$	6.06	3.03	6.06
Power $[W]$	72.96	80.64	80.64

For the half cell series-parallel configuration, two series strings of 21 cells will be place in parallel. However to protect the PV cells and prevent reverse currents, a blocking diode has to be added to both strings. Given that on average a diode has a voltage drop between 0.3V and 0.7V, this will result in a 2 to $4.5W$ power loss at STC, reducing the power output to between 76.14 - $78.64W$.

The power generated has to be converted to supply it to the motor or store it in the on board battery. Higher input currents will requires a heavier converter to stay efficient, so again a low I/V ratio is favourable. However the nominal battery voltage is $18V$ and a boost converter is used, so the output voltage of PV system should be below the battery voltage. This makes the half cell series configuration not fit for this converter setup. Analysing the other two possibilities, full cell series and half-cell series-parallel, the power generation of both setup is expected to be about equal due to the blocking diodes needed for a parallel configuration. The full cell series configuration is easier to implement, less complex and cheaper offering presumably the same performance. Hence the full cell series configuration has been chosen. The wiring of the configuration and the impact of partial shading will be discussed next in sections 4.5 and 4.6.

4.5. PV cell wiring

When choosing cell wiring, a wire type that is is able to transfer a high enough current for our configuration while creating the least amount of cable losses should be chosen, while keeping in mind that it should be also suitable for outdoor usage. Copper and aluminum materials are often used because these wire types are both efficient. Here copper has a greater conductivity, which results in its ability to carry a higher current than aluminum for same sized wires. Therefore a suitable copper wire would potentially add less weight to the configuration. When it comes to insulation, PV Wire, USE-2 and RHW-2 cables can be used in outdoor and wet conditions where their outer cabling is UV and moisture resistant. This is important as the wires could be exposed to such weather conditions when being used. The needed diameter-size of the wires is dependant on the amount of current that that will flow through it. The SunPower Maxeon Gen III - LE3 cell will not have a current higher than the short circuit current,

which is 6.43 Ampere. Therefore a 14 AWG size cable will be suitable. Based on these aspects, the 14 AWG XLP/USE-2/RHH/RHW-2 Building Wire is used.

This wire is implemented onto the chosen configuration as can be seen in figure 4.2. As you can see there are no wires used between solar cells, this is because they have built-in connectors. Furthermore, blue connectors are added to make sure the drone wings and lid are still demountable. Based on this setup, the total needed wire length is approximately 2.5 meters, this will give an additional weight of 88.13 gr (including connectors). The added resistance will be 0.021 Ohm. When a maximum current of 6.06 Ampere will flow through, this will cause a power loss of 0.76 W.

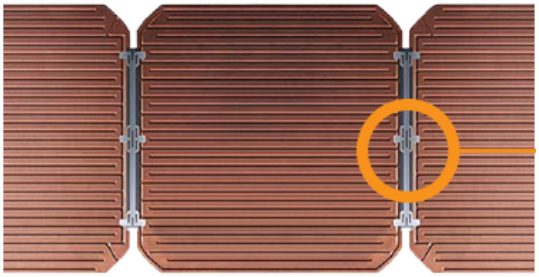

Figure 4.3: Maxeon Gen III built-in connector []

4.6. Partial shading

Partial shading can potentially have a large impact on the power generation of PV generators on UAV's. In order to quantify the impact that it can have on the Skywalker X8, the shade that's developed by the sun's angle onto the tip of the wings and the body is calculated. This can be seen in figures 4.4 and 4.5. In these figures, the length of the shade for the body and wing during a day are shown for the best- (June), worst- (December) and average case. For these calculations the sun is positioned to be sideways of the drone.

In the left picture can be seen that during December, when the light angle is on average quite low, the shade length is of such length that almost all cells are affected throughout the day. On average, at least one cell is affected by shades of the wing. In the right picture can be seen that for the average case and better, almost always no cells are impacted by the shade of the body. During December however, there is a steep graph where at least 2 cells are affected at all times.

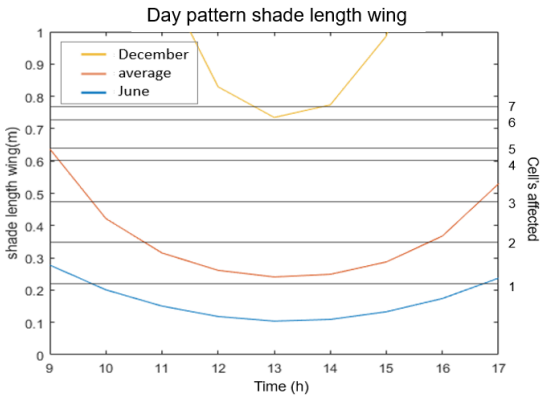

Figure 4.4: Shade length and affected cells of the wing

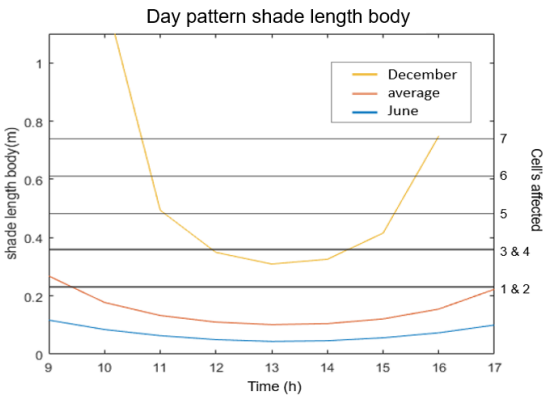

Figure 4.5: Shade length and affected cells of the body

Based on these results, there is concluded that partial shading impacts a significant amount of cells, mainly in early mornings, late afternoons and during winter when the solar angle is low. Usage of bypass diodes to maintain usability of the other solar cells does not seem to be a profitable solution. Therefore, in order maintain most usability of the solar cells, there is decided that partial shading effects should be avoided by adjusting flight paths accordingly. This means that the nose of the UAV should always be pointing towards or away from the sun's direction, to avoid shades falling on the drone. The Skywalker x8 with its chosen components make it possible to fly 3 times the area of the TU Delft, as can be seen in appendix D at the flight path section. Therefore there is enough margin to change flight paths to avoid partial shading while still being able to map the area of the TU Delft.

5
Modeling choices

To predict the performance of the PV generator, a model has to be created of the system. Modeling the PV generator can also be used to analyse the influence of different factors on the system. In this chapter modeling choices will be discussed, which then will be implemented in chapter 6.

5.1. Weather case creation

To analyse the PV generator, test cases have to be created that simulate the input of the PV generator for different weather circumstances. The test cases should cover a wide spectrum of weather situations to which the PV generator could be exposed. The test cases should cover the best, average and worst weather for the PV generator, so that the performance for the entire spectrum of weather situations can be predicted. Since the goals is to make an albedo map of the TU Delft campus, the test cases should be representative for the weather circumstances in Delft.

To create weather cases the weather data of a typical meteorological year at the TU Delft campus has been provided both in hourly and minutely resolution. This data contains a lot of different weather parameters. To make modeling of the PV generator feasible and limit the number of parameters that influence the performance of the system, a few assumptions have been made. The first assumption is that no partial shading will take place, since partial shading can be avoided when flying in the right direction relative to the solar azimuth. The second assumption is that all the PV cells are always oriented in horizontal to the surface of the ground. Finally, since the wind due to the flying speed (18 m/s at cruising speed) is much higher than the ground wind speed and the UAV will fly in both directions, the ground speed wind will be neglected when calculating the cell temperature.

With these assumptions, there are only two parameters relevant in the measured weather data. The global horizontal irradiance G_{Gh}, that is the total amount of radiation received from above on a horizontal surface. Since the cell is horizontal $\beta = 0°$ and G_{REFL} can be neglected because the PV cell is high above the ground. To calculate the global horizontal irradiance, equations 3.8 and 3.9 can be combined resulting in equation 5.1. Besides the irradiance, the ambient temperature is needed to calculate the cell temperature as discussed in section 5.3.

$$G_{Gh} = G_{DNI} \cdot cos(z) + G_{DIFF} \tag{5.1}$$

Knowing the relevant parameters, test cases can be created which reflect the best, average and worst weather conditions for the PV generator. The global horizontal irradiance is the most important parameter since it directly influences the amount of power generated. The selection of weather cases will therefore be determined by the global horizontal irradiance. In section 6.2 will be explained how the weather data is analysed and the weather cases are created.

5.2. Parameter value estimation

How to estimate the parameter values and which parameter values can be estimated, mainly depends on data that is available of the chosen cell. For the SunPower Maxeon Gen III, chosen in section 4.1, is only the data provide on the datasheet by the manufacture available. Extra measurements under controlled conditions were not possible, so this limits which parameter value can be estimated and the possible approaches.

In datasheet of manufactures are only a few specifications mentioned besides the temperature coefficients, namely the short circuit current, open circuit voltage and the maximum power point voltage and current. With this data three characteristic points of the I-V curve are known, namely $(0, I_{sc})$, (V_{mp}, I_{mp}) and $(V_{oc}, 0)$. One more known characteristic is that the derivative of the P-V curve at the maximum power point should equal zero, since this is the maximum of the P-V curve. This makes that four boundary conditions can be set when estimating the parameter values. The two-diode model however has seven parameters values that have to be estimated as explained in section 3.2.5, which cannot be done with four boundary conditions. The single-diode model on the other hand only requires the estimation of five parameter values and with setting one parameter to a certain value the other parameter values can be estimated [5]. The single diode model will be further elaborated in section 5.4 and the derivation of the expressions for the parameter values calculations can be seen in appendix A.2.

5.3. Sandia thermal model

In the case of implementing solar cells on a drone, the wind speed plays a particularly large role. The wind is defined as the effective speed of airflow over the module. Because of the high flying speed of the Skywalker X8, we defined the wind as the airflow caused by this flying speed, which is 18m/s. The Sandia thermal model is chosen to model cell temperature, as it takes wind speed WS into consideration while being a simple an easy implementable model. This model is stated in equation 5.2.

$$T_C = T_{amb} + G_{TOT} \cdot e^{a+b \cdot WS} \tag{5.2}$$

Coefficients a and b have to be determined with empirical data. a is a variable that refers to the case in which there's no wind present and b indicates the effect of the wind on the cell temperature. When a and b are determined with linear regression on a large set of empirical data, the accuracy was 95% [10]. Since it was not possible to gather empirical data, values for a and b had to be found for a similar situation. A overview of values for the coefficients a and b have been found in [10]. Here different values are stated for different types of modules and installations. The values for the insulated back installation are chosen for our setup, since this setup is most similar to our Styrofoam UAV. For the sake of simplicity, the wind speed is chosen to be constant at 18 m/s, as this is the average speed of the chosen UAV.

5.4. Single diode model

There are many types of models to simulate a PV cell. When choosing a model, it is preferred to go for a model that is simple while accurate. The ideal model, single diode model and two diode model were considered. These models are all electrical circuit equivalents of a PV cell and their functionalities are explained in 3.2. The ideal model is the simplest, as it consists of only a current source and a diode. However, due to its simplicity it leaves some non-idealities out of the equation making it is less accurate and not suitable for our use. The single diode model is similar to the ideal model, but it includes a shunt resistance and a series resistance. This makes this model more accurate than the ideal model. The two-diode model is similar to the single-diode model but also considers the difference in flow of circuit at low current values due to charge recombination in the semiconductor's depletion region. This makes the two-diode model theoretically the most accurate option while maintaining simplicity. However, the two-diode model is based on more variables than the single-diode model. Many of these variables cannot be found based on the PV data sheet and need to be empirically measured. As this is not an option, many of these values would therefore need to be estimated. This would lead to a less accurate model. Taking this information into account, the single diode model seems to be the best suited option. The needed variables for this model will be calculated via the variable parameter estimation model, which is explained in 5.2. This model will be generated via Simulink.

6

Implementation

In this chapter the implementation of the aspects mentioned in the previous chapters is discussed. Starting with the total PV configuration where an overview is provided of the implemented system. Next the different components of the implemented system are considered.

6.1. Total PV configuration

To model the total PV configuration as would be implemented on the Skywalker X8, multiple different sub-models are needed. The total setup of this configuration can be found in figure 6.1. The goal of this model is to simulate the chosen PV cell configuration, where for different weather inputs a current, voltage and power output will be generated. This output will then be used as an input for the overall simulation of the drone. To do this, weather cases are inputted in the weather model. From this case, a certain irradiance G_{tot} and ambient temperature T_{amb} will be outputted and used as an input for the single diode model and Sandia thermal model. The Sandia thermal model will calculate the cell's temperature T_{cell} , which will be used as an input for the single diode model. Furthermore, some data from the chosen PV cell will be used to calculate the variables I_{pv}, I_s, a, R_v, R_{sh} and k_i. These parameters will be inputted in the single diode model too, together with the T_{ref}, G_{ref} and Ir_{abs}. The single diode model will be transformed into a 19-cell series configuration and with above stated inputs a current and voltage will be outputted. To analyse the outputs, a I-V curve and a P-V curve will be generated. The implementation of these sub-models are explained in section 6.2 to 6.5 .

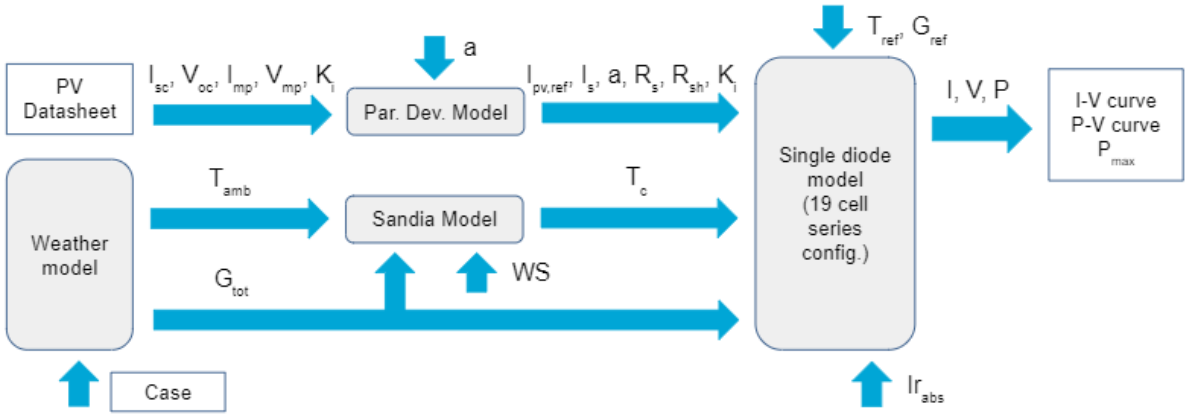

Figure 6.1: Diagram of modelling system [6]

6.2. Weather model

To create test cases that cover a wide spectrum of weather situations, the provided weather data of a typical meteorological year at the TU Delft Campus had to be analysed. For this the hourly weather data has been used to analyse the global horizontal irradiance throughout the year at different moments throughout the day. For every month the best, average and worst amount of irradiance has been calculated, from which became clear that June is the month with the highest amount of irradiance and December the month with the least. The results can be seen in section 7.1 and the implemented MATLAB code in section C.1. Therefore June and December have been used to create weather cases that reflect the best and worst circumstances for the PV generator. However, since the irradiance varies a lot throughout a month, for both June and December three weather cases have been created based on the minutely weather data. These three cases are the best, average and worst day of the month. The best day is the day with the highest total amount of irradiance between 9:00 and 17:59 and the worst day the lowest total amount of irradiance. For the average day the average amount of irradiance throughout the month has been taken for every minute. The irradiance of the average case is less volatile since the irradiance is averaged over around 30 days. Besides the best and worst month of the year, the yearly average is relevant to give insight in to the average irradiation throughout the year. This can be used to calculate the average performance of the PV generator throughout the year and together with the other cases the performance of the PV generator can be calculated for a wide spectrum of weather situations.

6.3. Parameter value estimation

The parameter values to be estimated for the single diode model are I_{pv}, I_s, a, R_s and R_{sh}, which can be calculated using the equations in section 3.2.5. These equations are derived from the four boundary conditions which are imposed by the datasheet values of the PV cell specifications. The datasheet values of the PV cell chosen can be seen in table 4.2. The MATLAB implementation can be seen in section C.2, this script starts with the datasheet values, than the parameter values are calculated. To finally verify if the parameter values result in characteristic PV curves that match the datasheet values. Before the parameter values can be calculated, a value for a has to be chosen, a typical value for a is between 1 and 1.5 for single junction solar cells. The parameter values can be calculated using A.10, A.11, A.4 and finally A.2. The parameter values depend on the value chosen for a, so by adjusting a appropriate values can be found for the other parameters. After calculating the parameter values, the I-V curve is plotted using the single diode model to verify if the model matches the values stated in the datasheet. The calculated values and verification will presented in section 7.2.

6.4. Sandia thermal model

The Sandia thermal model is implemented in Simulink as can be seen in figure 6.2. Here you can see its formula, as is stated in section 5.3 is directly implemented. The coefficients a and b are taken to be -2.81 and -0.0455 respectively. The temperature is added with 273 because for the overall model Kelvin is used as a unity for temperature. Furthermore, the inputs of the Sandia model are temperature T, windspeed WS and irradiance G, where for windspeed a constant value of 18 m/s is used.

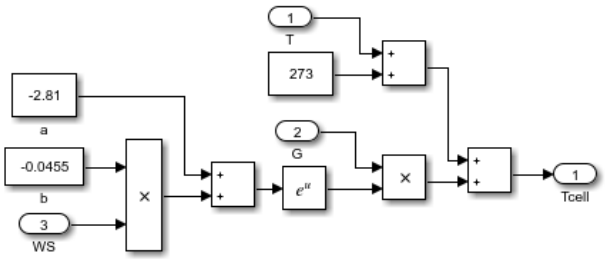

Figure 6.2: Sandia thermal model in Simulink

6.5. Single diode model

The single diode model is implemented in Simulink as can be seen in figure 6.3. Here the blocks of the reverse saturation current, saturation current, shunt current and photo current are created using the formula's stated in chapter 3.

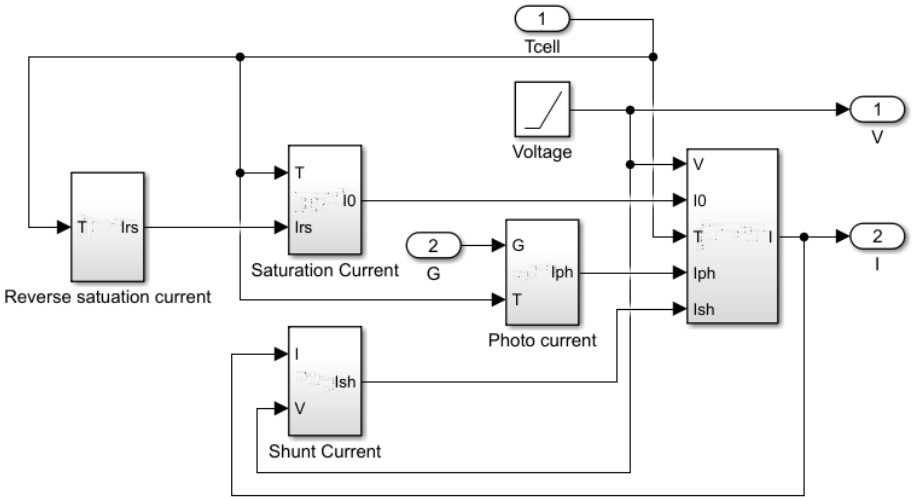

Figure 6.3: Single diode model in Simulink

Before being able to run this model, some initial values must be stated. These values are listed in table 6.1. The values for the current temperature coefficient, open-circuit voltage and short-circuit current are found in the PV datasheet. The electron charge and Boltzmann's constant are fixed constants. The nominal temperature is 25 degrees Celsius under STC conditions. The number of series connected PV cells is 19 as is mentioned in the PV configuration design chapter. The band gap energy is chosen as 1.1 eV as this corresponds with the band gab energy for a monocrystalline solar cell. The values for the ideality factor, series resistance and shunt resistance are estimated as was explained in section 6.3.

Table 6.1: Variables used for single diode model

Specification	Variable name	Value
Current temperature coefficient	Ki	0.0029 W/m2
Electron charge	q	1.6e-19 C
Boltzmann's constant	k	1.38e-23 J/K
Ideality factor of the diode	a	1
Band gab energy	Eg	1.1 eV
Series resistance	Rs	1.063954 $m\Omega$
Shunt resistance	Rsh	4.981578 Ω
Nominal temperature	Tn	298 K
Open-circuit voltage	Voc	13.756 V
Short-circuit current	Isc	6.43 A
Number of series connected PV cells	Ns	19

This model uses the cell temperature of the Sandia thermal model and the irradiance found by the weather model as an input and creates a current and voltage output. These outputs will be used to create I-V curves and P-V curves for different irradiances to validate if our models are correct. Furthermore these outputs will be used as inputs for the overall drone simulation.

7 Results

In this chapter the results will be presented of the implemented design. Starting with the created weather cases, presenting the cell and system characteristics and combining these results for the power output of the PV system for every weather case. With the generated power output and data from the general UAV simulation the flight range has been calculated. Finally multiple UAV configurations are compared and their flight range is analysed.

7.1. Weather analysis and cases

The created weather cases that resulted from the implementation described in section 6.2 are presented below.

The yearly irradiance at different times can be seen in figure 7.1 based on the hourly weather data. From this figure becomes clear that June and December are respectively the best and worst month regarding irradiance. Furthermore can be seen that the amount of irradiance is the highest around 13H and strongly dependent on the month, which is caused by the difference in sun elevation.

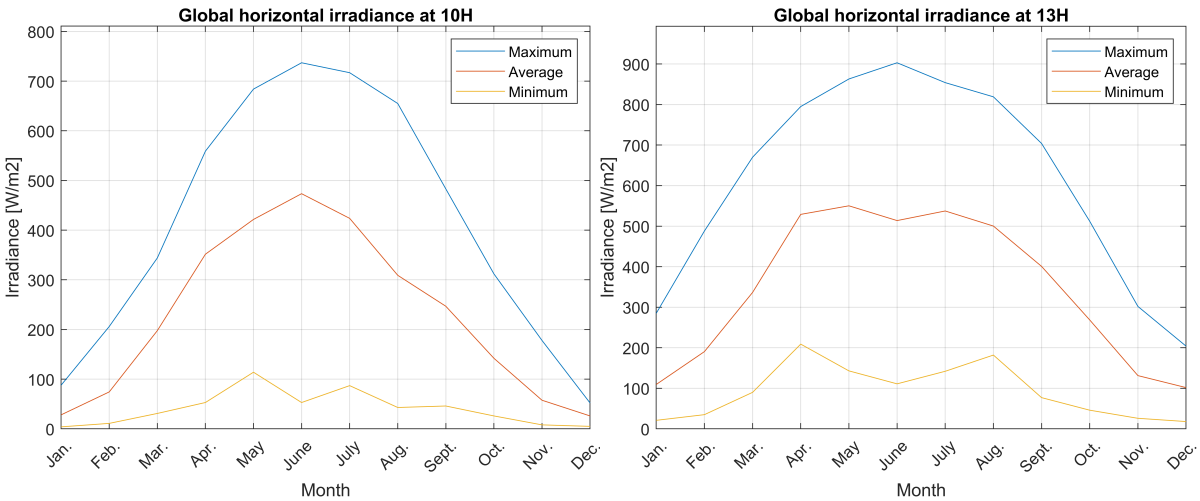

(a) Yearly irradiance at 10H

(b) Yearly irradiance at 13H

Figure 7.1: Global horizontal irradiance throughout the year

Based on the weather data analysis the weather cases have been created based on June, December and the yearly average. The weather cases can be seen in figures 7.2 and 7.3, which show a wide variety in the amount of irradiance. Also the volatility of the irradiance becomes clear for the maximum and minimum case weather cases.

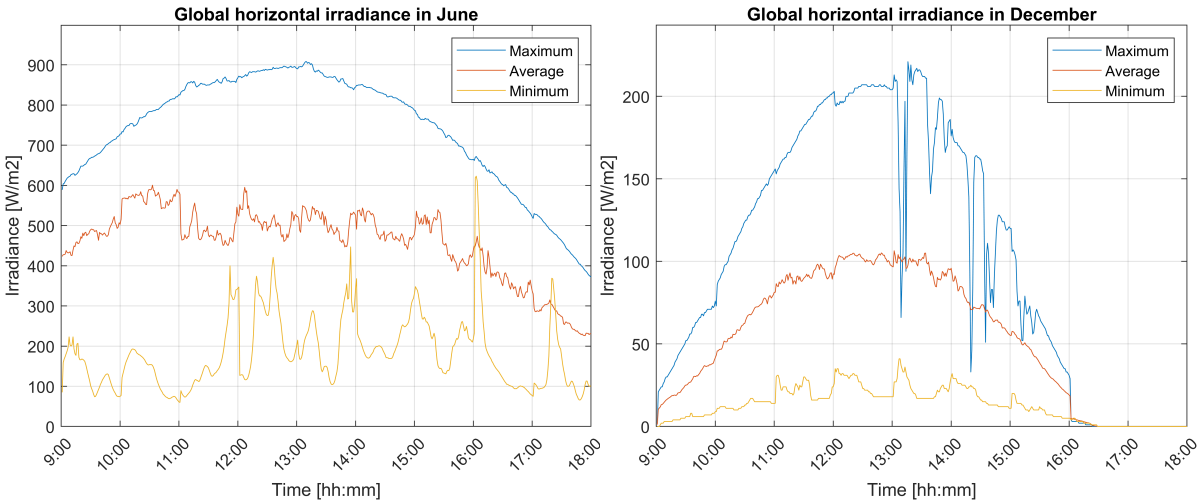

(a) Weather cases June

(b) Weather cases December

Figure 7.2: Monthly weather cases based on minutely weather data

7.2. PV cell values and characteristics

To model the PV cell using the single diode model, parameter values had to be calculated and verified. Then a single PV cell could be modelled and tested against various irradiances and temperatures.
To calculate the parameters a value for a had to be chosen. From the calculations became clear that for a value of 1.1 or higher, the series resistance R_s resulted in a negative value. Therefore a value of 1 for the ideality factor a has been chosen, resulting in a acceptable value for R_s, but a rather low value for R_{sh}. All the parameter values are as follows:

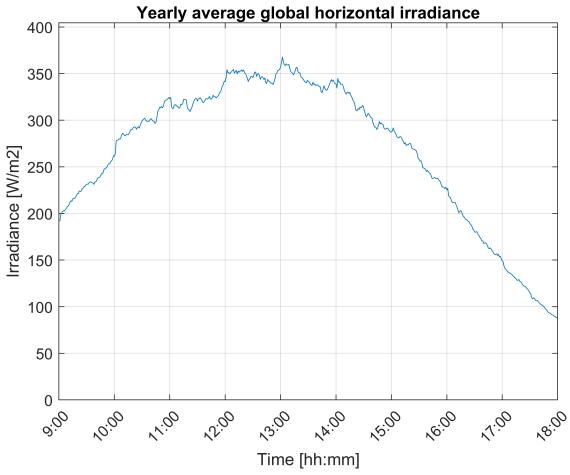

Figure 7.3: Yearly average weather case based on minutely weather data

- $a = 1$
- $I_{pv} = 6.431373\ A = 41.46865\ mA/cm^2$
- $I_s = 3.576601\ nA = 0.02306145\ nA/cm^2$
- $R_s = 1.063954\ m\Omega = 165.0086\ m\Omega \cdot cm^2$
- $R_{sh} = 4.981578\ \Omega = 772.5929\ \Omega \cdot cm^2$

Using equation 3.3, the I-V and P-V curves have been calculated for STC conditions to verify if the curves match the datasheet values. In figure 7.4 the curves are plotted and the datasheet values are marked, from which becomes clear that the points of characteristic curves match datasheet values and the calculated parameter values satisfy the boundary conditions set by the datasheet values.

With the calculated parameters the single diode model has been simulated and the resulting I-V and P-V curves can been seen in figure 7.5. Both the effect of the irradiance and the temperature are shown. The temperature has both an effect on the current and voltage and therefore on the power of the PV cell. The values provided by the datasheet and the calculated values for the model can be seen in table 7.1.

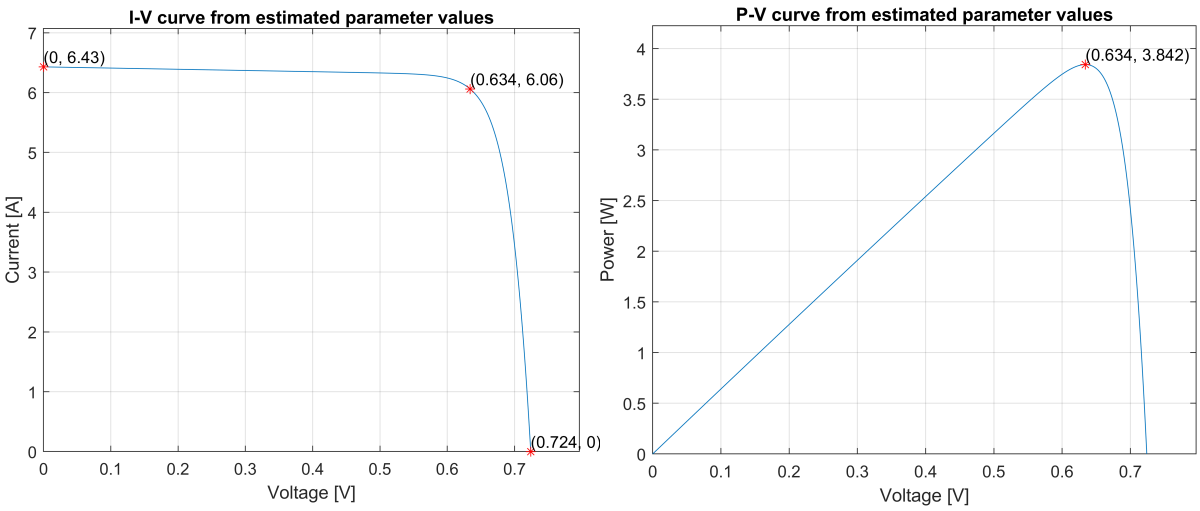

(a) Estimated I-V curve of PV cell

(b) Estimated P-V curve of PV cell

Figure 7.4: Estimation of a single SunPower Maxeon Gen 3 - Le3 PV cell

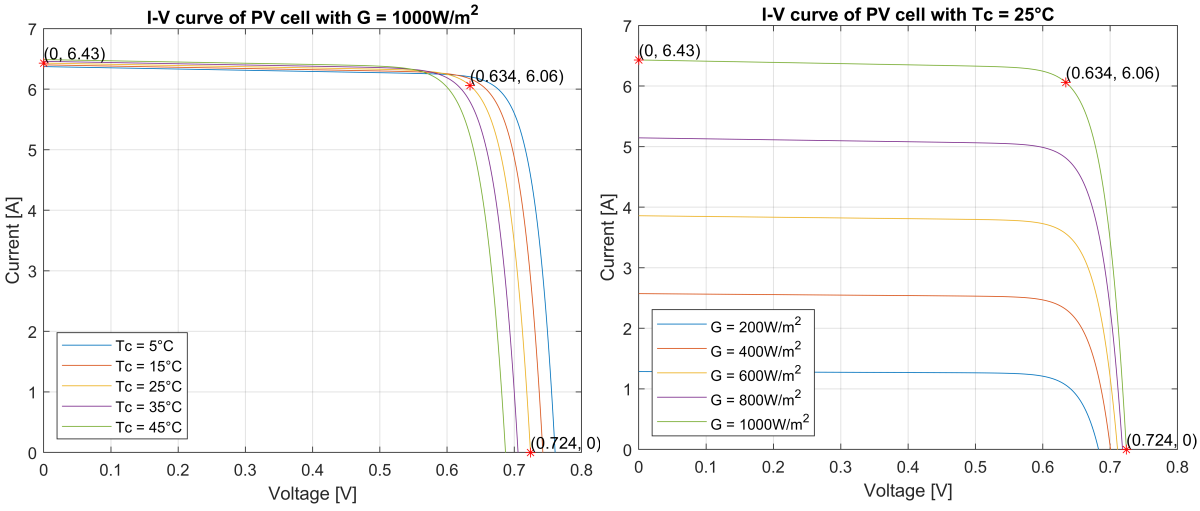

(a) Temperature sweep

(b) Irradiance sweep

Figure 7.5: I-V curves of single SunPower Maxeon Gen 3 - Le3 PV cell

Table 7.1: Temperature coefficient comparison

Temperature coefficient	Datasheet	Model
Voltage $[mV/°C]$	-1.74	-1.85
Current $[mA/°C]$	2.9	2.90
Power $[\%/°C]$	-0.29	-0.283

7.3. PV system characteristics and power output

The simulation of the PV system gives an overview of the performance and the characteristics of the entire PV system. Combining the PV system with the weather cases resulted in the theoretical output power of the PV generator under various weather conditions.

To calculate the characteristic curves of the PV system multiple aspects have been combined. The series configuration of 19 cell is combined with the Sandia thermal model for the cell temperature and the wire resistance is added for a more accurate system approximation. The I-V and P-V curves can be seen in

figure 7.6, in the legend of the plot the cell temperature is listed since the cell temperature depends on the amount of irradiance.

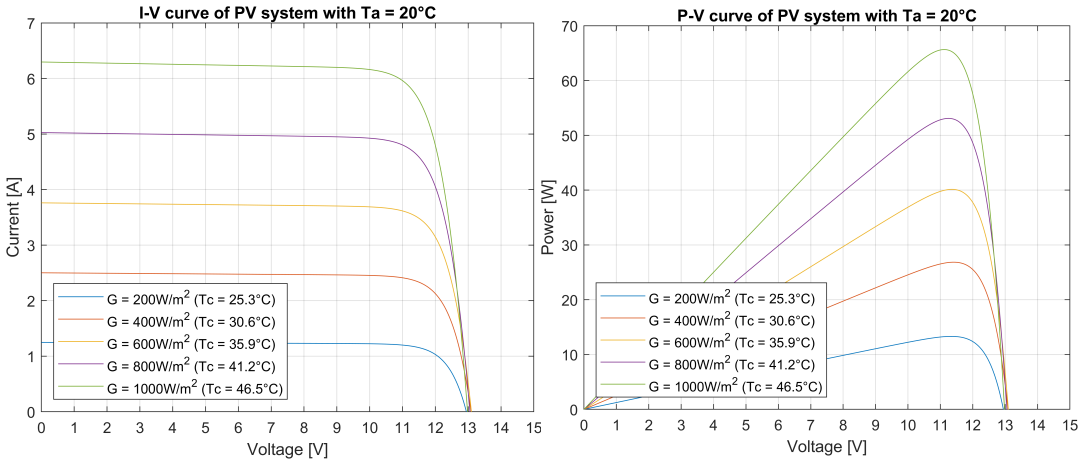

(a) Estimated I-V curve of PV system

(b) Estimated P-V curve of PV system

Figure 7.6: PV system performance for various irradiances

For the calculation of the power output of the PV system under different weather conditions, the seven weather cases with irradiance and ambient temperature are used as input. If the maximum power point is perfectly tracked, the power output of the PV system is shown in figures 7.7 and 7.8. Due to the large differences in irradiance between the different weather cases, the power output varies between zero and approximately $53W$.

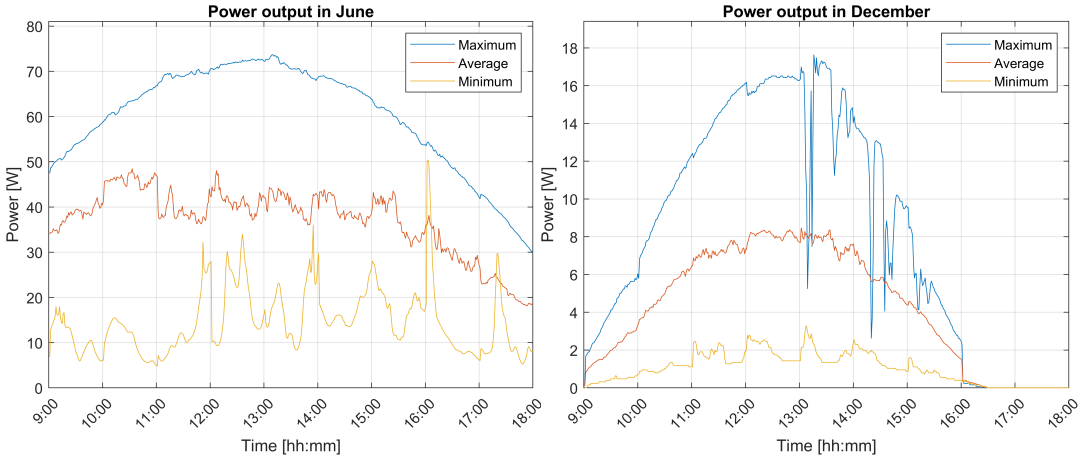

(a) Power output June

(b) Power output December

Figure 7.7: Power output at maximum power point

7.4. UAV flight range and comparison

The weight of the total UAV as a big impact on the flight range. Since the weight has a big impact on the flight range multiple configurations have been analysed. The configurations with the corresponding weight are listed in table 7.2. Here can be seen that the solar system, this includes the power converter and other electronics for the PV generator to operate properly, adds 240g without cell protection and 600g with cell protection. Since the cell protection more than doubles the weight of the solar system, both the case with and without protection is analysed. The power draw of the motor for the UAV with solar system with and without cell protection has been calculated when flying at a constant height and optimal speed. Combining the power draw with the power output of the PV system shown in figures 7.7 and 7.8, the range can be calculated for the various weather cases. The range is shown in figures 7.9, 7.10 and 7.11 for both with and without cell protection. The horizontal lines at 137.3 *km* and 189.7 *km* correspond with the range of an UAV without modifications and an UAV with larger battery.

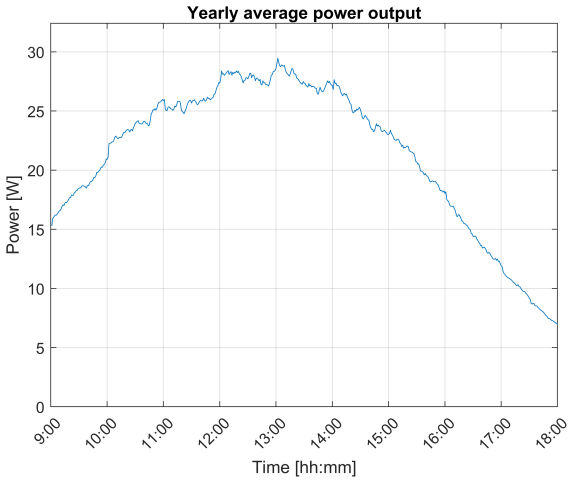

Figure 7.8: Power output at maximum power point

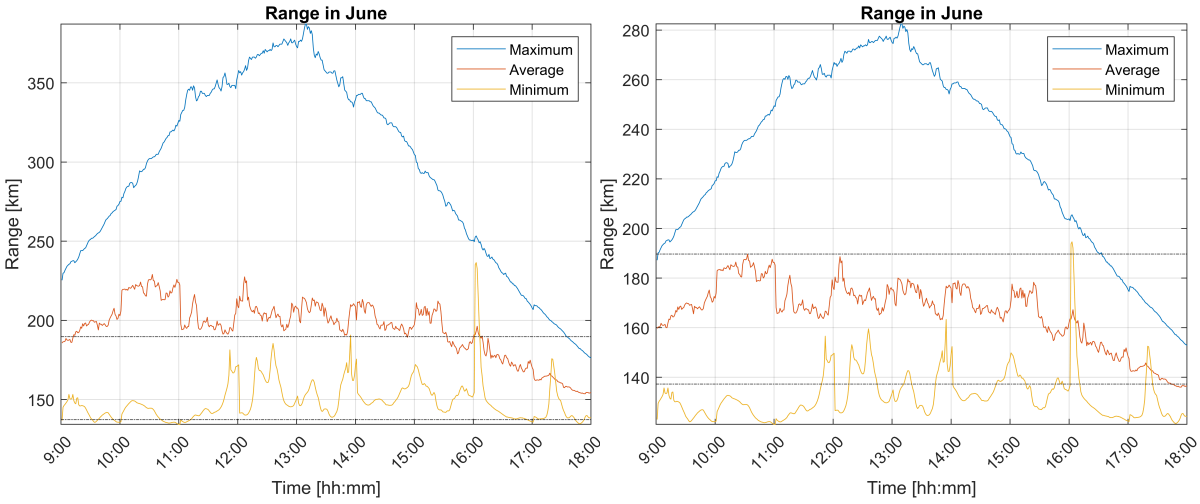

(a) without cell protection

(b) with cell protection

Figure 7.9: Range of UAV with solar system in June

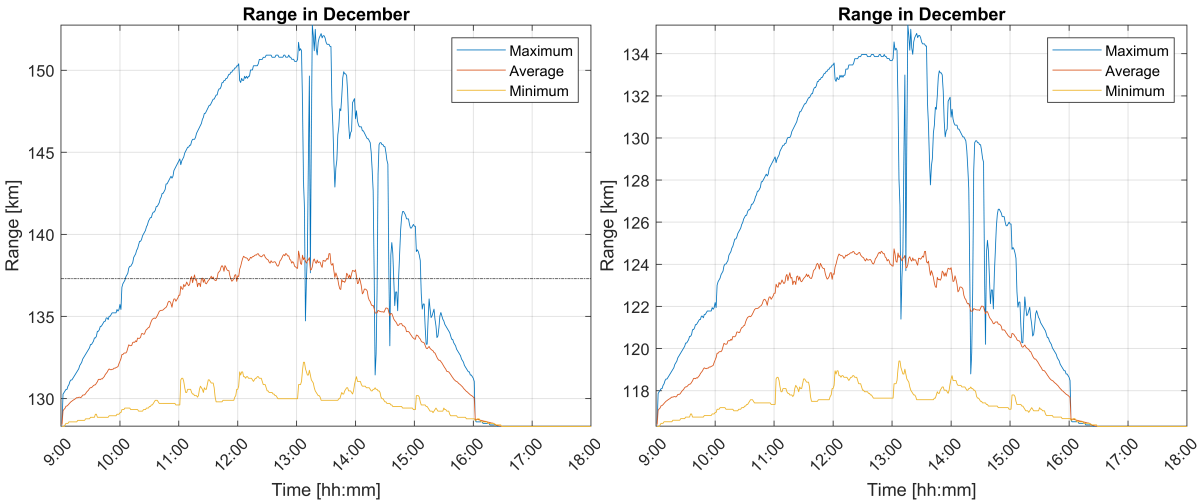

(a) without cell protection (b) with cell protection

Figure 7.10: Range of UAV with solar system in December

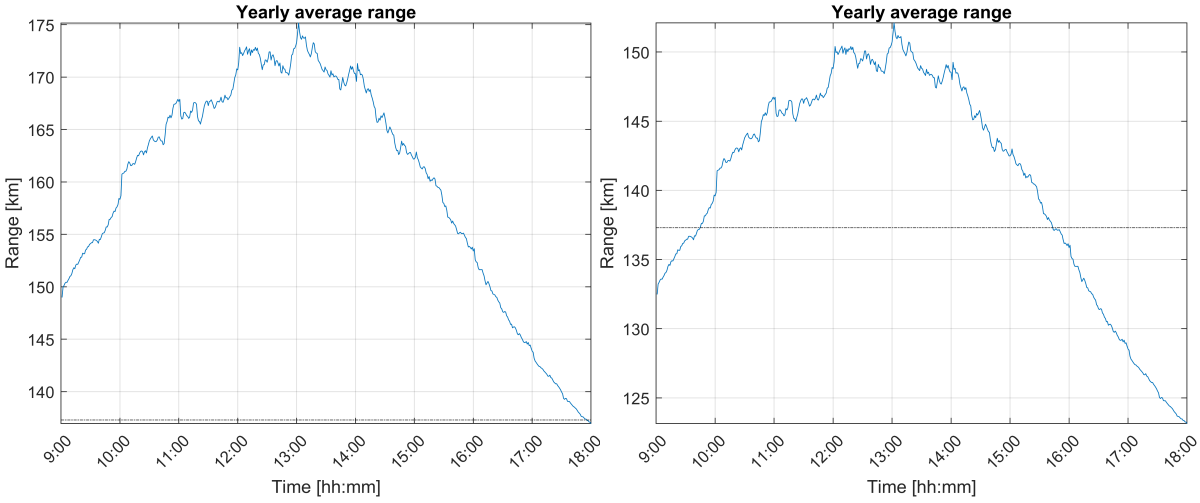

(a) without cell protection (b) with cell protection

Figure 7.11: Yearly average range of UAV with solar system

To place the performance of the UAV system with a solar system in perspective, the range for two different setups has been calculated as well. These setups are the UAV without modifications and the UAV with a larger 360Wh battery instead of the 216Wh battery. In table 7.2 the flight range of the configurations are listed. The flight range of the UAV without modifications and the UAV with larger battery are plotted with horizontal lines in figures 7.9, 7.10 and 7.11 for comparison.

Table 7.2: Flight range comparison for various configurations

Configuration	Battery size [Wh]	Weight [g]	Power draw [W]	Flight range [km]
UAV without modifications	216	3000	89.46	137.3
UAV with solar system without cell protection	216	3240	99.15	>128.3 and <250
UAV with solar system with cell protection	216	3620	112.7	>116.3 and <208
UAV with larger battery	360	3700	115.4	189.7

8

Discussion and conclusion

The overall goal of this project is to design a PV powered drone that can create an albedo map of an area that is equal or bigger than the area of the Technical University of Delft. In this chapter the results of the project are discussed and a conclusion is given. Next to this, the feasibility of the usage of cell protection is discussed, different system setups are compared, and an overall conclusion is made. Lastly, some further recommendations are made and future work is stated.

8.1. Discussion and conclusion

From figures 7.9 to 7.10 in the result chapter can be found that without protective layers the flight range of the UAV system with PV generator varies between 129 and 250 km, dependent on the irradiance. For the same system with protective layers, the flight range varies from 117 to 208 km. Based on the chosen flight path, the total flight range that is needed to map the area of the TU Delft is 48.75 km. This is elaborated on in Appendix D. With our UAV system we would be able to map the area of 2.4 to 5.1 times the area of area of the TU Delft. Therefore, there can be concluded that our goal has been achieved.

Feasibility cell protection usage

When looking at figure 7.11, the following conclusions can be made. On average, a UAV system with a PV generator that has cell protection will only exceed a system without a PV generator between 10:00 and 15:00. Since a flight would take around 00:37 hour (without setup and battery swap time) it would therefore still be able to meet our requirement regarding making five flights throughout the day. Therefore we can conclude that even though protection causes a reduction in flight range, it is still acceptable for usage. However, as this limits the possibility to fly in early mornings and late afternoon if you can want the PV generator to consume more power than it generates, it is recommended to use lighter cell protective layers.

Comparison different system setups

When comparing different UAV systems, the following conclusions can be drawn:

- In figure 7.11 (a) can be seen that on average between 9:00AM and 5:30PM the flight range is increased by adding a PV generator system onto the Skywalker X8. Therefore, it can be concluded that on average it is useful to implement a PV generator system in comparison to the same system without PV generator.
- In figure 7.10 (a) can be seen that it is on an average day in December the flight range will decrease. Therefore, it can be concluded that it is not beneficial to fly in December with the UAV system that includes the PV generator.
- In figure 7.9 (a) can be seen that even on an average day in June, the flight range for the PV generator system will mostly not exceed the flight range accomplished by the additional battery system. It will only be beneficial to use the PV generator system over additional batteries when

the solar irradiance exceeds 550 W/m^2. Therefore, it can be concluded that it is more beneficial to implement a UAV system with additional batteries than an system with a PV generator for weather cases of the TU Delft.

- Although the use of a bigger battery could in many cases give a better performance in terms of flight range, the use of a PV generator could still give you other advantages. For example, it would be possible to recharge the batteries between flights without the need of a connection to electricity grid, an additional generator or replacement batteries. Also, the PV generator is more sustainable as its energy is green.

8.2. Recommendations

Recommendation usage at the TU Delft

With the currently used Skywalker X8 model and PV generator system, there are some limitations regarding when it's profitable to fly at the TU Delft. Without protective layers it's best to fly when irradiances are above 125 W/m^2. This means that on average there should be flown at times between between 10:00AM and 5:30PM. With protective layers it's best to fly when irradiances exceed 240 W/m^2. This means that on average there should be flown at times between between 10:00AM and 3:00PM.

Recommendation usage other countries

For the Skywalker X8 model with PV generator system, it might be a good option to fly in other countries, as global horizontal irradiances could be significantly higher in some parts of the world.

Protection layers are implemented in the configuration, because they are necessary for electrical and weather protection. In this case the PV generator will be profitable over a similar system without PV system when irradiances exceed 240 W/m^2. If we assume for the sake of simplicity that a day consists of 12 hours of daylight, a day will need to produce 2.88 kWh/m^2 to become profitable. This means that on average it will be profitable to fly in the countries coloured light green to light pink at figure 8.1.

An UAV with PV system will be profitable over a system with additional batteries when irradiances exceed 780 W/m^2.If we again assume for the sake of simplicity that a day consists of 12 hours of daylight, a day will need to produce 9.36 kWh/m^2 to become profitable. This means that on average it will not be more profitable to fly with a PV generator system over a system with extra batteries anywhere in the world.

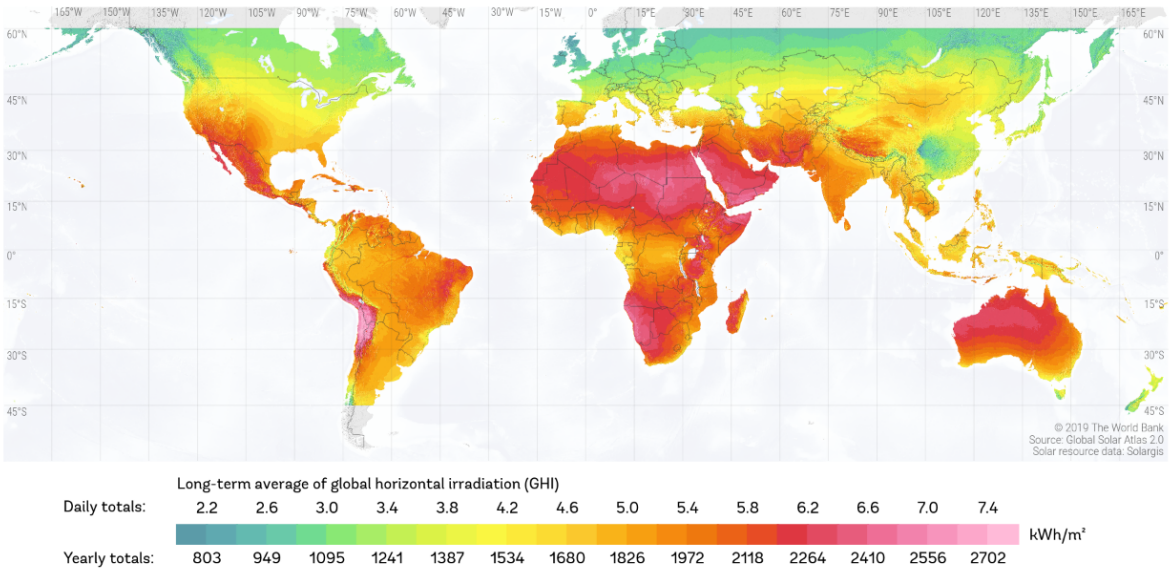

Figure 8.1: Global Horizontal irradiance by []

8.3. Future work

The currently developed PV generator can be used to simulate a PV generator system on a UAV. However, in order to further enhance the accuracy of the simulation, some further improvements can be made:

- As partial shading could play quite an important role in the power generation of the PV generator, a more thorough model could be made that takes into account the sun's light angle and the corresponding shades created by the body and the wing tips. Based on these findings either a suitable flight path should be calculated that prevents partial shading effects or a configuration could be considered that is least impacted by partial shading.
- The current model is based on strictly horizontally positioned solar cells. However, in reality some solar cells are bent due to the curvature of the wings and body of the UAV. This difference in angular position can impact the power generation of a PV cell. Thus, in order to create a more accurate model, curvatures of the PV cells could be taken into account.
- In order to protect the PV cells, front- and back sheets are used together with an encapsulant. The optical losses have been assumed to be about 3% in the simulations presented in the thesis, However, to further increase accuracy of the simulation, more accurate optical models should be developed and implemented.

Thus far, this model is based on available data and theoretical models. To further elaborate the model, it's beneficial to generate empirical data for the following purposes:

- The single diode model is established by parameters that are currently measured as is explained in section 6.3. This measurement is a close approximation but can be made more precise using empirical data of the PV cells' I-V curves under different irradiances.
- The Sandia thermal model bases the cell temperature on the windspeed and the coefficients a & b among other variables. The windspeed is taken to be 18 m/s, which is the average UAV speed. Empirical windspeed data of the TU Delft campus could be used to redeem this general estimation for a more precise output.
- Mismatch losses is a frequently occurring phenomenon. However, these losses originate from non ideal production of solar cells and can therefore only be measured when the system in physically created and tested.

The above stated points can be implemented to create an accurate model. Nonetheless, the most accurate way to test the flight range increase that would be achieved by the PV generator is by physically implementing the system. Also, in order to optimize the currently generated power output, they chosen UAV model could be reconsidered. A model that has a larger surface to weight ratio could potentially be able to generate more power.

A

Appendix

A.1. Symbols

- I_{pv} - Photocurrent $[A]$
- I_s - Saturation current $[A]$
- a - Ideality factor of the diode
- R_s - Series resistance $[\Omega]$
- R_{sh} - Shunt resistance $[\Omega]$
- V_T - Thermal voltage $[V]$
- k - Boltzmann's constant $= 1.38064852 \times 10^{-23}[J/K]$
- q - Elementary charge $= 1.60217662 \times 10^{-19}[C]$
- $I_{pv,ref}$ - Reference photocurrent at STC $[A]$
- K_i Current temperature coefficient $[A/K]$
- T_c - Cell temperature $[K]$
- T_{ref} - Reference temperature at STC $= 298[K]$
- G - Irradiance $[W/m^2]$
- G_{ref} - Reference irradiance at STC $= 1000[W/m^2]$
- V_{oc} - Open circuit voltage $[V]$
- I_{sc} - Short circuit current $[A]$
- V_{mp} - Maximum power point voltage $[V]$
- I_{mp} - Maximum power point current $[A]$
- P_{mp} - Maximum power point power $[W]$
- T_{amb} - Ambient temperature $[K]$
- WS - Windspeed $[m/s]$
- N_s - Number of cells connected in series
- E_g - Energy bandgap of the silicon $[eV]$
- K_{ev} - Boltzmann's constant $= 8.6173324 \times 10^{-5}[eV/K]$
- a - Experimental coefficient Sandia thermal model

- b - Experimental coefficient Sandia thermal model
- Ir_{abs} - Irradiance absorption [%]
- T_n - Nominal temperature [$Celsius$]
- G_{DNI} - Direct normal irradiance [W/m^2]
- G_{DIFF} - Diffuse irradiance [W/m^2]
- G_{REFL} - Reflected irradiance[W/m^2]
- α - Azimuth angle [$degree$]
- β - PV cell tilt [$degree$]
- γ - Angle between the cell and the south direction [$degree$]
- ζ - Zenith angle [$degree$]

A.2. Derivation of parameter value estimation

Describing the current-voltage (I-V) relationship of the single diode model can be done using equation 3.3, where the parameter values of I_{pv}, I_s, a, R_s and R_{sh} are unknown and should be estimated. For the parameter a the value has to be chosen, so that the other parameters can be calculated using the boundary conditions. The value of a is typically between 1 and 1.5 for single junction PV cells [5]. Starting with the short circuit conditions in equation 3.3, $V = 0$ and $I = I_{sc}$ results in the following equation:

$$I_{sc} = I_{pv} - I_s \left[exp\left(\frac{I_{sc}R_s}{aV_T} \right) - 1 \right] - \frac{I_{sc}R_s}{R_{sh}} \tag{A.1}$$

Analysing the value of the separate terms in this equation, the value of the second term $I_s \left[exp\left(\frac{I_{sc}R_s}{aV_T} \right) - 1 \right]$ is at least a 100 times smaller than the other terms in the equations [5]. Hence the second term can be neglected, resulting in an expression for I_{pv}.

$$I_{pv} = \frac{R_{sh} + R_s}{R_{sh}} I_{sc} \tag{A.2}$$

Using the open circuit conditions, $V = V_{oc}$ and $I = 0$, gives the following expression when using equation 3.3.

$$0 = I_{pv} - I_s \left[exp\left(\frac{V_{oc}}{aV_T} \right) - 1 \right] - \frac{V_{oc}}{R_{sh}} \tag{A.3}$$

Combining equations A.2 and A.3, the expression for the saturation current I_s can be derived.

$$I_s = \frac{(R_{sh} + R_s)I_{sc} - V_{oc}}{R_{sh} exp\left(\frac{V_{oc}}{aV_T} \right)} \tag{A.4}$$

The third boundary condition is set by the maximum power point, $V = V_{mp}$ and $I = I_{mp}$. This characteristic point is again filled in equation 3.3 and results in the following expression.

$$I_{mp} = I_{pv} - I_s \left[exp\left(\frac{V_{mp} + I_{mp}R_s}{aV_T} \right) - 1 \right] - \frac{V_{mp} + I_{mp}R_s}{R_{sh}} \tag{A.5}$$

Again the relative magnitude of the terms has been analysed and similar to equation A.1, the second term can be neglected. When the remaining equation is combined with earlier derived expressions A.2, A.4 and A.5, the following equation without I_{pv} and I_s can be derived.

$$I_{mp} = I_{sc} - \left(I_{sc} - \frac{V_{oc} - R_s I_{sc}}{R_{sh}}\right)\left[exp\left(\frac{V_{mp} + I_{mp}R_s - V_{oc}}{aV_T}\right)\right] - \frac{V_{mp} + I_{mp}R_s - I_{sc}R_s}{R_{sh}} \tag{A.6}$$

Finally the fourth boundary condition, the derivative of the P-V curve at the maximum power point should equal zero, is to ensure that the peak of the P-V curve is at the maximum power point. In equation A.7 the derivative of the power is shown and set to zero to satisfy the fourth boundary condition.

$$P = IV, \qquad \frac{\delta P}{\delta V} = V\frac{\delta I}{\delta V} + I = 0 \tag{A.7}$$

Filling in the maximum power point, $V = V_{mp}$ and $I = I_{mp}$, in equation A.7 gives the following expression.

$$\left(\frac{\delta I}{\delta V}\right)\Big|_{[I_{mp}, V_{mp}]} = -\frac{I_{mp}}{V_{mp}} \tag{A.8}$$

Taking the derivative with respect to V of equation 3.3, results in the following expression.

$$\frac{\delta I}{\delta V} = -\frac{I_s}{aV_T}\left(1 + \frac{\delta I}{\delta V}R_s\right)\left[exp\left(\frac{V + IR_s}{aV_T}\right)\right] - \frac{1}{R_{sh}}\left(1 + \frac{dI}{dV}R_s\right) \tag{A.9}$$

Combining equations A.2, A.4 and A.6 with equation A.9, an implicit expression of the series resistance R_s and datasheet parameters can be derived, equation A.10.

$$\frac{aV_T V_{mp}(2I_{mp} - I_{sc})}{(V_{mp}I_{sc} + V_{oc}(I_{mp} - I_{sc}))(V_{mp} - I_{mp}R_s) - aV_T(V_{mp}I_{sc} - V_{oc}I_{mp})} = exp\left(\frac{V_{mp} + I_{mp}R_s - V_{oc}}{aV_T}\right) \tag{A.10}$$

Finally the equation above A.10 can be combined with equation A.6, for an expression for R_{sh}.

$$R_{sh} = \frac{(V_{mp} - I_{mp}R_s)(V_{mp} - R_s(I_{sc} - I_{mp}) - aV_T)}{(V_{mp} - I_{mp}R_s)(I_{sc} - I_{mp}) - aV_T I_{mp}} \tag{A.11}$$

Starting with equation A.10, the value for R_s can be estimated using the data provided on the datasheet. With R_s known, equation A.11 can be used to calculated R_{sh}. Finally equations A.2 and A.4 can be used for calculating I_{pv} and I_s, completing the value estimation of the parameters needed for the single-diode model. The implementation of the parameter value estimation will be discussed in section 6.3.

B

Figures

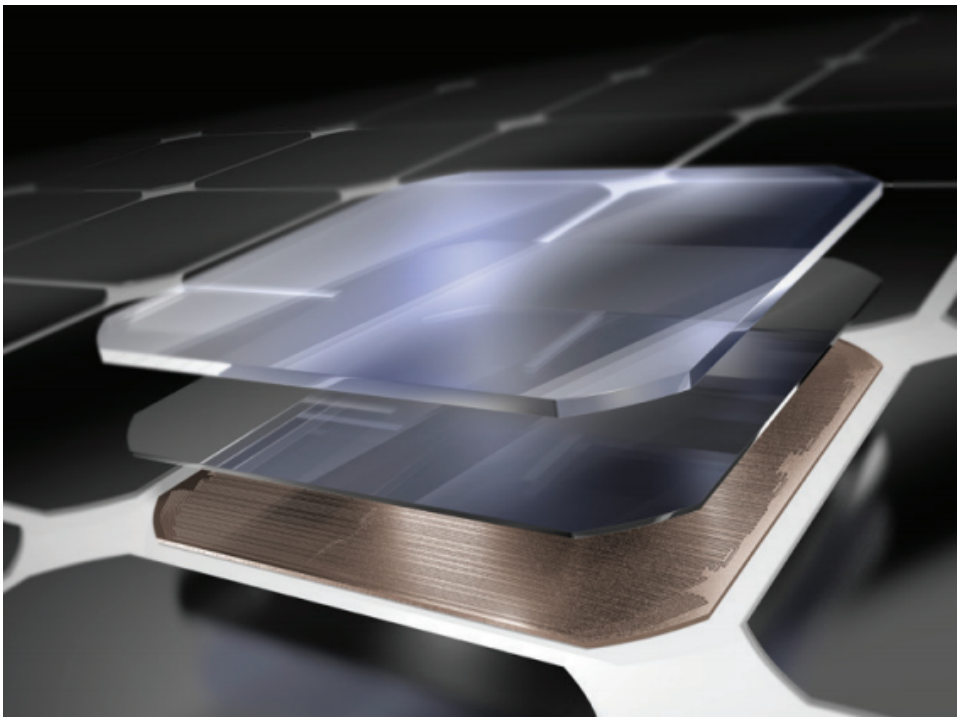

Figure B.1: Maxeon Gen 3 cell layout

Figure B.2: Maxeon Gen III bendability

B.1. Cell placement

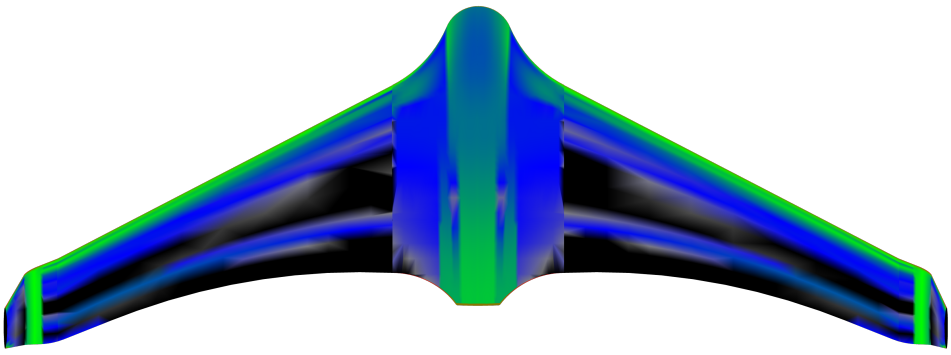

Figure B.3: Top view curvature of UAV

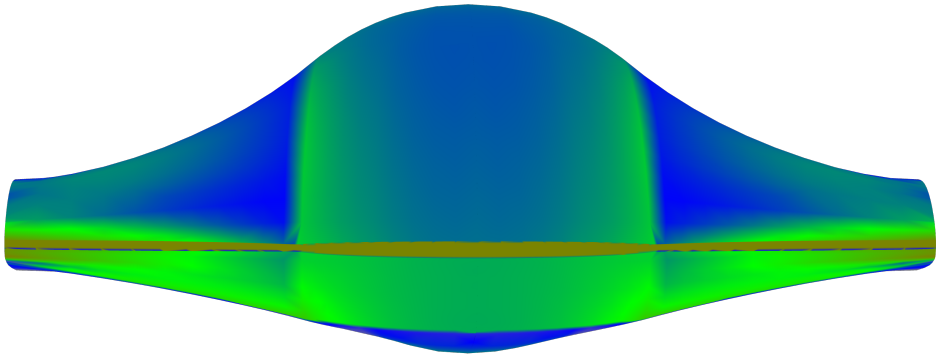

Figure B.4: Front view curvature of UAV

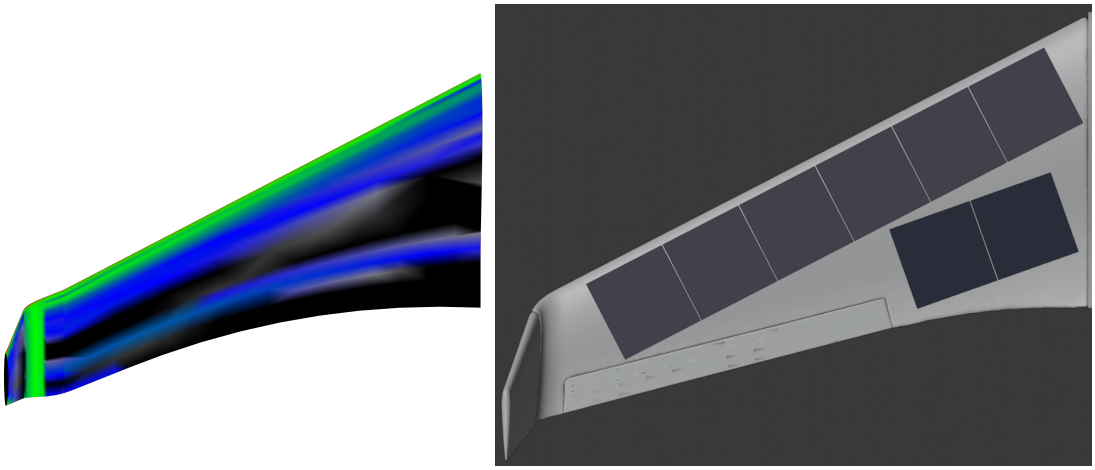

(a) The curvature

(b) The cell placement

Figure B.5: Top view of the wing

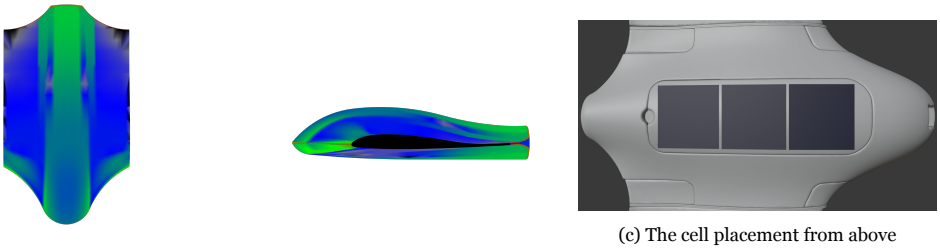

(a) The curvature from above

(b) The curvature from the side

(c) The cell placement from above

Figure B.6: View of the body

B.2. Characteristic curves

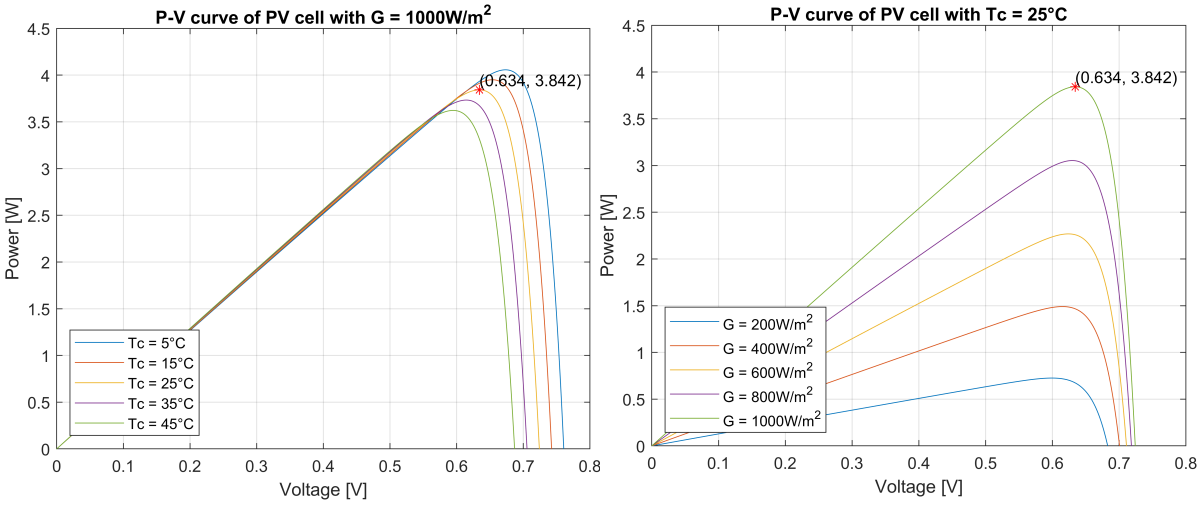

(a) Temperature sweep

(b) Irradiance sweep

Figure B.7: P-V curves of single SunPower Maxeon Gen 3 - Le3 PV cell

C

MATLAB code

C.1. Weather

weather_analysis.m

```
% weather_analysis.m
% Authors: Rik van der Hoorn - 4571150
%          Jasmijn Koning - 4329759
% Last modified: 11-06-2020
% Status: completed, tested and commented
%
% Load weather data Delft and analyse its content

close all;
clear all;

%% variable settings
filename = 'data\Delft-hour.csv';
hours = 9:18; % weather times of interest
n_sel = 1; % number of best/worst weather days for average best/worst
store_fig = true; % store generated figures

varNames = {'m', 'dm', 'h', 'G_Gh', 'Ta'}; % parameters of interest
varTypes = {'double', 'double', 'double', 'double', 'double'};

year_data = readtable(filename); % load weather data to table from csv

%% hourly analysis
for hour = hours % loop through set hours
    %% allocated space for results
    data_max = table('Size', [12, length(varNames)], 'VariableTypes', varTypes, ...
        'VariableNames', varNames);
    data_avg = table('Size', [12, length(varNames)], 'VariableTypes', varTypes, ...
        'VariableNames', varNames);
    data_min = table('Size', [12, length(varNames)], 'VariableTypes', varTypes, ...
        'VariableNames', varNames);

    %% select weather data
    hour_data = year_data(year_data.h == hour, varNames); % select data of interest ...
        with correct hour

    for month = 1:12
        month_data = hour_data(hour_data.m == month,:); % select month for calculations

        %% perform calculations and store analysis
        data_avg(month,:) = num2cell(mean(month_data{:,:},1));
        [~,rows_max] = maxk(month_data.G_Gh, n_sel);
        data_max(month,:) = num2cell(mean(month_data{rows_max,:},1));
        [~,rows_min] = mink(month_data.G_Gh, n_sel);
```

```
41          data_min(month,:) = num2cell(mean(month_data{rows_min,:},1));
42      end
43
44      %% plot hourly weather data analysis and store
45      figure()
46      plot(data_max.G_Gh)
47      hold on
48      plot(data_avg.G_Gh)
49      plot(data_min.G_Gh)
50      ylim([0 max(data_max.G_Gh)*1.1])
51      xlim([1 height(data_avg)])
52
53      month_label = [{'Jan.'}, {'Feb.'}, {'Mar.'}, {'Apr.'}, {'May'}, {'June'}, {'July'}, ...
            {'Aug.'}, {'Sept.'}, {'Oct.'}, {'Nov.'}, {'Dec.'}];
54      set(gca, 'XTick', 1:12)
55      set(gca, 'xticklabel', month_label.')
56      set(gca, 'XTickLabelRotation', 45)
57
58      legend('Maximum', 'Average', 'Minimum')
59      xlabel('Month')
60      ylabel('Irradiance [W/m2]')
61      title(['Global horizontal irradiance at ' num2str(hour) 'H'])
62
63      if store_fig
64          exportgraphics(gca,['figures\G_Gh_' num2str(hour) 'H.png'],'Resolution',600)
65      end
66  end
```

weather_cases_hourly.m

```
1   % weather_cases_hourly.m
2   % Authors: Rik van der Hoorn - 4571150
3   %          Jasmijn Koning - 4329759
4   % Last modified: 11-06-2020
5   % Status: completed, tested and commented
6   %
7   % Load hourly weather data Delft and create hourly weather cases
8
9   close all;
10  clear all;
11
12  %% variable settings
13  filename = 'data\Delft-hour.csv';
14  hours = 9:18; % weather hours of interest
15  months = [6 12]; % months of interest for weather cases
16  n_sel = 1; % number of best/worst weather days for average best/worst
17
18  store_cases = true; % store weather cases
19  store_fig = true; % store generated figures
20
21  varNames = {'m', 'dm', 'h', 'G_Gh', 'Ta'}; % parameters of interest
22  varTypes = {'double', 'double', 'double', 'double', 'double'};
23  month_names = [{'January'}, {'February'}, {'March'}, {'April'}, {'May'}, {'June'}, ...
        {'July'}, {'August'}, {'September'}, {'October'}, {'November'}, {'December'}];
24
25  data_year = readtable(filename); % load weather data to table from csv
26  case_data = table(); % table for final results
27
28  %% case creation of selected months
29  for month = months % loop through chosen months
30      %% allocated space for best/average/worst of month
31      case_max = table('Size', [length(hours), length(varNames)], 'VariableTypes', ...
            varTypes, 'VariableNames', varNames);
32      case_avg = table('Size', [length(hours), length(varNames)], 'VariableTypes', ...
            varTypes, 'VariableNames', varNames);
33      case_min = table('Size', [length(hours), length(varNames)], 'VariableTypes', ...
            varTypes, 'VariableNames', varNames);
34      case_year = table('Size', [length(hours), length(varNames)], 'VariableTypes', ...
            varTypes, 'VariableNames', varNames);
```

```
35
36      %% select weather data
37      data_month = data_year(data_year.m == month, varNames); % select data of interest ...
            with correct month
38
39      %% loop through days of the month and find best/worst day
40      num_days = height(data_month)/24; % number of days in month
41      G_Gh_month = zeros(num_days,1); % array with total irradiance of the days
42
43      for day = 1:num_days
44          G_Gh_day = data_month(data_month.dm == day, 'G_Gh'); % select irradiance of the ...
                day
45          G_Gh_month(day) = sum(G_Gh_day{hours,:}); % calculate total irradiance of day ...
                within selected hours
46      end
47
48      [~,rows_max] = maxk(G_Gh_month, n_sel); % best days
49      [~,rows_min] = mink(G_Gh_month, n_sel); % worst days
50
51      %% calculate best/average/worst values of month and store
52      idx = 1;
53      for hour = hours % calculate values for hours of interest
54          data_month_hour = data_month(data_month.h == hour,:); % select hour data
55          case_avg(idx,:) = num2cell(mean(data_month_hour{:,:},1));
56          case_max(idx,:) = num2cell(mean(data_month_hour{rows_max,:},1));
57          case_min(idx,:) = num2cell(mean(data_month_hour{rows_min,:},1));
58          idx = idx + 1;
59      end
60
61      case_max.Properties.VariableNames{'dm'} = 'cases';
62      case_avg.Properties.VariableNames{'dm'} = 'cases';
63      case_min.Properties.VariableNames{'dm'} = 'cases';
64      case_max.cases = repmat("max", height(case_max), 1);
65      case_avg.cases = repmat("avg", height(case_avg), 1);
66      case_min.cases = repmat("min", height(case_min), 1);
67      case_data = [case_data; case_max; case_avg; case_min];
68
69      %% plot monthly weather case and store
70      figure()
71      plot(case_max.h, case_max.G_Gh)
72      hold on
73      plot(case_avg.h, case_avg.G_Gh)
74      plot(case_min.h, case_min.G_Gh)
75      ylim([0 max(case_max.G_Gh)*1.1])
76      legend('Maximum', 'Average', 'Minimum')
77      xlabel('Time [hours]')
78      ylabel('Irradiance [W/m2]')
79      title(sprintf('Global horizontal irradiance in %s', string(month_names(month))))
80
81      if store_fig
82          exportgraphics(gca,['figures\' sprintf('G_Gh_hourly_%s.png', ...
                string(month_names(month)))],'Resolution',600)
83      end
84  end
85
86  %% calculate yearly average and store
87  case_year = table('Size', [length(hours), length(varNames)], 'VariableTypes', varTypes, ...
        'VariableNames', varNames);
88
89  idx = 1;
90  for hour = hours % calculate values for hours of interest
91      data_year_hour = data_year(data_year.h == hour, varNames); % select hour data
92      case_year(idx,:) = num2cell(mean(data_year_hour{:,:},1)); % yearly average for hour
93      idx = idx + 1;
94  end
95
96  case_year.Properties.VariableNames{'dm'} = 'cases';
97  case_year.cases = repmat("year", height(case_year), 1);
98  case_data = [case_data; case_year];
99
100 %% plot yearly weather case and store
```

```
figure()
plot(case_year.h, case_year.G_Gh)
ylim([0 max(case_year.G_Gh)*1.1])
xlabel('Time [hours]')
ylabel('Irradiance [W/m2]')
title('Yearly average global horizontal irradiance')

if store_fig
    exportgraphics(gca,'figures\G_Gh_hourly_year_avg.png','Resolution',600)
end

%% storing weather cases
if store_cases
    writetable(case_data, 'data\weather_cases_hourly.csv')
    writetable(case_data, 'data\weather_cases_hourly.xlsx')
end
```

weather_cases_minutely.m

```
% weather_cases_minutely.m
% Authors: Rik van der Hoorn - 4571150
%          Jasmijn Koning - 4329759
% Last modified: 11-06-2020
% Status: completed, tested and commented
%
% Load minutely weather data Delft and create minutely weather cases

close all;
clear all;

%% variable settings
filename = 'data\Delft-min.xlsx';
hours = 9:18; % weather interval of interest
months = [6 12]; % months of interest for weather cases
n_sel = 1; % number of best/worst weather days for average best/worst

store_cases = true; % store weather cases
store_fig = true; % store generated figures

varNames = {'m', 'dm', 'h', 'mi', 'G_Gh', 'Ta'}; % parameters of interest
varTypes = {'double', 'double', 'double', 'double', 'double', 'double'};
month_names = [{'January'}, {'February'}, {'March'}, {'April'}, {'May'}, {'June'}, ...
    {'July'}, {'August'}, {'September'}, {'October'}, {'November'}, {'December'}];

data_year = readtable(filename); % load weather data to table from csv
case_data = table(); % table for final results

%% case creation of selected months
for month = months % loop through chosen months
    %% allocated space for best/average/worst of month
    case_max = table('Size', [(length(hours)-1)*60, length(varNames)], 'VariableTypes', ...
        varTypes, 'VariableNames', varNames);
    case_avg = table('Size', [(length(hours)-1)*60, length(varNames)], 'VariableTypes', ...
        varTypes, 'VariableNames', varNames);
    case_min = table('Size', [(length(hours)-1)*60, length(varNames)], 'VariableTypes', ...
        varTypes, 'VariableNames', varNames);
    case_year = table('Size', [(length(hours)-1)*60, length(varNames)], ...
        'VariableTypes', varTypes, 'VariableNames', varNames);

    %% select weather data
    data_month = data_year(data_year.m == month, varNames); % select data of interest ...
        with correct month

    %% loop through days of the month and find best/worst day
    num_days = height(data_month)/(24*60); % number of days in month
    G_Gh_month = zeros(num_days,1); % array with total irradiance of the days

    for day = 1:num_days % loop through days
        G_Gh_day = data_month(data_month.dm == day, 'G_Gh'); % select irradiance of the ...
```

```
            day
45          G_Gh_month(day) = sum(G_Gh_day{hours(1)*60:hours(end)*60-1,:}); % total ...
                irradiance from 9:00 until 18:00
46      end
47
48      [~,rows_max] = maxk(G_Gh_month, n_sel); % best days
49      [~,rows_min] = mink(G_Gh_month, n_sel); % worst days
50
51      %% calculate best/average/worst values of month and store
52      idx = 1;
53      for hour = hours(1:end-1) % calculate values for hours of interest
54          data_month_hour = data_month(data_month.h == hour,:); % select hour data
55          for minute = 0:59
56              data_month_minute = data_month_hour(data_month_hour.mi == minute,:); % ...
                    select minute data
57              case_avg(idx,:) = num2cell(mean(data_month_minute{:,:},1));
58              case_max(idx,:) = num2cell(mean(data_month_minute{rows_max,:},1));
59              case_min(idx,:) = num2cell(mean(data_month_minute{rows_min,:},1));
60              idx = idx + 1;
61          end
62      end
63
64      case_max.Properties.VariableNames{'dm'} = 'cases';
65      case_avg.Properties.VariableNames{'dm'} = 'cases';
66      case_min.Properties.VariableNames{'dm'} = 'cases';
67      case_max.cases = repmat("max", height(case_max), 1);
68      case_avg.cases = repmat("avg", height(case_avg), 1);
69      case_min.cases = repmat("min", height(case_min), 1);
70      case_data = [case_data; case_max; case_avg; case_min];
71
72      %% plot monthly weather case and store
73      figure()
74      plot(case_max.G_Gh)
75      hold on
76      plot(case_avg.G_Gh)
77      plot(case_min.G_Gh)
78      ylim([0 max(case_max.G_Gh)*1.1])
79      xlim([0 height(case_avg)])
80
81      time_label = [{'9:00'}, {'10:00'}, {'11:00'}, {'12:00'}, {'13:00'}, {'14:00'}, ...
            {'15:00'}, {'16:00'}, {'17:00'}, {'18:00'}];
82      set(gca, 'XTick', 0:60:height(case_avg))
83      set(gca, 'xticklabel', time_label.')
84      set(gca, 'XTickLabelRotation', 45)
85
86      legend('Maximum', 'Average', 'Minimum')
87      xlabel('Time [hh:mm]')
88      ylabel('Irradiance [W/m2]')
89      title(sprintf('Global horizontal irradiance in %s', string(month_names(month))))
90
91      if store_fig
92          exportgraphics(gca,['figures\' sprintf('G_Gh_minutely_%s.png', ...
                string(month_names(month)))],'Resolution',600)
93      end
94  end
95
96  %% calculate yearly average and store
97  idx = 1;
98  for hour = hours(1:end-1) % calculate values for hours of interest
99      data_year_hour = data_year(data_year.h == hour, varNames); % select relevant data ...
            and hour
100     for minute = 0:59
101         data_year_minute = data_year_hour(data_year_hour.mi == minute,:); % select ...
                minute data
102         case_year(idx,:) = num2cell(mean(data_year_minute{:,:},1)); % calculate yearly ...
                average
103         idx = idx + 1;
104     end
105 end
106
107 case_year.Properties.VariableNames{'dm'} = 'cases';
```

```
case_year.cases = repmat("year", height(case_year), 1);
case_data = [case_data; case_year];

%% plot yearly weather case and store
figure()
plot(case_year.G_Gh)
ylim([0 max(case_year.G_Gh)*1.1])
xlim([0 height(case_year)])

time_label = [{'9:00'}, {'10:00'}, {'11:00'}, {'12:00'}, {'13:00'}, {'14:00'}, ...
    {'15:00'}, {'16:00'}, {'17:00'}, {'18:00'}];
set(gca, 'XTick', 0:60:height(case_year))
set(gca, 'xticklabel', time_label.')
set(gca, 'XTickLabelRotation', 45)

xlabel('Time [hh:mm]')
ylabel('Irradiance [W/m2]')
title('Yearly average global horizontal irradiance')

if store_fig
    exportgraphics(gca,'figures\G_Gh_minutely_year_avg.png','Resolution',600)
end

%% storing weather cases
if store_cases
    writetable(case_data, 'data\weather_cases_minutely.csv')
    writetable(case_data, 'data\weather_cases_minutely.xlsx')
end
```

C.2. Parameter value estimation

parameter_value_estimation.m

```
% parameter_value_estimation.m
% Authors: Rik van der Hoorn - 4571150
%          Jasmijn Koning - 4329759
% Last modified: 15-06-2020
% Status: completed, tested and commented
%
% Calculate values of parameters for single diode model (Ipv, Is, a, Rs, Rsh)

close all;
clear all;

%% datasheet parameters and constants
Isc = 6.43; % short circuit current [I]
Voc = 0.724; % open voltage current [V]
Imp = 6.06; % maximum power point current [I]
Vmp = 0.634; % maximum power point voltage [V]

T = 298; % cell temperature in [K]

k = 1.3806e-23; % Boltzmann's constant [J/K]
q = 1.6022e-19; % elementary charge [C]
Vt = (k*T)/q; % thermal voltage [V]

%% variable settings
a = 1; % diode ideality factor
Vstep = 0.001; % voltage step size for calculating I-V and P-V curves
store_fig = true; % store generated figures

%% value estimation of parameters
syms Rs
l_eq = (a*Vt*Vmp*(2*Imp-Isc)) / ...
    ((Vmp*Isc+Voc*(Imp-Isc))*(Vmp-Imp*Rs)-a*Vt*(Vmp*Isc-Voc*Imp));
r_eq = exp((Vmp+Imp*Rs-Voc)/(a*Vt));
Rs = vpasolve(l_eq == r_eq, Rs);

```

```
Rsh = ((Vmp-Imp*Rs)*(Vmp-Rs*(Isc-Imp)-a*Vt)) / ((Vmp-Imp*Rs)*(Isc-Imp)-a*Vt*Imp);
Is = ((Rsh+Rs)*Isc - Voc) / (Rsh*exp(Voc/(a*Vt)));
Ipv = ((Rsh+Rs)*Isc) / Rsh;

%% calculate I-V and P-V curves with estimated values
Vsweep = 0:Vstep:Voc;
Iout = zeros(1,length(Vsweep));

for i = 1:length(Vsweep)
    V = Vsweep(i);
    syms I
    l_eq = I - Ipv + (V + I*Rs) / Rsh;
    r_eq = -Is*(exp((V+I*Rs)/(a*Vt))-1);
    Iout(i) = vpasolve(l_eq == r_eq, I);
end

Pout = Iout.*Vsweep;

%% plot I-V and P-V curves and mark characteristic points
figure()
plot(Vsweep,Iout)
hold on
x = [0 0.634 0.724];
y = [6.43 6.06 0];
labels = {'(0, 6.43)','(0.634, 6.06)','(0.724, 0)'};
plot(x,y,'r*')
text(x,y,labels,'VerticalAlignment','bottom','HorizontalAlignment','left')

ylim([0 max(Iout)*1.1])
xlim([0 Voc*1.1])
xlabel('Voltage [V]')
ylabel('Current [I]')
title('I-V curve from estimated parameter values')

if store_fig
    exportgraphics(gca,'figures\I-V_curve_estimation.png','Resolution',600)
end

figure()
plot(Vsweep,Pout)
hold on
x = 0.634;
y = 3.842;
labels = {'(0.634, 3.842)'};
plot(x,y,'r*')
text(x,y,labels,'VerticalAlignment','bottom','HorizontalAlignment','left')

ylim([0 max(Pout)*1.1])
xlim([0 Voc*1.1])
xlabel('Voltage [V]')
ylabel('Power [W]')
title('P-V curve from estimated parameter values')

if store_fig
    exportgraphics(gca,'figures\P-V_curve_estimation.png','Resolution',600)
end
```

C.3. PV cell analysis

pv_cell.m

```
% pv_cell.m
% Authors: Rik van der Hoorn - 4571150
%          Jasmijn Koning - 4329759
% Last modified: 15-06-2020
% Status: completed, tested and commented
%
% Calculate I-V characteristics of the
```

```
% SunPower Maxeon Gen III - Le3 PV cell
%
% Inputs:   G - irradiance [W/m2]
%           Tc - cell temperature [K]
%           Vstep - voltage step size for voltage sweep [V]
% Output:   V - output voltage array [V]
%           I - corresponding output current array [A]

function [Vsweep, Iout] = pv_cell(G, Tc, Vstep)
    %% PV cell model parameters
    Voc = 0.724; % open voltage current [V]

    Gref = 1000; % reference irradiance at STC [W/m2]
    Tref = 298; % reference temperature at STC [K]
    Ipv_ref = 6.431373; % reference photocurrent at STC [A]
    Rsh_ref = 4.981578; % reference shunt resistance at STC [ohm]
    Eg_ref = 1.17 - 4.73e-4*(Tref^2/(Tref + 636)); % reference bandgap energy of the ...
        silicon at STC [eV]
    Is_ref = 3.576601e-12; % reference saturation current [A]

    a = 1; % ideality factor
    Rs = 1.063954e-3; % series resistance [ohm]
    Ki = 2.9e-3; % current temperature coefficient [A/K]

    k = 1.38064852e-23; % 'Boltzmanns constant [J/K]
    k_ev = 8.6173324e-5; % 'Boltzmanns constant [eV/K]
    q = 1.60217662e-19; % elementary charge [C]

    %% calculate I-V and P-V curves with estimated values
    Vt = (k*Tc)/q; % thermal voltage [V]
    Ipv = (Ipv_ref + Ki*(Tc - Tref))*G/Gref; % photocurrent [A]
    Rsh = Rsh_ref*(Gref/G); % shunt resistance [ohm]
    Eg = 1.17 - 4.73e-4*(Tc^2/(Tc + 636)); % bandgap energy of the silicon [eV]
    Is = Is_ref*(Tc/Tref)^3*exp((Eg_ref/(a*k_ev*Tref)) - (Eg/(a*k_ev*Tc))); % ...
        saturation current [A]

    Vsweep = 0:Vstep:Voc*1.1; % voltage sweep
    Iout = zeros(1,length(Vsweep));

    for i = 1:length(Vsweep)
        V = Vsweep(i);
        syms I % calculate I according to single diode model
        eq = Ipv - Is*(exp((V+I*Rs)/(a*Vt))-1) - (V + I*Rs) / Rsh_ref;
        Iout(i) = vpasolve(I == eq, I);
    end
end
```

pv_cell_analysis.m

```
% pv_cell_analysis.m
% Authors: Rik van der Hoorn - 4571150
%          Jasmijn Koning - 4329759
% Last modified: 15-06-2020
% Status: completed, tested and commented
%
% File used to analyse the I-V and P-V characteristics of the
% SunPower Maxeon Gen III - Le3 PV cell

close all;
clear all;

%% Plot I-V curve with various temperatures
G = 1000; % global horizontal irradiance [W/m2]
Tc_sweep = [278 288 298 308 318]; % cell temperature [K]
Vstep = 0.01; % voltage step size for voltage sweep [V]
store_fig = true;

figure()
for Tc = Tc_sweep
```

```
21      [V,I] = pv_cell(G, Tc, Vstep); % calculate I-V characteristics of PV cell
22      plot(V,I)
23      hold on
24      ylim([0 7])
25      xlim([0 0.8])
26      set(gca, 'XTick', 0:0.1:0.8)
27  end
28
29  legend('Tc = 5°C', 'Tc = 15°C', 'Tc = 25°C', 'Tc = 35°C', 'Tc = 45°C', 'Location', ...
        'southwest')
30  xlabel('Voltage [V]')
31  ylabel('Current [I]')
32  title('I-V curve of PV cell with G = 1000W/m^{2}')
33
34  if store_fig
35      exportgraphics(gca,'figures\I-V_cell_temp_sweep.png','Resolution',600)
36  end
37
38  %% Plot P-V curve with various temperatures
39  figure()
40  for Tc = Tc_sweep
41      [V,I] = pv_cell(G, Tc, Vstep); % calculate I-V characteristics of PV cell
42      plot(V,I.*V)
43      hold on
44      ylim([0 4.5])
45      xlim([0 0.8])
46      set(gca, 'XTick', 0:0.1:0.8)
47  end
48
49  legend('Tc = 5°C', 'Tc = 15°C', 'Tc = 25°C', 'Tc = 35°C', 'Tc = 45°C', 'Location', ...
        'southwest')
50  xlabel('Voltage [V]')
51  ylabel('Power [P]')
52  title('P-V curve of PV cell with G = 1000W/m^{2}')
53
54  if store_fig
55      exportgraphics(gca,'figures\P-V_cell_temp_sweep.png','Resolution',600)
56  end
57
58  %% Plot I-V curve with various irradiances
59  Tc = 298; % cell temperature [K]
60  G_sweep = [200 400 600 800 1000]; % global horizontal irradiance [W/m2]
61
62  figure()
63  for G = G_sweep
64      [V,I] = pv_cell(G, Tc, Vstep); % calculate I-V characteristics of PV cell
65      plot(V,I)
66      hold on
67      ylim([0 7])
68      xlim([0 0.8])
69      set(gca, 'XTick', 0:0.1:0.8)
70  end
71
72  legend('G = 200W/m^{2}', 'G = 400W/m^{2}', 'G = 600W/m^{2}', 'G = 800W/m^{2}', 'G = ...
        1000W/m^{2}', 'Location', 'southwest')
73  xlabel('Voltage [V]')
74  ylabel('Current [I]')
75  title('I-V curve of PV cell with Tc = 25°C')
76
77  if store_fig
78      exportgraphics(gca,'figures\I-V_cell_irr_sweep.png','Resolution',600)
79  end
80
81  %% Plot P-V curve with various irradiances
82  figure()
83  for G = G_sweep
84      [V,I] = pv_cell(G, Tc, Vstep); % calculate I-V characteristics of PV cell
85      plot(V,I.*V)
86      hold on
87      ylim([0 4.5])
88      xlim([0 0.8])
```

```
89      set(gca, 'XTick', 0:0.1:0.8)
90  end
91
92  legend('G = 200W/m^{2}', 'G = 400W/m^{2}', 'G = 600W/m^{2}', 'G = 800W/m^{2}', 'G = ...
        1000W/m^{2}', 'Location', 'southwest')
93  xlabel('Voltage [V]')
94  ylabel('Power [P]')
95  title('P-V curve of PV cell with Tc = 25°C')
96
97  if store_fig
98      exportgraphics(gca,'figures\P-V_cell_irr_sweep.png','Resolution',600)
99  end
```

C.4. PV power output

pv_system_power_simu.m

```
1  % pv_system_power_simu.m
2  % Authors: Rik van der Hoorn - 4571150
3  %          Jasmijn Koning - 4329759
4  % Last modified: 14-06-2020
5  % Status: completed, tested and commented
6  %
7  % Load minutely weather cases Delft and calculate power output of PV system
8  % using the simulink implementation of the PV system. The wire resistance
9  % is neglected, the irradiance absorption of the protection layers is
10 % included
11
12 close all;
13 clear all;
14
15 %% variable settings
16 filename = 'data\weather_cases_minutely.csv';
17 a_sandia = -2.81; % a coeficient of sandia thermal model
18 b_sandia = -0.0455; % b coeficient of sandia thermal model
19 windspeed = 18; % windspeed for sandia thermal model
20 pro_abs = 0.03; % irradiance absorption of protection layers
21
22 store_power = true; % store power output of weather cases
23 store_fig = true; % store generated figures
24
25 months = [6  12]; % months numbers of weather cases
26 month_names = [{'January'}, {'February'}, {'March'}, {'April'}, {'May'}, {'June'}, ...
       {'July'}, {'August'}, {'September'}, {'October'}, {'November'}, {'December'}];
27
28 %% load case data and add cell temperature
29 case_data = readtable(filename);
30 case_data.Tc = case_data.Ta + case_data.G_Gh*exp(a_sandia + b_sandia*windspeed);
31
32 %% create arrays for data storage of simulations
33 Pout = zeros(height(case_data),1);
34 Vout = zeros(height(case_data),1);
35 Iout = zeros(height(case_data),1);
36
37 for i = 1:height(case_data) % loop operation conditions
38     %% simulate case situation
39     Tc = case_data.Tc(i);
40     G_Gh = case_data.G_Gh(i)*(1-pro_abs);
41     sim_data = sim('pv_module_automated');
42
43     %% calculate power output
44     [~, Mpp_idx] = max(sim_data.yout{1}.Values.Data);
45     Iout(i) = sim_data.yout{3}.Values.Data(Mpp_idx);
46     Vout(i) = sim_data.yout{2}.Values.Data(Mpp_idx);
47 end
48
49 power_data = case_data;
50 power_data.Pout = Vout.*Iout;
```

```
power_data.Vout = Vout;
power_data.Iout = Iout;

for month = months
    %% plot power output for monthly weather cases and store
    power_data_month = power_data(power_data.m == month,:);
    Pout_max = power_data_month{strcmp(power_data_month.cases, 'max'), 'Pout'};
    Pout_avg = power_data_month{strcmp(power_data_month.cases, 'avg'), 'Pout'};
    Pout_min = power_data_month{strcmp(power_data_month.cases, 'min'), 'Pout'};

    figure()
    plot(Pout_max)
    hold on
    plot(Pout_avg)
    plot(Pout_min)
    ylim([0 max(Pout_max)*1.1])
    xlim([0 length(Pout_avg)])

    time_label = [{'9:00'}, {'10:00'}, {'11:00'}, {'12:00'}, {'13:00'}, {'14:00'}, ...
        {'15:00'}, {'16:00'}, {'17:00'}, {'18:00'}];
    set(gca, 'XTick', 0:60:length(Pout_avg))
    set(gca, 'xticklabel', time_label.')
    set(gca, 'XTickLabelRotation', 45)

    legend('Maximum', 'Average', 'Minimum')
    xlabel('Time [hh:mm]')
    ylabel('Power [W]')
    title(sprintf('Power output in %s', string(month_names(month))))

    if store_fig
        exportgraphics(gca,['figures\' sprintf('Power_simu_minutely_%s.png', ...
            string(month_names(month)))],'Resolution',600)
    end
end

%% plot power output for yearly weather case and store
Pout_year = power_data{strcmp(power_data.cases, 'year'), 'Pout'};

figure()
plot(Pout_year)
ylim([0 max(Pout_year)*1.1])
xlim([0 length(Pout_year)])

time_label = [{'9:00'}, {'10:00'}, {'11:00'}, {'12:00'}, {'13:00'}, {'14:00'}, ...
    {'15:00'}, {'16:00'}, {'17:00'}, {'18:00'}];
set(gca, 'XTick', 0:60:length(Pout_year))
set(gca, 'xticklabel', time_label.')
set(gca, 'XTickLabelRotation', 45)

xlabel('Time [hh:mm]')
ylabel('Power [W]')
title('Yearly average power output')

if store_fig
    exportgraphics(gca,'figures\Power_simu_minutely_year_avg.png','Resolution',600)
end

%% storing weather cases
if store_power
    writetable(power_data, 'data\weather_cases_power_simu_minutely.csv')
    writetable(power_data, 'data\weather_cases_power_simu_minutely.xlsx')
end
```

C.5. UAV flight range

range_calculations.m

```
% range_calculations.m
```

```
% Authors: Rik van der Hoorn - 4571150
%          Jasmijn Koning - 4329759
% Last modified: 16-06-2020
% Status: completed, tested and commented
%
% Load generated power data and calculate range for UAV with PV system with
% and without cell protection

close all;
clear all;

%% variable settings
filename = 'data\weather_cases_power_minutely.csv';
store_fig = true; % store generated figures
months = [6 12]; % months numbers of weather cases
month_names = [{'January'}, {'February'}, {'March'}, {'April'}, {'May'}, {'June'}, ...
    {'July'}, {'August'}, {'September'}, {'October'}, {'November'}, {'December'}];

p_pv_light = 99.15; % power usage for UAV with PV without cell protection (3240g)
p_pv_heavy = 112.7; % power usage for UAV with PV with cell protection (3620g)

r_uav = 137.3; % range UAV without modifications (3000g)
r_pv_light_base = 128.3; % range without PV power generation
r_pv_heavy_base = 116.3; % range without PV power generation
r_bat = 189.7; % range UAV with larger battery (3700g)

eff_pv = 0.9; % transmission and converter efficiency

%% calculations
power_data = readtable(filename);

power_data.r_pv_light = r_pv_light_base./((p_pv_light - ...
    power_data.Pout.*eff_pv)./p_pv_light);
power_data.r_pv_heavy = r_pv_heavy_base./((p_pv_heavy - ...
    power_data.Pout.*eff_pv)./p_pv_heavy);

for month = months
    %% plot power output for monthly weather cases and store
    power_data_month = power_data(power_data.m == month,:);
    range_max = power_data_month{strcmp(power_data_month.cases, 'max'), 'r_pv_light'};
    range_avg = power_data_month{strcmp(power_data_month.cases, 'avg'), 'r_pv_light'};
    range_min = power_data_month{strcmp(power_data_month.cases, 'min'), 'r_pv_light'};

    figure()
    plot(range_max)
    hold on
    plot(range_avg)
    plot(range_min)
    yline(r_uav, '-.k')
    yline(r_bat, '-.k')
    ylim([min(range_min) max(range_max)])
    xlim([0 length(range_avg)])

    time_label = [{'9:00'}, {'10:00'}, {'11:00'}, {'12:00'}, {'13:00'}, {'14:00'}, ...
        {'15:00'}, {'16:00'}, {'17:00'}, {'18:00'}];
    set(gca, 'XTick', 0:60:length(range_avg))
    set(gca, 'xticklabel', time_label.')
    set(gca, 'XTickLabelRotation', 45)

    legend('Maximum', 'Average', 'Minimum')
    xlabel('Time [hh:mm]')
    ylabel('Range [km]')
    title(sprintf('Range of UAV with PV system in %s', string(month_names(month))))

    if store_fig
        exportgraphics(gca,['figures\' sprintf('Range_PV_no_protec_minutely_%s.png', ...
            string(month_names(month)))],'Resolution',600)
    end
end

for month = months
```

```
68      %% plot power output for monthly weather cases and store
69      power_data_month = power_data(power_data.m == month,:);
70      range_max = power_data_month{strcmp(power_data_month.cases, 'max'), 'r_pv_heavy'};
71      range_avg = power_data_month{strcmp(power_data_month.cases, 'avg'), 'r_pv_heavy'};
72      range_min = power_data_month{strcmp(power_data_month.cases, 'min'), 'r_pv_heavy'};
73
74      figure()
75      plot(range_max)
76      hold on
77      plot(range_avg)
78      plot(range_min)
79      yline(r_uav, '-.k')
80      yline(r_bat, '-.k')
81      ylim([min(range_min) max(range_max)])
82      xlim([0 length(range_avg)])
83
84      time_label = [{'9:00'}, {'10:00'}, {'11:00'}, {'12:00'}, {'13:00'}, {'14:00'}, ...
            {'15:00'}, {'16:00'}, {'17:00'}, {'18:00'}];
85      set(gca, 'XTick', 0:60:length(range_avg))
86      set(gca, 'xticklabel', time_label.')
87      set(gca, 'XTickLabelRotation', 45)
88
89      legend('Maximum', 'Average', 'Minimum')
90      xlabel('Time [hh:mm]')
91      ylabel('Range [km]')
92      title(sprintf('Range of UAV with PV system in %s', string(month_names(month))))
93
94      if store_fig
95          exportgraphics(gca,['figures\' sprintf('Range_PV_protect_minutely_%s.png', ...
                string(month_names(month)))],'Resolution',600)
96      end
97  end
98
99  %% plot power output for yearly weather case and store
100 range_year = power_data{strcmp(power_data.cases, 'year'), 'r_pv_light'};
101
102 figure()
103 plot(range_year)
104 hold on
105 yline(r_uav, '-.k')
106 yline(r_bat, '-.k')
107 ylim([min(range_year) max(range_year)])
108 xlim([0 length(range_year)])
109
110 time_label = [{'9:00'}, {'10:00'}, {'11:00'}, {'12:00'}, {'13:00'}, {'14:00'}, ...
        {'15:00'}, {'16:00'}, {'17:00'}, {'18:00'}];
111 set(gca, 'XTick', 0:60:length(range_year))
112 set(gca, 'xticklabel', time_label.')
113 set(gca, 'XTickLabelRotation', 45)
114
115 xlabel('Time [hh:mm]')
116 ylabel('Range [km]')
117 title('Yearly average range of UAV with PV system')
118
119 if store_fig
120     exportgraphics(gca,'figures\Range_PV_no_protect_minutely_year_avg.png','Resolution',600)
121 end
122
123 %% plot power output for yearly weather case and store
124 range_year = power_data{strcmp(power_data.cases, 'year'), 'r_pv_heavy'};
125
126 figure()
127 plot(range_year)
128 hold on
129 yline(r_uav, '-.k')
130 yline(r_bat, '-.k')
131 ylim([min(range_year) max(range_year)])
132 xlim([0 length(range_year)])
133
134 time_label = [{'9:00'}, {'10:00'}, {'11:00'}, {'12:00'}, {'13:00'}, {'14:00'}, ...
        {'15:00'}, {'16:00'}, {'17:00'}, {'18:00'}];
```

```
135 set(gca, 'XTick', 0:60:length(range_year))
136 set(gca, 'xticklabel', time_label.')
137 set(gca, 'XTickLabelRotation', 45)
138
139 xlabel('Time [hh:mm]')
140 ylabel('Range [km]')
141 title('Yearly average range of UAV with PV system')
142
143 if store_fig
144     exportgraphics(gca,'figures\Range_PV_protect_minutely_year_avg.png','Resolution',600)
145 end
```

D

Drone Documentation

BACHELOR END PROJECT

DRONE DOCUMENTATION

June 19, 2020

– Solar Powered drones –
Laura Muntenaar (4554213),
Martin Geertjes (4324285),
Rik van der Hoorn (4571150),
Jasmijn Koning (4329759),
Jetse Spijkstra (4466667),
Sjoerd Groot (4694368),

Contents

1 Introduction 1

2 UAV selection 2
- 2.1 Multi-rotor . . . 2
- 2.2 Single-rotor . . . 3
- 2.3 Fixed-wing . . . 3
- 2.4 Fixed-wing hybrid . . . 3
- 2.5 UAV type selection . . . 4
- 2.6 UAV selection . . . 6

3 Component selection 7
- 3.1 Auto-pilot . . . 7
- 3.2 Propeller . . . 7
- 3.3 Motor . . . 8
- 3.4 Speed controller . . . 9
- 3.5 Battery . . . 9
- 3.6 Camera . . . 10

4 System overview 11
- 4.1 Introduction . . . 11
- 4.2 Costs . . . 11
- 4.3 Component fit . . . 12
- 4.4 Inter-Component relationship . . . 13

5 Flight simulation 14
- 5.1 Introduction . . . 14
- 5.2 Aerodynamic model . . . 14
  - Simulink implementation of the aerodynamics . . . 14
  - Mass and angle of attack sweep . . . 16

6 Final simulation 18
- 6.1 Introduction . . . 18
- 6.2 Simulink Implementation . . . 18
- 6.3 Results of final simulation . . . 19
- 6.4 Flight path calculation . . . 20
- 6.5 Power consumption in flight . . . 22

Bibliography 24

A Components 25

B Results 31

1

Introduction

With renewables being on the rise, green solutions are being investigated for every market. This thesis revolves around the idea that the flight range and flight time of commercially available drones could possibly be elongated by the addition of solar panels. In order to do this, a drone is proposed which has the ability to accommodate solar panels and thus can provide its on board system with additional power to elongate the flight range.

This thesis is structured as follows. First the UAV type is selected, then the actual drone frame and the additional components are selected. Finally the drone is simulated and final results are elaborated on.

2

UAV selection

For the UAV selection, it is important to understand which types of UAVs there are. Four types of UAVs are considered and discussed: multi-rotor, single-rotor,fixed-wing and fixed-wing hybrid.

2.1. Multi-rotor

A quadcopter is what is generally thought of when thinking of a UAV, which is a subclass of the multi-rotor class. Typically it is driven by four rotors, where the direct opposite rotors spin in the opposite direction. This type of UAV is the easiest to engineer, since as long as the rotors are spaced in a symmetrical way it will fly without problems. Stability and flexibility are two of the main advantages of a quadcopter; it can suspend itself in the air and take photos from a still position. Furthermore, it can move very flexibly, in any direction at any given time, which may prevent crashes in tightly packed neighbourhoods. Finally it will not need a lot of space for take-off since it can take-off vertically. However, there are also some disadvantages to this design, among which is the fact that it is less-efficient than airplane solutions [6]. Secondly it is difficult to keep the camera angle compared to the ground constant, since the angle of the quadcopter changes when moving and hovering. One of the most important advantages is the fact that a quadcopter could have a large area available for the placement of PV panels, which would benefit the purpose of our project. An extensive overview of advantages and disadvantages of a quadcopter are listed in table 2.1.

Figure 2.1: Quadcopter example [8]

Table 2.1: Advantages and disadvantages of a quadcopter

Advantages	*Disadvantages*
Easy to engineer	Less energy efficient than airplane solutions
Can take still photos	Photos while moving changes camera angle
Very flexible movements	Simple square shape is more fragile
Possibly a lot of area for solar panels	Low payload

2.2. Single-rotor

A single-rotor, or helicopter, type of UAV is contrary to the fact that it is called a single-rotor type, two rotors. These rotors consist of a large rotor and a smaller, tail rotor. These types of UAVs are much more efficient than it's multi-rotor counterpart [10], but still less efficient than a fixed-wing solution according to [6]. Besides that, such a solution has little to no suitable room for solar solutions. Therefore, these types will not be further considered since they are not a suitable solution for solar powered UAVs.

Figure 2.2: Single rotor example [1]

2.3. Fixed-wing

Next to this distinction, another type of drone can also be investigated, the fixed-wing. Fixed-wing type UAVs are entirely different in build and using purposes. Where rotor types are able to suspend themselves in mid-air, fixed-wing UAVs are constantly moving at a certain horizontal speed. They remain at altitude by the lift force generated by the wings, which counteracts the gravitational force. This way, it moves in a more efficient way than a rotor type UAV. This, and the fact that it is always moving, is why it is very suitable for long distance operations, such as mapping. The main disadvantage of a fixed-wing solution is that it is less flexible in moving around mid-air and needs either a runway (a small grass field is usually enough) or some sort of launching base to propel it into the air

Table 2.2: Advantages and disadvantages of a fixed-wing UAV

Advantages	*Disadvantages*
More energy efficient	No photos from still position / cannot suspend in mid-air
Constant angle while moving (at equal altitude)	Only suitable area for solar panels is on the wings
More robust shape	Needs a runway or launching mechanism
Higher payload	

2.4. Fixed-wing hybrid

The final type researched is a fixed-wing hybrid UAV. This type of UAV has VTOL (Vertical Take-Off and Landing) capabilities and can take-off and land vertically as the name suggests, while in the air flies like a fixed-wing UAV. With this design the aim is to combine the benefits of a multi-rotor with the flying efficiency of a fixed-wing UAV. However this leads to a complex design and a bigger chance of complications during flying.

(a) Fixed wing drone [12]

(b) Fixed wing hybrid [7]

Figure 2.3: Fixed wing vs Fixed wing hybrid

2.5. UAV type selection

For the drone selection, a few criteria are important. The table on the next page shows these criteria per section for the four types of drones we distinguished. All the way on the right, the weight per criteria is indicated, with '10' being the most important and '1' being not important at all. From this table it becomes clear that a fixed wing is the best option, especially when the red factors are taken into account. The quadcopter has a low payload capacity and mounting the PV cells would be difficult. For the single-rotor UAV, the placement of the PV cells would also be difficult. The concept of a VTOL UAV is quite new, so the simulation would be difficult to make and the complexity of the design would make it more difficult to make it solar powered. Next to that, it would also be rather expensive.

UAV Types		Multi-rotor	Fixed-wing	Single-rotor	Fixed-wing hybrid	Importance
General specs	Range	short	long	short	long	10
	Speed	limited	variable	variable	variable	4
	Efficiency	low	high	medium	medium	10
	Flight time	20-30 min	couple of hours	higher than multi-rotor	higher than multi-rotor	10
	Payload capacity	small	medium	high	variable	8
Controllability	In air stability/ camera control	high	medium	high	high	8
	Runway	VTOL	yes	VTOL	VTOL	2
	Skill training	not needed	required	required	required	2
	Controllability	easy	medium	easy	easy	7
	Ability to stay at same height	oke	oke	oke	oke	8
Robustness	Maintenance	not often	not often	often	often	2
	Waterproof	per case	per case	per case	per case	2
	Shockproof	per case	per case	mostly not	per case	4
Adjustability	Possiblity changing casing	per case	per case	per case	per case	1
	Attachment solar cells	not easy (payload capacity)	easy	low	medium	10
	Impact of changes on efficiency	high	low	Low	low	6.5
	Efficiency optimalization	low	high	medium	high	10
	Rotor adjustability	high	Medium/High	high	medium	2
	PV potential/Area	High	Medium/High	None	Medium	8
Other	Risk of use	possibly	possibly	yes (strong big blades)	possibly	5
	Easily simulatable	medium	yes if drag constants are known	medium	no	8
	Costs	low	medium	high	high	7
	Datasheet	per case	Per case	per case	per case	5
	Remarks					
	Link					

2.6. UAV selection

In the last section, the decision was made to design a fixed-wing UAV. To optimize the performance of the drone all the components needed for the drone are chosen manually and described in chapter 3. To select a frame, the payload capacity has to be high enough to carry all the components and a decent camera for albedo mapping. Furthermore, it should be possible to attach PV cells on the frame. There are a lot of frames available, but in the end the frame of the Skywalker X8 was chosen as it was a frame that was commercially available, easily implemented for simulations and has a large wing area. Next to this, it was a relatively cheap UAV. Models of the frame have been found as well to analyse the aerodynamics of the frame needed for modeling of the entire UAV.

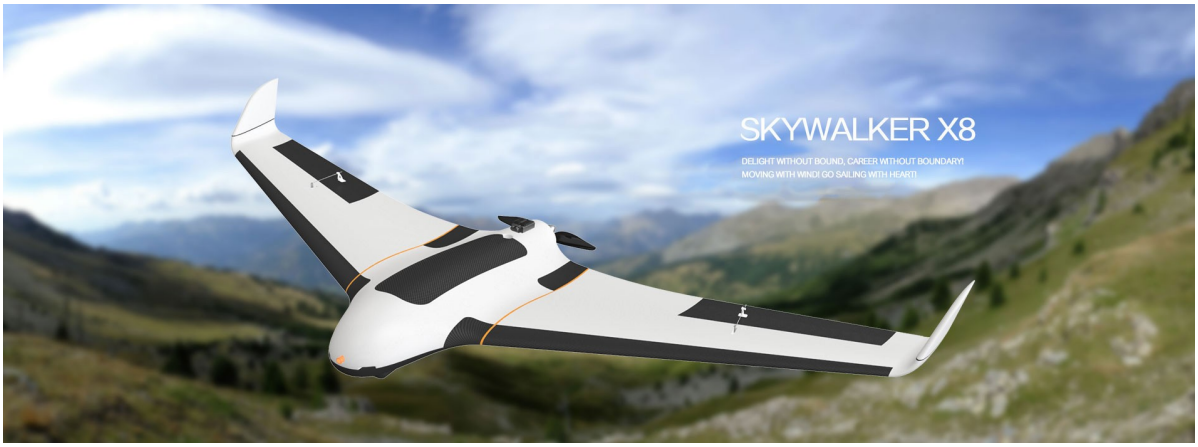

Figure 2.4: The Skywalker X8 [15]

The Skywalker X8 is a fixed wing, single rotor UAV. The specifications of the Skywalker X8 are as follows:

Model	Skywalker X8
Wingspan	2122 mm
Length	820 mm
Payload volume	9550 cm^3
Mean aerodynamic chord	357mm
Max wing curve	8.9 degrees
Typical cruising speed	65 km/hr
Maximum speed	85 km/hr
Body weight	880 g
Maximum take off weight	3200-4200 g

Table 2.3: Frame specifications

The specifications show a large payload volume and high payload capacity for all the components and equipment. Large wings to place the PV cells on, but with a wingspan of 2122mm and the possibility to detach the wings from the body, compact enough for transportation. Finally it is important that there are models available of the frame and aerodynamic specifications can be found or calculated to simulate the characteristics of the frame.

3

Component selection

In this chapter the different components that were chosen for the implementation of our system are discussed. To complete the skywalker X8, an Auto-pilot, propeller, motor, speed controller, battery and a camera needed to be selected.

3.1. Auto-pilot

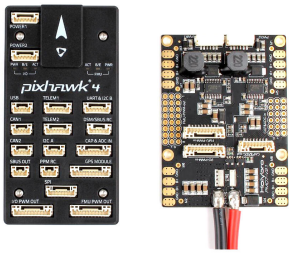

Figure 3.1: Chosen Auto-pilot [3]

The autopilot is a mini computer that controls the motor and servos during the flight using sensor and telecommunication hardware. The requirements for our autopilot are the following:

1. It is commercially available product.
2. Works with other selected components and is easy to implement.
3. Can fly stand-alone.
4. Easy to set way points/flight route to fly.
5. Functionality to implement safety instructions.

Because the the auto-pilot will not be simulated in Simulink and no physical implementation will be made. Little research was done for this component. The above mentioned requirements were taken into account but no comparison was made between all the available auto-pilots on the commercial market. For our application we have chosen the Holybro Pixhawk 4, because this device is affordable and meets our requirements. See the appendix A.2 for the further specifications.

3.2. Propeller

The propeller is able to convert the rotational energy into thrust force. Generally, the greater the propeller area, the higher the thrust force and propeller efficiency, as long as the motor is able to supply the required torque. Also, the propeller needs to fit on the UAV. The recommended maximum propeller size for the frame that was chosen, is 11" x 7", so for the propeller this size is taken. To have useful propeller data, a Graupner Nylon 11" x 7", which is covered in PropCalc [17], was used. The test data provided by this program is shown in figure 3.3, where efficiency is plotted against the speed.

Figure 3.2: Chosen Propeller [5]

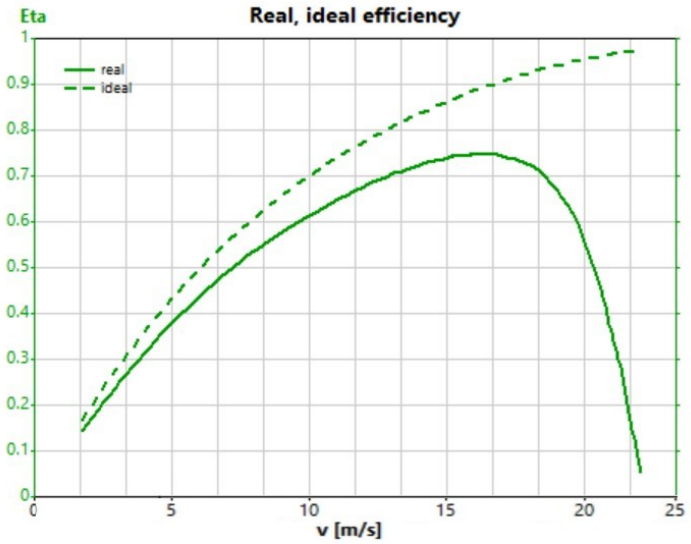

Figure 3.3: Propeller efficiency of the Graupner Nylon 11" x 7"[17]

3.3. Motor

For the motor, the goal is not to create the most efficient drone but to prolong the flight time as long as possible. The most important consideration that is taken into account is the KV. The KV, or RPM/V, depicts how much the RPM of the motor will increase per volt. The KV is linearly dependent on the torque, as is seen in Equation 3.1, where K_t is the torque constant. Furthermore, it is beneficial to have the motor operate at a higher voltage, as this results in a higher efficiency [13].

Figure 3.4: Chosen Motor [2]

$$K_V = \frac{1}{K_t} \tag{3.1}$$

Subsequently, higher torque is needed to drive a higher diameter propeller as a higher diameter propeller has more air resistance or, in other words, can propell more air around. This is why the lowest recommended KV motor was chosen, which is the Turnigy Aerodrive 4250 KV500. However, next to this, the motor should also be able to deliver a power of at least 200W, as this is the expected consummated power by keeping the UAV in the air. The chosen model's specifications are shown in table 3.1.

Specification	Unit
Motor model	Turnigy Aerodrive 4250 KV500
KV	500 RPM/V
Maximum power (5S)	1350W
Maximum current	57A
Burst current	70A
Weight	269g

Table 3.1: Motor specifications

3.4. Speed controller

A speed controller is responsible for the three-phase control of the motor. Therefore it must be able to handle the maximum rated current of the motor, which is 60 A. Other requirements regarding the selection of the speed controller is that it should be light weighted and commercially available.

Figure 3.5: Chosen Speed controller[11]

For the selection of the speed controller the following speed controllers were condisered; the Aerostar RVS 60A Electronic Speed Controller w/Reverse Function 5A BEC, YEP 60A (2 6S) SBEC Brushless Speed Controller, Turnigy Plush-32 60A Speed Controller w/BEC and the HobbyKing 60A ESC 4A SBEC. From these options, the Aerostar RVS speed controller was chosen for a number of reasons. First, this controller is able to handle a 60A motor rating that is able to handle the voltage of a five series battery cell configuration. It is also light weight in comparison with the Yep en Turnigy speed controllers, namely 20 gram. Furthermore, it has a build-in Battery Eliminator Circuit (BEC) and the efficiency is known.

The specifications of the chosen speed controller can be found in table 3.2

Specification	Unit
Motor model	Aerostar RVS 60A Electronic Speed Controller w/Reverse Function 5A BEC
Maximum current	60A
Weight	44g
Size	56 x 30 x 14mm
Efficiency	83-87% (Higher efficiency at lower voltages)

Table 3.2: ESC specifications

3.5. Battery

When choosing a battery, a trade-off regarding the battery size should be made. A bigger battery capacity will not always extend the flight range because the weight will also impact the payload and so the power consumption. Therefore, a light weighted but high capacity battery is preferred and a high energy to mass ratio is wanted. The battery also needs to be sufficient for the high current demands of the motor, it must be commercial available and the characteristics of the battery need to be specified for the simulations.

Figure 3.6: Chosen battery[14]

When taking these specifications into consideration, it can be found that li-ion batteries offer the highest energy density and have a storage efficiency close to 100%. The lithium nickel cobalt manganese-oxide (NCM) compound meets the requirements for high specific capacity (mAh/g) and this technology is commercial available.

Within the different commercial NCM li-ion cells, the following types are compared; the Sanyo NCR2070C, Molicel INR21700-P42A, the Samsung INR21700-40T, the Samsung INR21700-30T and the Molicel INR20700A. There was found a good energy/mass ratio of 0.224wh per gram for the Molicel INR21700-P42A. This cell is also able to deliver a high maximum output current of 45A.

After comparing different configurations of this battery cell, the configuration with 5 cells in series and 3 of these series configurations in parallel meets the required capacity, input voltage and the continues current.

Also the weight, volume and expected price fits in the range of the drone specifications. Therefore, this configuration is chosen. The specification of this battery pack can be found in table 3.3. For every series string, a safety component is added that prevents high charge and discharge currents flowing trough the battery. The specifications of this safety component can be found in the appendix.

Specification	unit
Battery model	Molicel INR21700-P42A
Voltage	18.5V
Capacity	12000 mAh
Max continues current	135 A
Weight	990 gr
Volume	115.8 cm3

Table 3.3: Battery Pack specs

3.6. Camera

To be able to create Albedo maps, a camera is needed that is able to create high quality images. Since there are flight-height restrictions imposed by the Dutch government that withholds UAV's to fly higher than certain heights, the camera should be able to create quality images around 120m. To be able to do this it should have a maximum ground spatial distance (GSD) of 20cm at a shutter time less or equal to 1/1000s. Another requirement is that the camera should be able to create RAW linear images to make sure the images are easily edited for Albedo map creating. The camera should have stabilisation in order to be less affected by the turbulence of the UAV and lastly, it should be lightweight and as cheap as possible. The options that were considered were the GoPro MAX, HERO8 Black, AKASO V50, Insta360 ONE X, HERO 7 Black and the Sony Alpha-6000 because these camera's are all compact while having considerably good specifications. However, based on above mentioned specifications the The Sony Alpha-6000 camera with SELP1650 lens is chosen.

Figure 3.7: Chosen Camera [4]

The specifications of the chosen camera can be found in table 3.4

Specification	unit
Camera model	Sony Alpha-6000 camera with SELP1650 lens
Weight	460 gr
Pixels	24.3 MP
Frames per second	11 (in burst mode)
Shutter time	1/4000 s
Maximum field of view	83 degree
Aperture	f/2.8
ISO	100-25600
focal point	15-60mm
focal length	35-75mm
Image output	RAW and JPEG

Table 3.4: Camera specifications

4

System overview

4.1. Introduction

This chapter describes the system overview. First an overview of the weight and cost of the UAV is given. Then the selected components and the selected drone are 3D modeled to show the fit of the described system. Then the inter-component wiring is described and the total system overview is explained.

4.2. Costs

To ensure that the UAV will fly as efficiently as possible, the system needs to be optimized for weight. Next to this, as a business plan has to be generated, the system also has to be optimized for cost. The total weight and cost of all the components and the UAV are described in table 4.1.

Table 4.1: Total weight and cost of UAV

Component	Weight (grams)	Estimation (€)	Costs incl. tax (€)
Body	880	140	239.9
Motor	269	40	38.37
ESC	60	30	30.74
Servo (2x)	40	15	14.22
Propellor	20	15	8.95
Auto pilot/controller	37	180	159.3
Gps for auto pilot	32		
Receiver FrSky R9	5.8	30	29.95
Camera	344	550	650
lens for camera	116		
Battery (18V, 12Ah = 216Wh)	1050	86	123
3x Battery protection	45		45
Wiring and mounting	100		
FrSky Taranis X9 Lite remote ctrl	nvt	120	109
PV panels	616.6	nvt	213.32
Total	**3615.4**	1206	1661.75

4.3. Component fit

After the selection of all the components and the drone, a model of the components can be fitted into the drone. Although the physical UAV will not be created, an estimate of the component fit and thus the weight distribution can be made. Table 4.2 shows the components referenced in chapter 3 and their respective dimensions.

Table 4.2: Overview of the component dimensions

Component	Length (cm)	Width (cm)	Height (cm)	Total volume (cm^2)	Total volume + 2cm marge (cm^2)
Battery	13,2	6,6	7	609.84	1176.48
Camera	12.0	6.7	4.5	361.8	791.7
Motor	not relevant (own space)	not relevant(own space)	not relevant(own space)		
Speed controller	5.6	3.0cm	1.4	23.52	129.2
Propellor	not relevant (own space)	not relevant (own space)	not relevant (own space)		
**DC-DC controller(power management solar panels)	4.5	2.5	2.0	22.5	117
*micro controller - power management	10.16	5.33	2.0	108.3056	356.5312
flight controller(+ auto pilot)	5.5	3.8	1.55	32.395	154.425
**power system	10	5	2	100	336
GPS Module	5.0	5.0	2.5	62.5	220.5
TOTAL				1320.8606	3281.8362

Figure 4.1 shows the 3D fit of the components in the UAV in solid works. Here, the battery is placed more towards the front (the main box visible) to center the weight of the components around the center of mass of the UAV. Thus stabilizing the UAV.

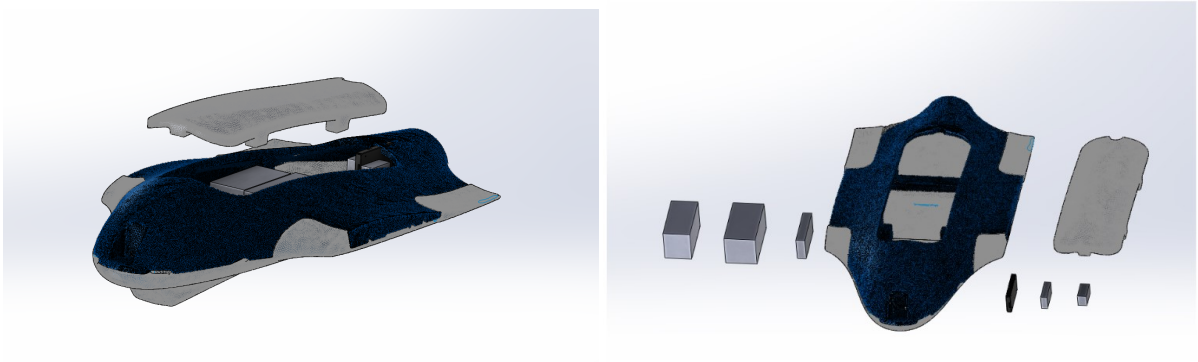

(a) Top view of components in UAV

(b) From Left to right: Camera, Battery, Power system, Autopilot, Speed Controller, DC-DC

Figure 4.1: Top view and closed view of components in the uav

4.4. Inter-Component relationship

Figure 4.2 shows the general overview of the total system. The power supplies are displayed in blue. On the left, the battery cells are connected to the battery management system. This manages the internal cell voltage and ensures enough power is supplied to the secondary systems, such as the ESC and BEC, which is actually integrated inside the ESC but is displayed separately for the completeness of the model. Below, the PV system is interconnected with the power converter. The power converter, subsequently, is supplied with the necessary control data from the (MPPT) micro controller.

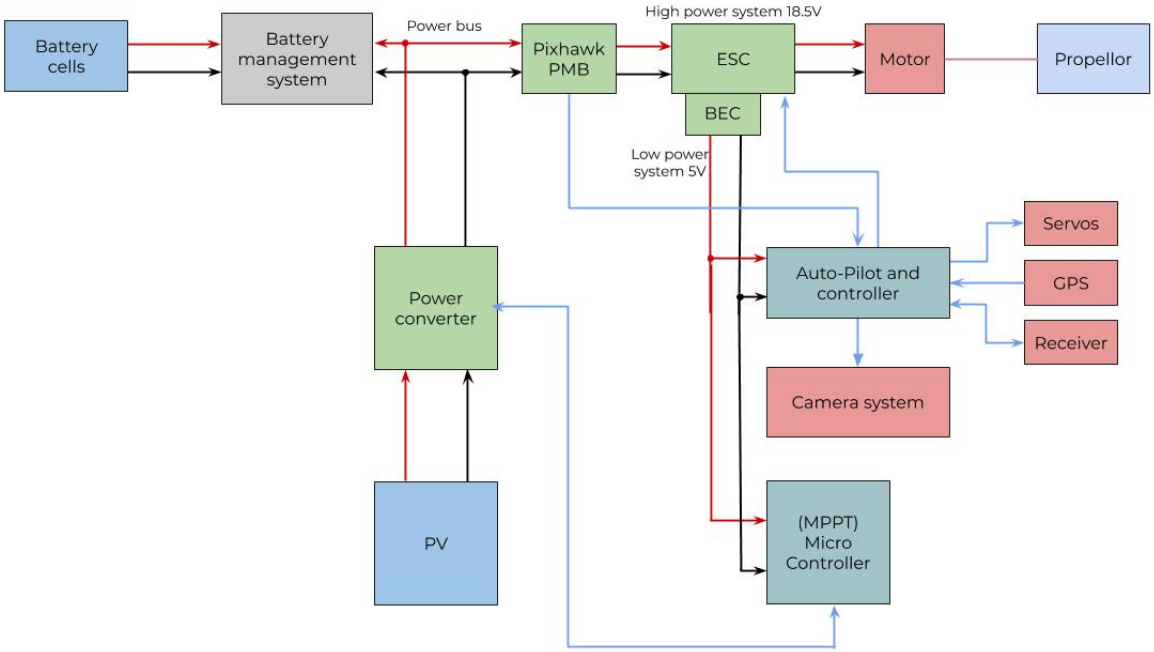

Figure 4.2: System overview diagram

5

Flight simulation

5.1. Introduction

This chapter describes the modelling of the drone. To accurately represent the drone the aerodynamic forces need to be modelled as they influence the power and energy needed for flight. First the general modelling of an air vehicle is explained, then the implementation of the Aerodynamic model in simulink is elaborated on. Next the integration of the electrical And Aerodynamic model is explained. At last, the effect of the aircraft mass and aircraft angle is investigated with the implementation of a mass sweep and an angle sweep.

5.2. Aerodynamic model

When looking at an aircraft, 4 main forces can be identified. The Lift, Drag, Thrust and gravitation force indicate the way the aircraft will fly. Figure 5.1 shows these four forces and their respective orientation with the UAV.

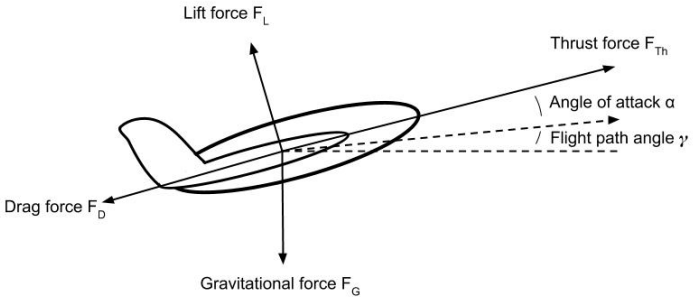

Figure 5.1: Forces on the plane

The Lift force is the result of the airflow above and over the wing lowering the air pressure on the top of the wing, which pulls the wing up-wards and will thus push the aircraft up-wards. It is generally seen as the force which counteracts gravity.

The drag force is the result of the air resistance which the UAV encounters whilst moving through the air. This can be viewed as the amount of force it takes to move the UAV through air. The counteract force to drag is the thrust force. The thrust force indicates the force the motor provides to move the aircraft forward.

Figure 5.1 also shows the angle of attack and the flight path angle. The flight path angle (γ) is the angle of the aircraft path with respect to the ground. The angle of attack (α) is the angle between the incoming air the aircraft experiences with respect to the angle of the aircraft.

The aerodynamic model of the airplane is based on the measurement results and aerodynamic simulations presented in [9] and the electric aircraft Model in Simscape [18].

Simulink implementation of the aerodynamics

The main goal of the aerodynamic model is to determine the power that the motor should provide. The architecture of the model is similar to the implementation of [18] however our model does take the angle of attack into account for determining the lift and drag coefficients as seen in Figure 5.2.

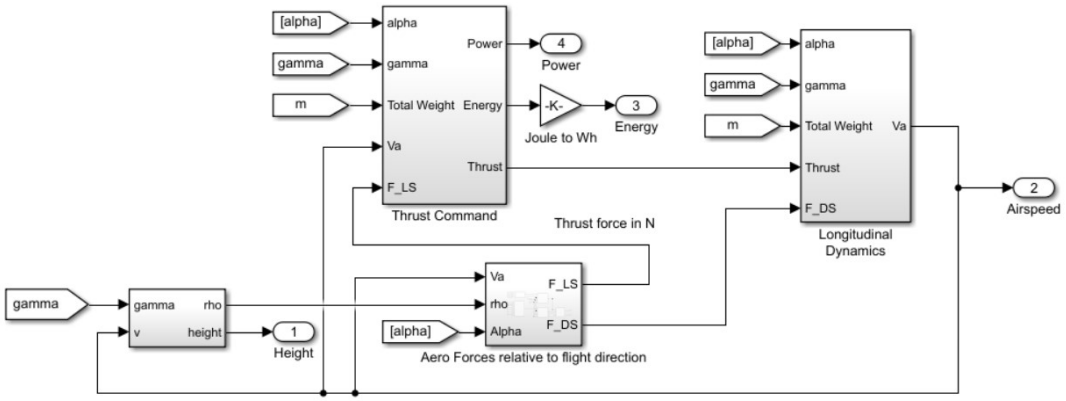

Figure 5.2: Aerodynamics overview

Aerodynamic forces

Table 5.1: Aerodynamic coefficients used as measured by [9]

C_{L_0}	0.0867
C_{L_α}	4.0203
C_{D_0}	0.0197
$C_{D_{\alpha 1}}$	0.0791
$C_{D_{\alpha 2}}$	1.0555

First, the lift and drag coefficients, C_L and C_D respectively, are derived from the angle of attack α according to Equation 5.1 and 5.2.

$$C_L = C_{L_0} + C_{L_\alpha}\alpha \tag{5.1}$$

$$C_D = C_{D_0} + C_{D_{\alpha 1}}\alpha + C_{D_{\alpha 2}}\alpha^2; \tag{5.2}$$

The lift and drag forces, F_L and F_D respectively, are then calculated using the airspeed V_a, air pressure ρ, wing area S_{wing} and the coefficients described above.

$$F_L = \frac{1}{2}\rho V_a^2 S_{wing} C_L \tag{5.3}$$

$$F_D = \frac{1}{2}\rho V_a^2 S_{wing} C_D \tag{5.4}$$

Forces reference system

Three reference frames are present in the simulation as seen in Figure 5.3. Firstly the inertial frame (green) is relative to the ground. This is used for the gravity that is always pointing down. The stability frame (blue) is in the orientation that the airplane is flying. This is the orientation that is relevant to calculate if the airplane accelerates/decelerates and if the lift and motor force counteract the gravity. The third reference frame is the body frame (black) pointing in the same direction as the airplane. This differs from the stability frame because of the angle of attack of the airplane.

The forces of lift, drag and the motor are in the body frame reference. These are therefore rotated by the angle α to go from the body frame to the stability frame.

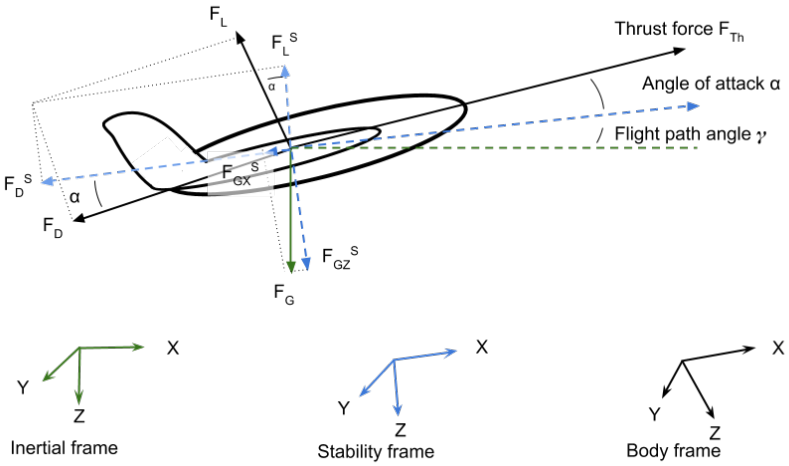

Figure 5.3: Reference systems of Aerodynamic forces

Thrust command and longitudal dynamics

The required thrust F_{th}, is calculated based on the difference between aerodynamic lift and opposing force of the weight. The propulsion power P, is determined by multiplying the thrust force by the airspeed.

$$F_{th} = \frac{1}{\sin(\alpha)}(F_G^S - F_L^S) \tag{5.5}$$

$$P = F_{th} V_a \tag{5.6}$$

Where F_G^S F_L^S are the gravitational force with respect to the stability frame visible in 5.3. From this thrust, the drag and gravitational forces in the stability reference frame, F_{Gx}^S and F_D^S respectively and the total airplane mass m, the acceleration $\dot{v}$ is determined. The airspeed is determined by integrating this acceleration.

$$\dot{v} = -F_{Gx}^S - \frac{F_D^S}{m} + \frac{F_{th_x}^S}{m} \tag{5.7}$$

By integrating the airspeed and taking the flightpath angle into account the height of the plane is tracked and the corresponding air density is determined.

If the airplane didn't had enough lift to counteract the gravity the motor thrust will become larger, this will increase the airplane velocity and this results in more lift generated. This feedback loop ensures that the aircraft will acquire a steady state, ascending or descending according to the flight path angle.

Mass and angle of attack sweep

Figure 5.4 was obtained by simulating the airplane model. On the vertical axis the Maximum flight range, the maximum flight duration the cruising speed and the cruising power draw is shown. In each simulation the airplane starts off thrown at a height of 2 meter and an airspeed of 2 m/s. The plane is instructed to climb to a height of 120m and than to maintain level flight until the battery is empty.

This simulation is performed for different airplane weights and different alpha values to obtain the maximum range for all weight configurations.

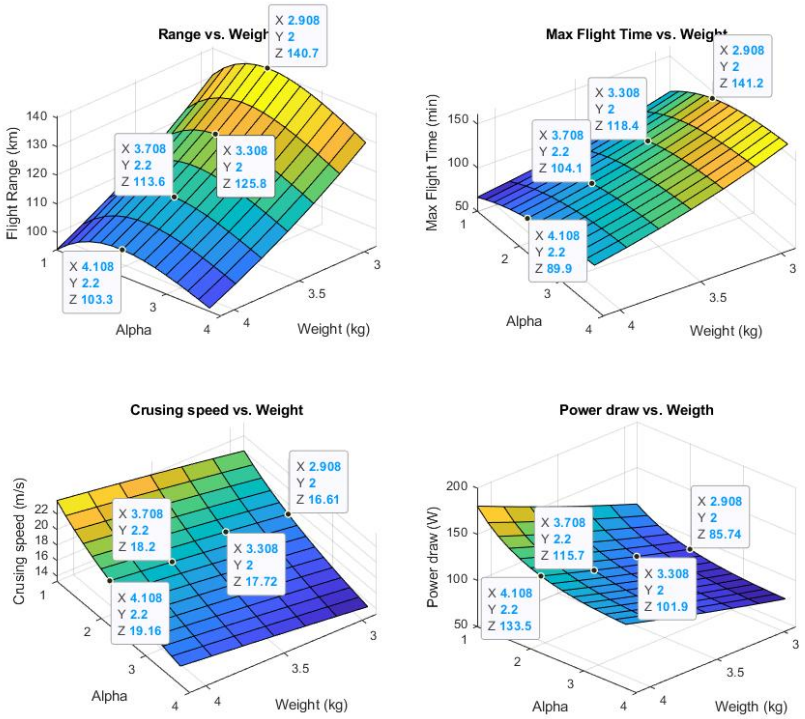

Figure 5.4: Simulation results under varying weight and angle of attack (alpha in degrees)

6

Final simulation

6.1. Introduction

This chapter elaborates on the final simulation done. In this simulation, all the sub-systems were integrated into one big simulation. Fist the simulink is explained after which the results are discussed.

6.2. Simulink Implementation

The overview of the final simulation can be viewed in 6.1. Here, on the left, the battery and the PV power are inputted which provide power to the system. The PV power can be turned on or off to simulate a cloudy day or a sunny day. The on the top right, the flight controller and the aerodynamic model can be found. These simulate the take-off, level flight and landing by adjusting the flight path angle in the aerodynamic model.

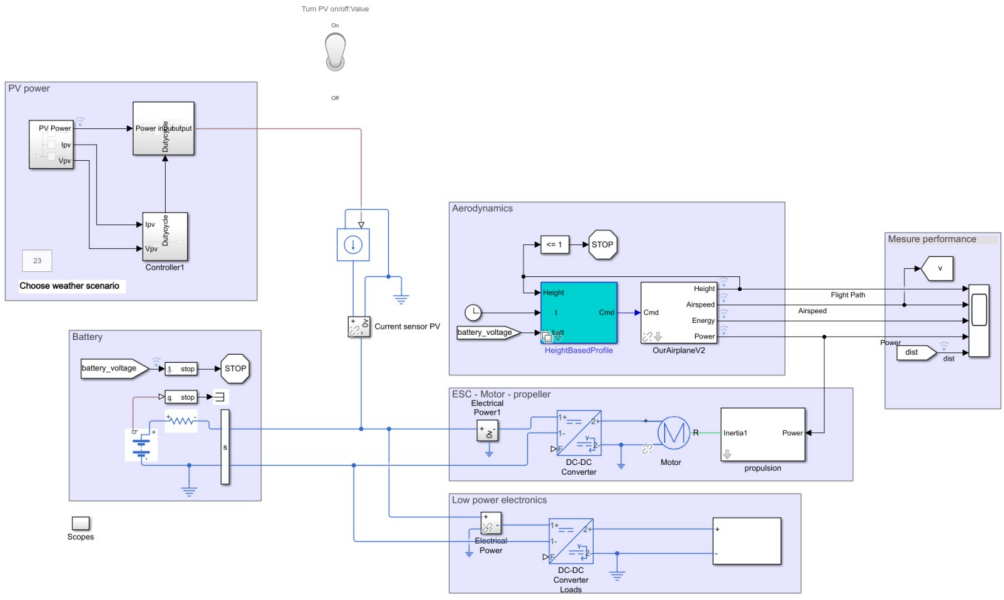

Figure 6.1: Final electrical simulation of the aircraft

The middle block shows the propeller and the motor. The aerodynamic model output the power needed to stay in the air. The propeller and motor then adjust accordingly to provide the necessary torque. Lastly, the bottom block, represents all the secondary systems which need power like the auto-pilot or the speed controller.

6.3. Results of final simulation

Figure 6.2 shows the additional flight range that the PV panels provide. On the left, the worst case scenario is displayed in which the solar irradiance is 129 W/m^2 and the temp equals 21.1 degrees Celsius. Here the flight range is decreased with 4% by the addition of PV as the PV panels add more weight and dus more power is needed than the PV panels deliver. On the Right, the best case scenario is displayed. In this case, the the solar irradiance is 782 W/m^2 and the temp equals 18.5 degrees Celsius. Here the flight range is increased by 83%.

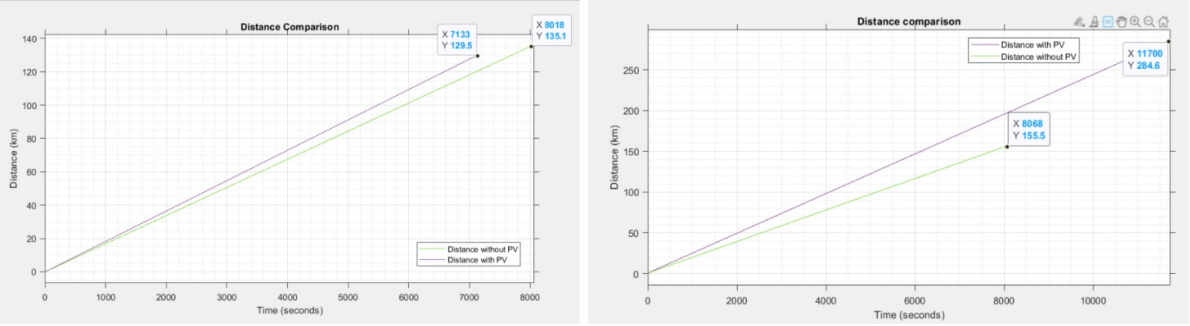

Figure 6.2: Addition to flight range from PV under different weather scenario's

Figure 6.3 shows the overall results of he total simulation, this figure can be found as a larger figure in appendix B.2. In the figure, the purple line represents the simulation in which PV panels are used. The green line represents the simulation without the PV panels. The right On he top left, the increased flight time becomes visible. We can see that the drone will fly for a long period of time before it lands. On the bottom left, it becomes visible that the discharging of the battery goes slower when PV panels are added.

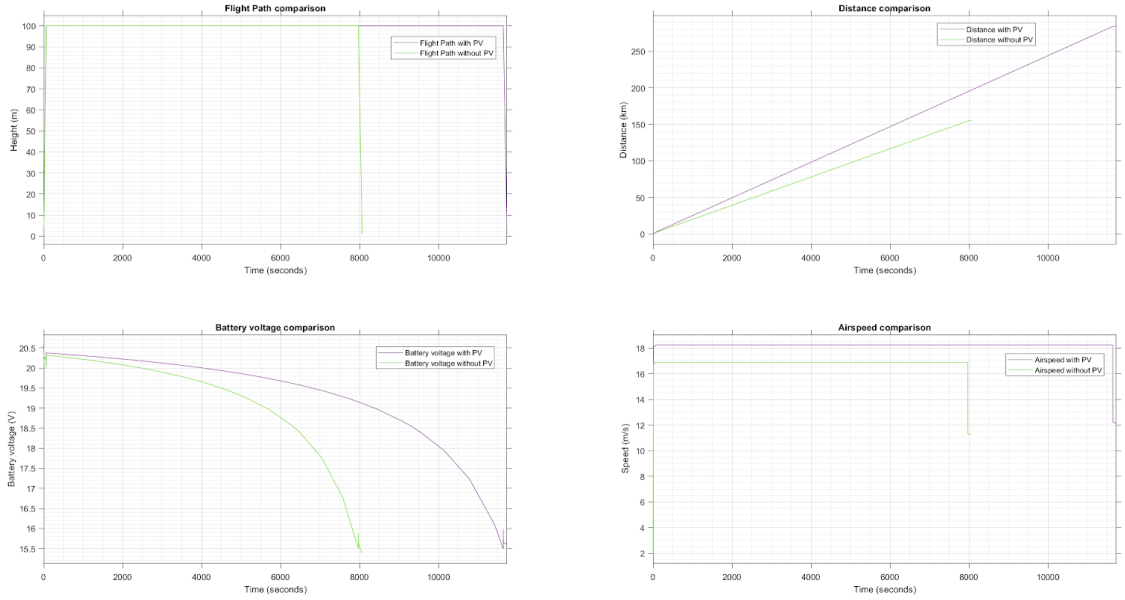

Figure 6.3: Comparison of flight path with and without PV

On the left, the difference in range becomes clear. In this particular situation, as mentioned in 6.2, the solar panels added 83% increase in range.

6.4. Flight path calculation

The flight path of the UAV is dependent on UAV and camera specifications based on the program of requirements, its path should be able generate high quality images while being time efficient. The image will have a good quality when the ground sampling distance (GSD) is lower than 20 cm [16]. The GSD can be calculated using formula 6.1.

$$GSD = \frac{p * H * 1000}{f * cosd(0.5 * FOV)} \tag{6.1}$$

Here p is the pixel size (micron), H is the flight height (m), f is the focal length (mm) and FOV is the field of view (degrees). The camera specifications can be found in section 3.6. The pixel size can be calculated using formula 6.2

$$p = \frac{s_w}{p_w} + \frac{\frac{s_h}{p_h}}{2} \tag{6.2}$$

Here s_w and s_h are the sensor width and sensor height respectively and p_w and p_h are the pixel width and pixel height respectively. Based on these calculations, the GSD is 17.93cm when flying at a height of 120m, which is sufficient. Now, another specification that is needed to guarantee the quality of the generated albedo map is image overlapping. There is a forward overlap of images needed of 65% and a sideward overlap of 40% [16]. The following formula's are used.

$$d_f max = \frac{v}{fps * 3600} \tag{6.3}$$

$$d_s need = \frac{\frac{(1-o_s ide) * H * s_w}{f}}{1000} \tag{6.4}$$

In formula 6.3 the forward distance between every picture d_{fmax} (m) is calculated based on the speed v of the UAV (m/s) and the frames per second fps (1/s), and is 1.6 meter. The needed side overlap d_{sneed} is calculated in formula 6.4 to be 48.5 meters. Lastly, in order to create a flight path, the turning radius of the UAV needs to be calculated. This is done via the following formula's.

$$R_f = \frac{(0.54 * v)^2}{11.26 * tand(30)} \tag{6.5}$$

$$R = \frac{\frac{R_f}{3.28}}{1000} \tag{6.6}$$

$$l_c = 0.5 * \pi * R \tag{6.7}$$

Here R_f is the possible radius in foot, which is dependent of the velocity v of the UAV. In formula 6.6, the radius is transformed from foot to kilometer. In formula 6.7 the minimum length of the turn is calculated. This is 363 meter. Based on previously mentioned outcomes, a flight path is chosen. This can be seen in figure 6.4.

The total flight range is calculated via formula 6.8. Here l_{fl} is the length of the flight lines, which is based on the length of the TU Delft and is 2.1km. l_{ctop} and l_{cdown} are the lengths of the turning circles for the top part of the figure and bottom part of the figure respectively, which are 686m and 609m . n_{rtop} and n_{rdown} are the number of turns for the top and bottom part respectively, which are 9 and 8. l_{to} and l_l are the take-off length and the length for landing respectively. They are both chosen to be 1 km to be on the safe side.

$$d_{tot} = (n_{fl} * l_{fl}) + (l_{ctop} * n_{rtop}) + (l_{cdown} * n_{rdown}) + l_t o + l_l \tag{6.8}$$

This gives a total flight path length of 48.75 km. The corresponding flight time, given that the speed of the UAV is 65km/h is 00:45 hours.

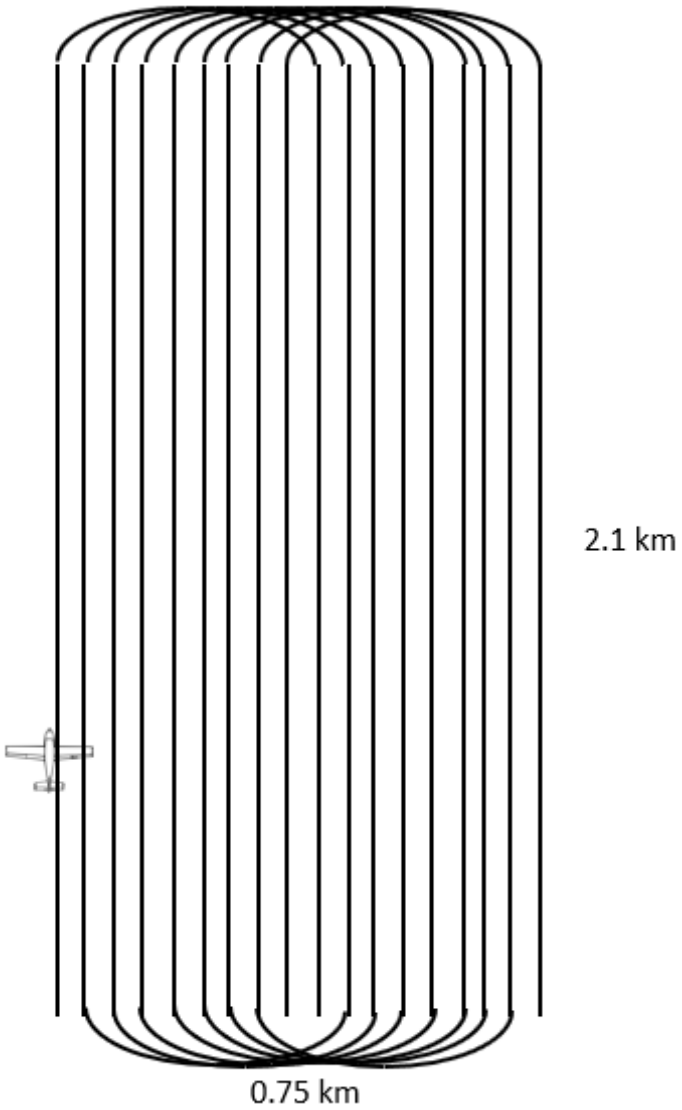

Figure 6.4: Flight path of the area of the TU Delft

6.5. Power consumption in flight

Figure 6.5 shows the power consumption by the system and the power generated from the battery and PV in the best case scenario. The Solar irradiation equals 887 W/m^2 and the temperature equals 21.2 degrees. From this graph, it becomes visible that the solar panels generate about 50W, the battery generates about 60W and the motor + secondary system consume about 110W. Figure 6.6 shows the power consumption by the system

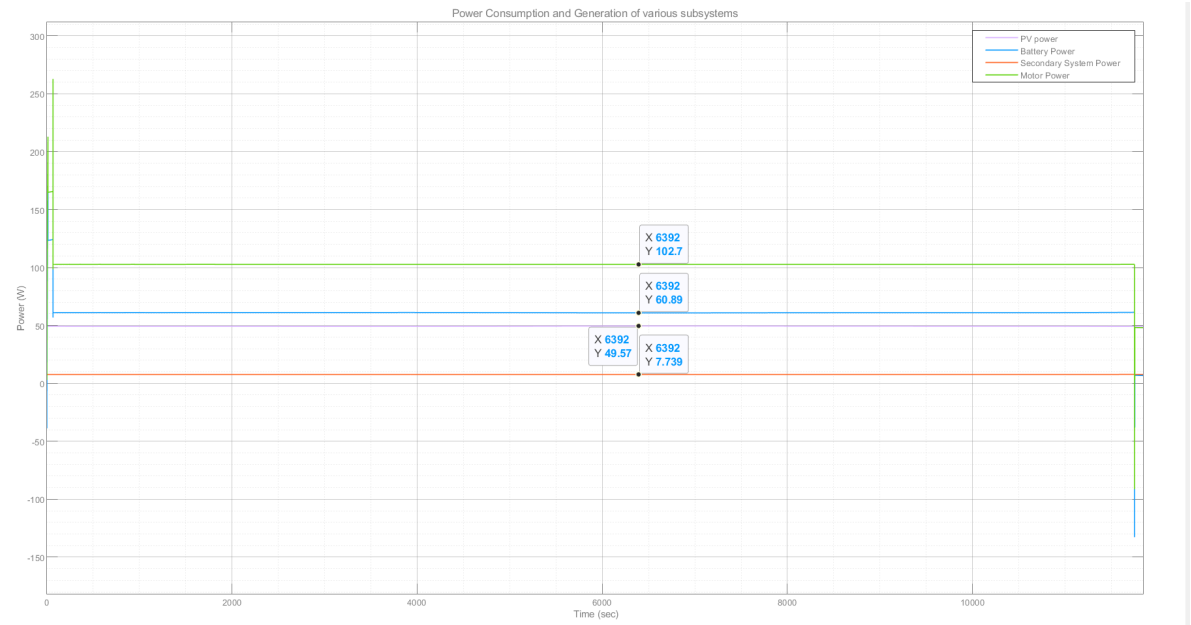

Figure 6.5: Power consumption of the system in the best case scenario

and the power generated from the battery and PV in the worst case scenario. The Solar irradiation equals 0 W/m^2 and the temperature equals 4.4 degrees. From this graph, it becomes visible that the solar panels generate 0W, the battery generates about 100W and the motor + secondary system consume about 110W.

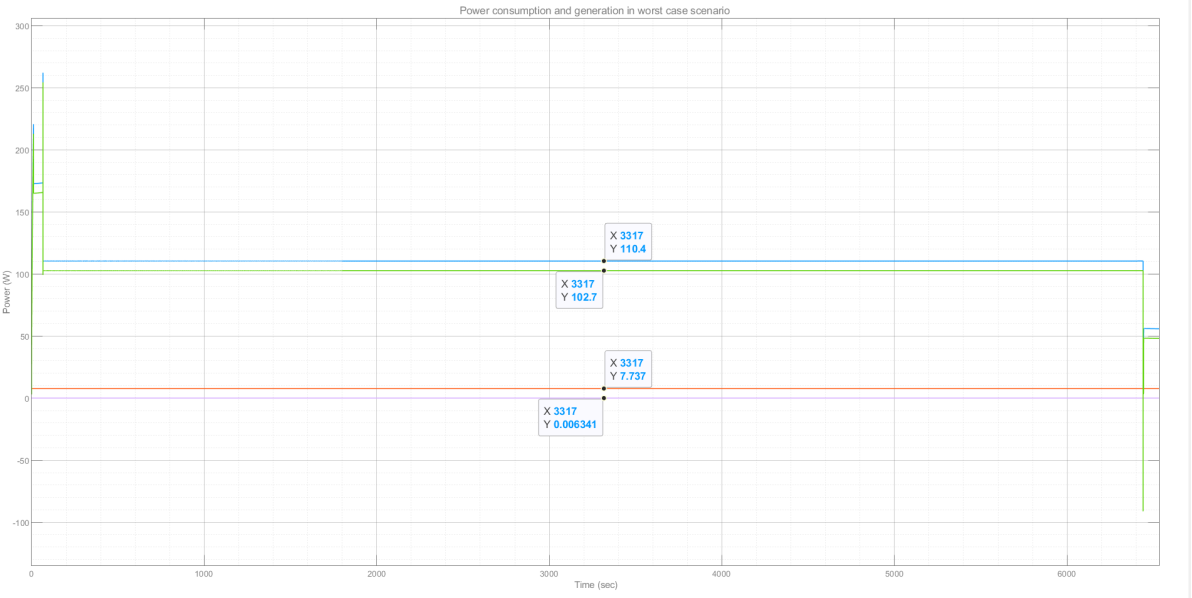

Figure 6.6: Power consumption of the system in the worst case scenario

Figure 6.6 shows the power consumption by the system and the power generated from the battery when no PV panels are added. From this graph, the battery generates about 82W and the motor + secondary system consume about 89W.

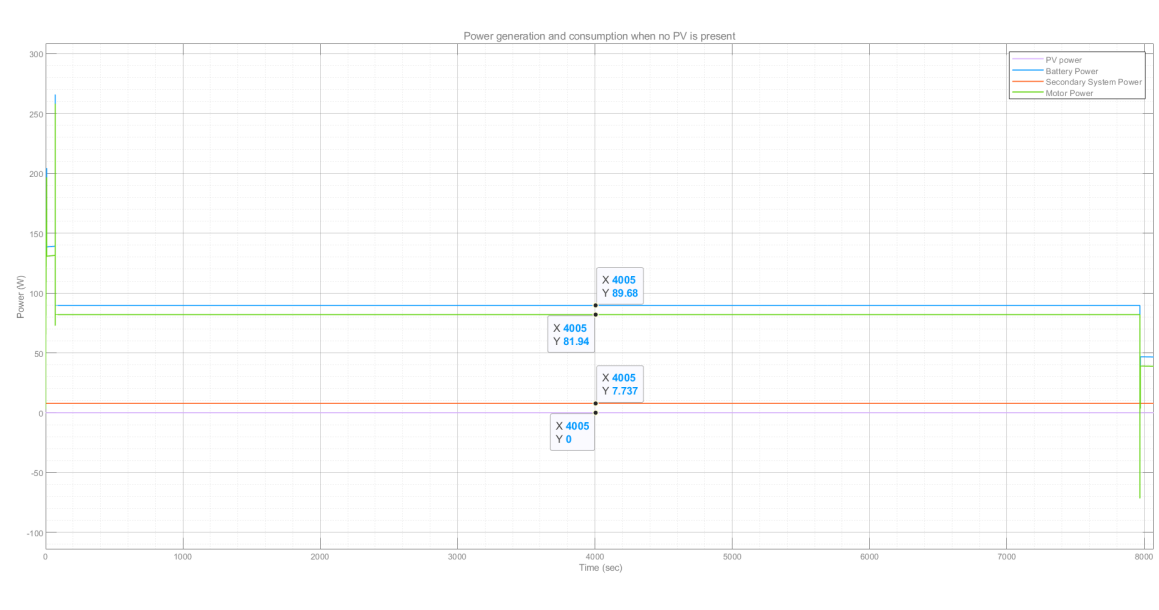

Figure 6.7: Power consumption of the system when no PV panels are added

Bibliography

[1] Alibaba. Single rotor drone. URL https://www.alibaba.com/product-detail/2018Years-Single-rotor-Drone-Agriculture-Sprayer_60761797076.html.

[2] Allegro. Silnik sk3 4250 kv500 4s-6s li-po turnigy rc. URL https://allegro.pl/oferta/silnik-sk3-4250-kv500-4s-6s-li-po-turnigy-rc-7150196451.

[3] Banggood. Holybro pixhawk 4. URL https://nl.banggood.com/Holybro-Pixhawk-4-PX4-Flight-Controller-STM32F765-32-Bit-ARM-for-RC-Drone-FPV-Racing-p-1302139.html?ID=534789&cur_warehouse=CN.

[4] Bol. Sony alpha 6000. URL https://www.bol.com/nl/p/sony-a6000-16-50mm/9200000025106838/.

[5] Hobby Direkt. Graupner propeller. URL https://www.hobbydirekt.de/Zubehoer/Luftschrauben/Nylon/Plastikpropeller/Prop-28x18cm-11x7-Zoll-Graupner-1316-28-18::37462.html?language=en.

[6] Dario Floreano and Robert J Wood. Science, technology and the future of small autonomous drones. *Nature*, 521(7553):460–466, 2015.

[7] Idea Forge. Hybrid fixed wing drone. URL https://www.ideaforge.co.in/drones/switch-uav/.

[8] Geekbuying. Quadcopter,. URL https://nl.geekbuying.com/item/SHRC-H2-Locke-2K-WIFI-\FPV-RC-Quadcopter-RTF-White-Two-Battery-413824.html.

[9] Kristofer Gryte, Richard Hann, Mushfiqul Alam, Jan Roháč, Tor Arne Johansen, and Thor I Fossen. Aerodynamic modeling of the skywalker x8 fixed-wing unmanned aerial vehicle. In *2018 International Conference on Unmanned Aircraft Systems (ICUAS)*, pages 826–835. IEEE, 2018.

[10] jojo. Types of drones – explore the different models of uav's, ?? URL http://www.circuitstoday.com/types-of-drones.

[11] Hobby King. Aerostar rvs 60a. URL https://hobbyking.com/nl_nl/aerostar-rvs-60a-electronic-speed-controller-w-reverse-function-and-5a-bec-2-6s.html.

[12] Betsy Lillian. sensefly's latest fixed-wing mapping drone is here, October, 2016. URL https://nl.geekbuying.com/item/SHRC-H2-Locke-2K-WIFI-\FPV-RC-Quadcopter-RTF-White-Two-Battery-413824.html.

[13] David Lundström, Kristian Amadori, and Petter Krus. Validation of models for small scale electric propulsion systems. In *48th AIAA Aerospace Sciences Meeting Including the New Horizons Forum and Aerospace Exposition*, page 483, 2010.

[14] Lygte. Molicel inr21700-p42a 4200mah (gray). URL https://lygte-info.dk/review/batteries2012/Molicel%20INR21700-P42A%204200mAh%20(Gray)%20UK.html.

[15] Rioku. Skywalker x8 drone, 2018. URL http://www.regimage.org/skywalker-x8-drone/.

[16] Birute Ruzgiene. Requirements for aerial photography. page 79, 12 2004.

[17] Helmut Schenk. Propeller calculator, ?? URL http://www.drivecalc.de/PropCalc/.

[18] Steve Miller Zhao Wang. Electric aircraft model in simscape, 2018. URL https://www.mathworks.com/matlabcentral/fileexchange/64991.

A

Components

Turnigy Aerodrive SK3 - 4250-500kv Brushless Outrunner Motor

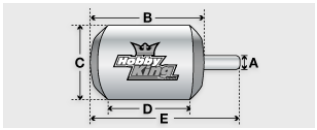

SKU: SK3-4250-500
425 g

Config Table

K_V	500 RPM/V
Weight	269 g
Max Current	57 A
Max Voltage	19 V
Power	1350 W
Internal resistance	18 mohm
Shaft (A)	5 mm
Length (B)	58 mm
Diameter (C)	42 mm
Can Length (D)	34 mm
Total Length (E)	80 mm

Figure A.1: Motor - Turnigy Aerodrive SK3 - 4250-500kv specifications

pixhawk® 4 mini

The power of Pixhawk® 4 in a compact form

Product Features

- Half the footprint of the *Pixhawk® 4*
- The same FMU processor and memory resources as the *Pixhawk 4*
- Aluminum casing for great thermal performance
- Easy to connect to commercial ESCs
- The latest sensor technology from Bosch® and InvenSense®
- Redundant IMUs for reliable performance
- NuttX real-time operating system
- Pre-installed with the most recent PX4 firmware

The *Pixhawk® 4* Mini autopilot is designed for engineers and hobbyists who are looking to tap into the power of *Pixhawk 4* but are working with smaller drones. *Pixhawk 4 Mini* takes the FMU processor and memory resources from the *Pixhawk 4* while eliminating normally unused interfaces. This allows the *Pixhawk 4 Mini* to be small enough to fit in a 250mm racer drone. The *Pixhawk 4 Mini* is easy to install; the 2.54mm (0.1in) pitch connector makes it easier to connect the 8 PWM outputs to commercially available ESCs.

Pixhawk 4 Mini was designed and developed in collaboration with Holybro® and Auterion®. It is based on the Pixhawk FMUv5 design standard and is optimized to run PX4 flight control software.

Figure A.2: Auto pilot - Pixhawk 4 mini specifications

TURNIGY Manual for Brushless Motor Speed Controller

Thank you for purchasing our Electronic Speed Controller (ESC). High power systems for RC model can be very dangerous; we strongly suggest you read this manual carefully. We have no control over the correct use, installation, application, or maintenance of our products, no liability shall be assumed nor accepted for any damages, losses or costs resulting from the use of the product. Any claims arising from the operating, failure or malfunctioning etc. will be denied. We assume no liability for personal injury, property damage or consequential loss resulting from our product or our workmanship. As far as is legally permitted, the obligation to compensation is limited to the invoice amount of the affected product.

Features:

- **Lithium battery Balance Discharge Monitoring and Protecting (BDMP) Design**, monitors in real time the discharge voltage of each lithium (Li-ion/Li-poly) cell in a battery pack. Don't worry about the over discharge problem again, your lithium battery pack will have a much longer life. **(Remark: This BDMP function is ONLY available for "SENTRY" series ESC)**
- Extreme low resistance, high current endurance.
- Full protection features: Low-voltage cutoff protection / Over-heat protection / Throttle signal lost protection
- 3 startup modes: Normal / Soft / Super-Soft, can be used for both fixed-wing aircraft or helicopter models
- Throttle range can be configured, fully compatible with all kinds of available transmitters.
- Smooth and accurate speed control, excellent throttle linearity.
- Microprocessor uses separate voltage regulator IC (except PULSAR-6A and PULSAR-10A), with high anti-jamming capability.
- Supports up to: 210000 RPM (2 poles), 70000 RPM (6 poles), 35000 RPM (12 poles) motors.
- The program card is a very small device which can be purchased additionally for easy programming the ESC in the field.
- With a program card, you can activate the music playing function of ESC, and there are 15 songs can be selected.

Specifications:

PLUSH Series

Class	Model	Cont. Current	Burst Current (>10s)	BEC Mode	BEC Output	Battery Cell: Li-ion Li-poly	Battery Cell: NiMH NiCd	User Programmable	Balance Discharge Protection	Weight	Size L*W*H
6A	PLUSH-6	6A	8A	Linear	5V/0.8	2	5-6	Available	N/A	6g	24*12*6
10A	PLUSH-10	10A	12A	Linear	5V/2A	2-4	5-12	Available	N/A	9g	27*17*6
12A	PLUSH-12	12A	15A	Linear	5V/1A	2-4	5-12	Available	N/A	12g	32*24*8
	PLUSH-12E	12A	15A	Linear	5V/2A	2-4	5-12	Available	N/A	13g	32*24*10
18A	PLUSH-18	18A	22A	Linear	5V/2A	2-4	5-12	Available	N/A	19g	45*24*11
25A	PLUSH-25	25A	35A	Linear	5V/2A	2-4	5-12	Available	N/A	22g	45*24*11
	PLUSH-25-OPTO	25A	35A	N/A	N/A	2-4	5-12	Available	N/A	21g	45*24*11
30A	PLUSH-30	30A	40A	Linear	5V/2A	2-4	5-12	Available	N/A	25g	45*24*11
40A	PLUSH-40	40A	55A	Switch	5V/3A	2-6	5-18	Available	N/A	35g	55*28*12
	PLUSH-40-OPTO	40A	55A	N/A	N/A	2-6	5-18	Available	N/A	32g	55*28*11
60A	PLUSH-60	60A	80A	Switch	5V/3A	2-6	5-18	Available	N/A	60g	70*31*14
	PLUSH-60-OPTO	60A	80A	N/A	N/A	2-6	5-18	Available	N/A	56g	70*31*13
80A	PLUSH-80	80A	100A	Switch	5V/3A	2-6	5-18	Available	N/A	62g	70*31*14
	PLUSH-80-OPTO	80A	100A	N/A	N/A	2-6	5-18	Available	N/A	58g	70*31*13

SENTRY Series

Class	Model	Cont. Current	Burst Current (>10s)	BEC Mode	BEC Output	Battery Cell: Li-ion Li-poly	Battery Cell: NiMH NiCd	User Programmable	Balance Discharge Protection	Weight	Size L*W*H
18A	SENTRY-18	18A	22A	Linear	5V/2A	2-4	5-12	Available	Available	24g	45*26*11
25A	SENTRY-25	25A	35A	Linear	5V/2A	2-4	5-12	Available	Available	27g	45*26*12
30A	SENTRY-30	30A	40A	Linear	5V/2A	2-4	5-12	Available	Available	29g	45*26*12
40A	SENTRY-40	40A	55A	Switch	5V/3A	2-6	5-18	Available	Available	40g	55*28*15
60A	SENTRY-60	60A	80A	Switch	5V/3A	2-6	5-18	Available	Available	65g	70*31*14
80A	SENTRY-80	80A	100A	Switch	5V/3A	2-6	5-18	Available	Available	67g	70*31*14

BASIC Series

Class	Model	Cont. Current	Burst Current (>10s)	BEC Mode	BEC Output	Battery Cell: Li-ion Li-poly	Battery Cell: NiMH NiCd	User Programmable	Balance Discharge Protection	Weight	Size L*W*H
18A	BASIC-18	18A	22A	Linear	5V/2A	2-4	5-12	Available	Available	24g	45*26*11
25A	BASIC-25	25A	35A	Linear	5V/2A	2-4	5-12	Available	Available	27g	45*26*12

BEC Output Capability	Linear Mode BEC(5V/2A)				Switch Mode BEC(5V/3A)	
	2S Li-Poly	3S Li-Poly	4S Li-Poly	5S Li-Poly	2S — 4S Li-Poly	5S Li-Poly
Standard micro servos(Max.)	5	4	3	2	5	4

IMPORTANT! The ESC named "xxx-xxx-OPTO" hasn't a built-in BEC, so an UBEC (Ultimate-BEC) or an individual battery pack should be used to power the receiver. And an individual battery pack is needed to power the program card when setting the programmable value of ESC, please read the user manual of program card for reference.

TURNIGY Manual for Brushless Motor Speed Controller

Wiring Diagram:

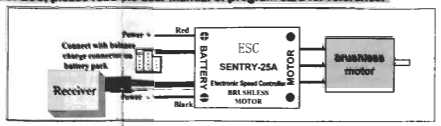

Lithium Battery Balance Discharge Monitoring and Protecting Adapter For "SENTRY" Series ESC:

We provide 2 kinds of Lithium Battery Balance Discharge Monitoring and Protecting Adapters for user to choose.

Adapter #1

Adapter #2

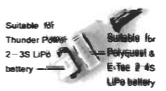

VERY IMPORTANT! You MUST connect the adapter with the balance charge connector on battery pack BEFORE connecting the main power to ESC. And if you use banana-shape connectors on main power wires (input wires), please connect the black wire (negative polarity) BEFORE red wire (positive polarity). So the right sequence is:

Balance discharge adapter → BLACK wire of main power → RED wire of main power

Feature Explanation:

1. **Brake Settings**: Brake Enabled / Brake Disabled, default is Brake Disabled
2. **Battery Type**: Li-xx(Li-ion or Li-poly) / Ni-xx(NiMh or Nicd), default is Li-xx.
3. **Low Voltage Protection Mode(Cutoff Mode)**: Reduce / Cutoff Output Power, default is Reduce the output power gradually.
4. **Low Voltage Protection Threshold(Cutoff Threshold)**: Low / Medium / High, default is Medium.
   - **When NOT using balance discharge monitoring and protecting function** (i.e. **Do Not** plug the balance charge connector into the balance discharge protecting socket on ESC, in this case , the ESC only monitors the voltage of whole battery pack)
     1) For Li-xx battery, number of battery cells are calculated automatically, low / medium / high cutoff voltage for each cell are: 2.6V/2.85V/3.1V. For example: 3 cells Li-Poly, when medium cutoff voltage is set, the cutoff voltage is: 2.85*3=8.55V.
     2) For Ni-xx battery, low / medium / high cutoff voltages are 0%/45%/60% of the startup voltage (i.e. the initial voltage of battery pack), and 0% means low voltage cutoff function is disabled. For example: 10 cells NiMH battery, fully charged voltage is 1.44*10=14.4V, when "medium" cutoff voltage is set, the cutoff voltage is : 14.4*45%=6.5V.
   - **When using balance discharge monitoring and protecting function** (i.e. Plug the balance charge connector on battery pack into the balance discharge protecting socket on ESC, in this case, the ESC monitors not only the voltage of whole battery pack but also the voltage of each cell). For Li-xx battery, low / medium / high cut off voltage for each cell are: 2.6V/2.85V/3.1V. When the voltage of any cell in battery pack is lower than the cutoff threshold, the protecting program is activated.
5. **Startup Mode**: Normal /Soft /Super-soft, default is Normal startup.
   Normal is good for fixed-wing aircraft. Soft and Super-soft are good for helicopters. The initial speed of soft / super-soft mode is very slow, 1 second (soft startup) / 2 seconds (super-soft startup) from startup to full speed. But if throttle is closed (throttle stick is moved to bottom) and opened again (throttle stick is moved upwards) within 3 seconds after the first startup, the restart will be temporarily changed to normal mode to get rid of the chances of crash caused by slow throttle response in aerobatic fly.
6. **Timing**: Low / Medium / High, default is Low.
   In normal cases, low timing can be used for most motors. But for high efficiency, we recommend the **Low** timing for 2 poles motor and **Medium** timing for 6 poles and above. For higher speed, **High** timing can be chosen.
   Important! After you changing the timing setting, please test your RC model on ground firstly!

Special Hint

Some high KV out-runner motors have very special configuration, the space between each alnico is very large, and lots of ESCs can't drive these motors. After updating the program, our ESCs have very good compatibility with them. But some RC fans still have several questions about the programmable value for some special motors. So we just give some suggestions as follows:

Motor \ Programmable Value Suggestion	Timing	Startup Mode
General in-runner motor	Low	Usually, aircraft uses "normal" startup mode helicopter uses "super-soft" startup mode
General out-runner motor	Low or Medium	
Align 420LF (Made in TAIWAN, out-runner)	High (MUST)	
450TH (Made in TAIWAN, out-runner)	Low	Soft (MUST)

Begin To Use Your New ESC

Please start up the ESC in the following sequence:

1. Move the throttle stick to bottom position and then switch on the transmitter.
2. Connect battery pack to ESC, the ESC begins the self-test process, a special tone " ♪123" is emitted, which means the voltage of battery pack is in normal range, and then N "beep" tones will be emitted, means the quantity of lithium battery cells. Finally a long "beep------" tone will be emitted, which means self-test is OK, the aircraft/helicopter is ready to go flying.
   - If nothing is happened, please check the battery pack and all the connections;

Figure A.3: Speed controller - Turnigy Plush 60

MOLICEL®

LITHIUM-ION RECHARGEABLE BATTERY

PRODUCT DATA SHEET

MODEL INR-21700-P42A

■ CELL CHARACTERISTICS

Capacity	Typical	4200 mAh 15.5 Wh
	Minimum	4000 mAh 14.7 Wh
Cell Voltage	Nominal	3.6 V
	Charge	4.2 V
	Discharge	2.5 V
Charge Current	Standard	4.2 A
Charge Time	Standard	1.5 hr
Discharge Current	Continuous	45 A
Typical Impedance	AC (1 KHz)	10 mΩ
	DC (10A/1s)	16 mΩ
Temperature	Charge	0°C to 60°C
	Discharge	-40°C to 60°C
Energy Density	Volumetric	615 Wh/l
	Gravimetric	230 Wh/kg

■ PHYSICAL CHARACTERISTICS

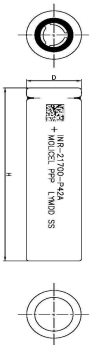

Shape	Cylindrical
Can	Steel
Diameter	21.7 mm (Max)
Height	70.2 mm (Max)
Weight	70 g (Max)

The information contained herein is for reference only and does not imply a performance guarantee or a product warranty. Specifications and characteristics are subject to change without prior notice.

For application specific information, please contact E-One Moli Energy Sales and Applications or the nearest MOLICEL® recognized agent.

■ Charge Characteristics

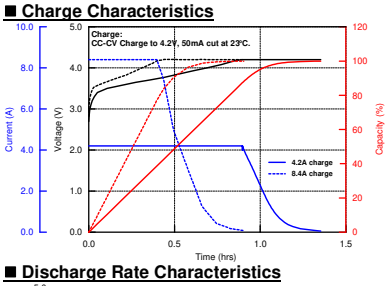

■ Discharge Rate Characteristics

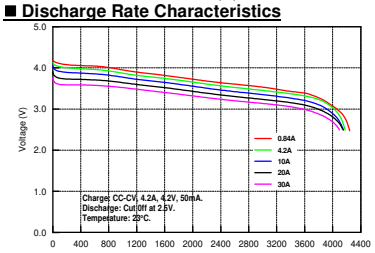

■ Discharge Temperature Characteristics

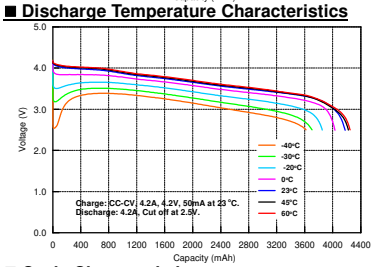

■ Cycle Characteristics

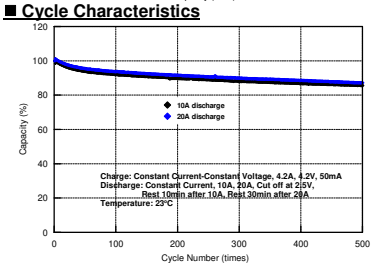

■ **Taiwan Facility**
10 Dali 2nd Rd., Shan-Hwa,
Tainan City, Taiwan, R.O.C.
Tel: 886-6-505-0666
Fax: 886-6-505-0777
mailto:service@molicel.com
http://www.molicel.com

■ **Canada Facility**
20 000 Stewart Crescent
Maple Ridge, BC, Canada, V2X 9E7
Tel: 1-604-466-6654
Fax: 1-604-466-6600
mailto:molicel@molicel.com
http://www.molicel.com

■ **Headquarters**
10F, 113, Sec.2, Zhung Shan N Rd.,
Taipei, Taiwan, R.O.C.
Tel: 886-2-2567-3500
Fax: 886-2-2567-6500

Figure A.4: Battery cel - Molicel P42A specifications

BMS Specifications For 5S /18.5V Li-ion Battery Pack			
Model: LIM-5S1045LI606			
No.	**Test item**		**Criterion**
1	Voltage	Charging voltage	DC:21V CC/CV
		Balance voltage for single cell	4.180V±50 mV
2	Current	Balance current for single cell	80mA±10mA
		Current consumption for single cell	≤6μA
		Maximal continuous Charging current	10A
		Maximal continuous Discharging current	45A
3	Over charge Protection	Over charge detection voltage	4.25V≤±0.025V
		Over charge delay time	1S
		Over charge recovery voltage	4.15V≤±0.025V
4	Over discharge protection	Over discharge detection voltage	2.8V≤± 0.1V
		Over discharge delay time	128ms
		Over discharge release voltage	3.0V≤±0.1V
5	Over current protection	Over current testing voltage	150mv ≤± 15mv
		Over current detection current	90A± 10A
		Over current delay time	12MS
		Release condition	Automatic Recovery
6	Short protection	Detection condition	Exterior short circuit
		Detection delay time	≤300us
		Release condition	Automatic Recovery
7	Resistance	Protection circuitry (MOSFET)	≤20mΩ
8	Temperature	Operating Temperature Range	-40~+65°C
		Storage Temperature Range	-40~+ 125°C
9	Size		L60*W60*T9mm
10	Weight		30g

Figure A.5: Specifications battery protection component

B

Results

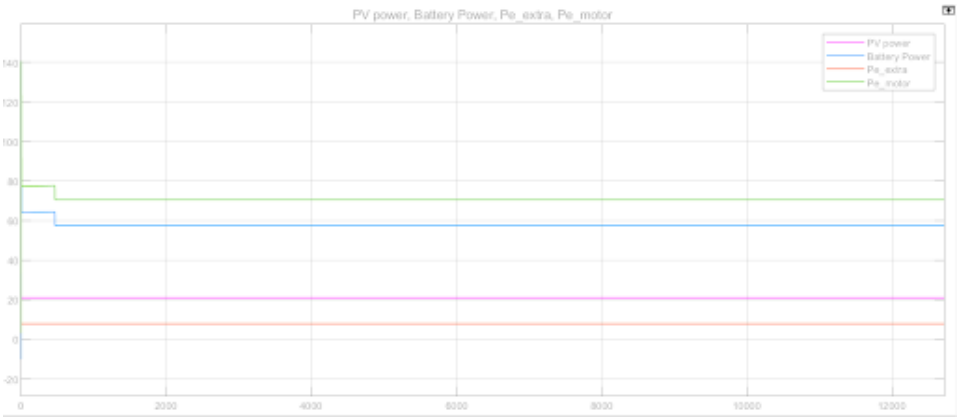

Figure B.1: Power distribution during flight

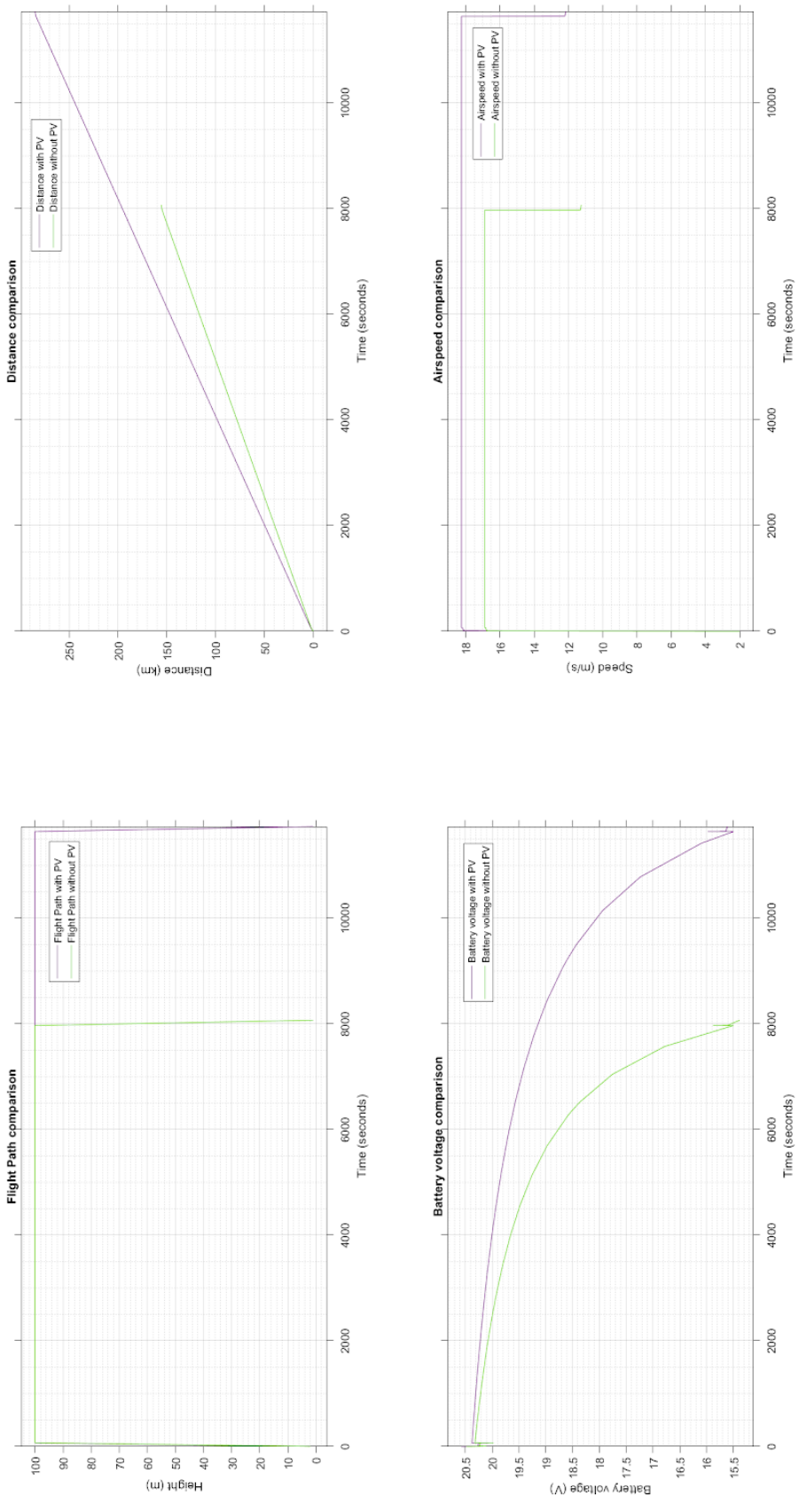

Figure B.2: Comparison between using PV panels and not using PV panels at a Solar irradiance of 782 W/m^2 and a Temp: 18.5 deg

E

Datasheets

E.1. SunPower Maxeon datasheet

SunPower Gen 3 Cell – 166 mm

Cell Physical Characteristics

Wafer:	Monocrystalline silicon
Design:	All back contact
Front:	Uniform, black antireflection coating
Back:	Tin-coated, copper metal grid
Cell Area:	Approximately 155cm^2
Cell Weight:	Approximately 6.6 grams
Cell Thickness:	150µm +/- 30µm

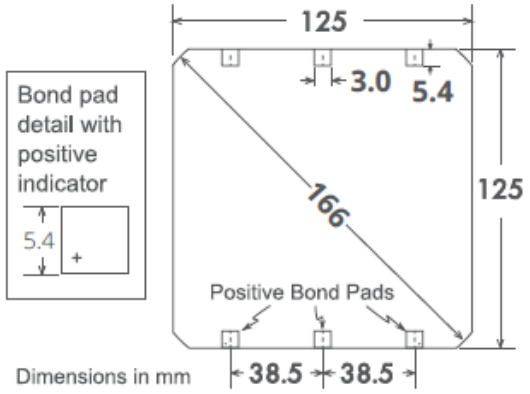

Bond pad area dimensions are 5.4mm x 3.0mm
Metal finger pitch between positive and negative fingers is 471um.
Positive/Negative pole bond pad sides have "+/-" indicators on leftmost and rightmost bond pads

Electrical Characteristics of a typical Maxeon Gen III Cell At Standard Test Conditions (STC)

STC: 1000W/m^2, AM 1.5G and cell temp 25°C

	Cell Bin	Pmpp (Wp)	Eff. (%)	Vmpp (V)	Impp (A)	Voc (V)	Isc (A)
Max Peak Performance	Me3	3.89	25.1	0.640	6.08	0.727	6.45
Max Premium Performance	Le3	3.84	24.8	0.634	6.06	0.724	6.43
Max High Performance	Ke3	3.77	24.4	0.627	6.02	0.721	6.41

Electrical parameters are nominal values.
Temp.Coefficients in SunPower Panels: Voltage: -1.74mV/°C, Current: 2.9mA/°C, Power: -0.29%/°C

Cell Bin	Cosmetic Quality	150 pcs
Me3	Highest	$21/cell
Le3	Highest	$8.8/cell
Ke3	Highest	$7.8/cell

Note:
- Pricing is not including tax and shipping
- Order less than 150 pcs will charge additional $25 for repacking and handling
- Cells have limited availability
- Spec sheets are available at SunPower website: https://us.sunpower.com/buy-solar-cells/

SUNNIVA TECH

SunPower Interconnect Tab

Interconnect Tab and Process Recommendations

SunPower recommends customers use SunPower's patented tin-plated copper strain-relieved interconnect tabs, which can be purchased from SunPower. These interconnects are easily solderable and compatible with lead free processing. Tabs weigh approximately 0.3 grams.

Our patented interconnect tabs are packaged in boxes of 3600 or 36,000 each.

http://us.sunpower.com/about/sunpower-technology/patents/

Interconnect Tab	150 pcs Unit Price
	$0.12/tab

Note:
- Pricing is not including tax and shipping
- Order without the cells will charge additional $10 for repacking and handling
- Tabs have limited availability

SUNNIVA TECH

Bibliography

[1] Bypass diodes in solar panels, -. URL https://www.electronics-tutorials.ws/diode/bypass-diodes.html.

[2] Askari Mohammad Bagher, Mirzaei Mahmoud Abadi Vahid, and Mirhabibi Mohsen. Types of solar cells and application. *American Journal of optics and Photonics*, 3(5):94, 2015.

[3] Dominique Bonkoungou, Zacharie Koalaga, and Donatien Njomo. Modelling and simulation of photovoltaic module considering single-diode equivalent circuit model in matlab. *International Journal of Emerging Technology and Advanced Engineering*, 3(3):493–502, 2013.

[4] Daniel Tudor Cotfas, Petru Adrian Cotfas, and Octavian Mihai Machidon. Study of temperature coefficients for parameters of photovoltaic cells. *International Journal of Photoenergy*, 2018, 2018.

[5] Javier Cubas, Santiago Pindado, and Marta Victoria. On the analytical approach for modeling photovoltaic systems behavior. *Journal of power sources*, 247:467–474, 2014.

[6] Alberto Dolara, Sonia Leva, and Giampaolo Manzolini. Comparison of different physical models for pv power output prediction. *Solar energy*, 119:83–99, 2015.

[7] Dupont. Micro-inverters vs. central inverters, -. URL https://www.dupont.com/products/what-makes-up-a-solar-panel.html.

[8] Ahmed A El Tayyan. A simple method to extract the parameters of the single-diode model of a pv system. *Turkish Journal of Physics*, 37(1):121–131, 2013.

[9] Mohamed A. Awadallah Fawzan Salema. Detection and assessment of partial shading in photovoltaic arrays. *Journal of Electrical Systems and Information Technology*, (3):23–32, 2016.

[10] MK Fuentes. A simplified thermal model of photovoltaic modules. *Sandia National Laboratories Report, SAND85-0330*, 1985.

[11] Abdessattar Hassanalian, Mostafa & Abdelkefi. Classifications, applications, and design challenges of drones: A review. *Progress in Aerospace Sciences*, -:34, 2017.

[12] Ramaprabha RamabadranDr B L Mathur. Impact of partial shading on solar pv module containing series connected cells. *International Journal of Recent Trends in Engineering*, 2, 2009.

[13] C.Gomes M.A. Radzi M.I.Rezadad & S. Hajighorbani M.R. Maghami, H. Hizam. Power loss due to soiling on solar panel: A review. *Renewable and Sustainable Energy Reviews*, 59:1307 – 1316, 2016.

[14] D. Picault, B. Raison, S. Bacha, J. Aguilera, and J. De La Casa. Changing photovoltaic array interconnections to reduce mismatch losses: a case study. pages 37–40, 2010.

[15] JM Pó, A Los, and WGJHM van Sark. Assessment of stc conversion methods under outdoor test conditions. In *Proceedings/26th European Photovoltaic Solar Energy Conference and Exhibition*, pages 3458–3462. WIP-Renewable Energies, 2011.

[16] E Radziemska and Eugeniusz Klugmann. Photovoltaic maximum power point varying with illumination and temperature. *Journal of Solar Energy Engineering*, 2006.

[17] Haleakala Solar & Roofing. What is the difference between monocrystalline and polycrystalline solar panels?, 2019. URL https://www.haleakalasolarroofing.com/what-is-the-difference-between-monocrystalline-and-polycrystalline-solar-panels/.

[18] Clemens Schwingshackl, Marcello Petitta, Jochen Ernst Wagner, Giorgio Belluardo, David Moser, Mariapina Castelli, Marc Zebisch, and Anke Tetzlaff. Wind effect on pv module temperature: Analysis of different techniques for an accurate estimation. *Energy Procedia*, 40:77–86, 2013.

[19] Markku Tilli, Mervi Paulasto-Krockel, Matthias Petzold, Horst Theuss, Teruaki Motooka, and Veikko Lindroos. *Handbook of silicon based MEMS materials and technologies*. Elsevier, 2020.